UNIVERSITÀ DEGLI STUDI DI NAPOLI FEDERICO II

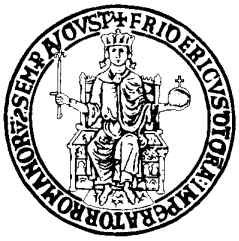

DEPARTMENT OF CHEMICAL SCIENCES
PhD IN CHEMICAL SCIENCES
XXXI CYCLE

STRUCTURE OF POTENTIAL LPS AGONIST AND ANTAGONISTS FROM DIFFERENT BACTERIAL SOURCES

Mateusz Pallach

Tutor
Prof. Alba Silipo

Supervisor
Prof. Gerardino D'Errico

Co-tutor
Prof. Antonio Molinaro

Summary

Gram-negative bacteria can be found in various habitats, they interact with humans, different animals, plants or other organisms as symbionts or parasites, can be used for industrial purpose goods production like bioethanol or drugs upon application of genetic engineering, for production of food and beverages. Moreover, they can be found in unhaltable niches for higher organisms, comprising tremendous concentrations of salt, extremely low/high pH or temperature, different organic compounds. Nearly all Gram-negative bacteria possess an outer membrane (OM) whose outer leaflet is predominantly composed of lipopolysaccharides (LPS). These amphiphilic glycoconjugates are built of three chemically, biologically and genetically distinct domains including: the lipid A, inner glycolipid moiety anchoring the LPS to the OM; - the hydrophilic moiety comprising a core

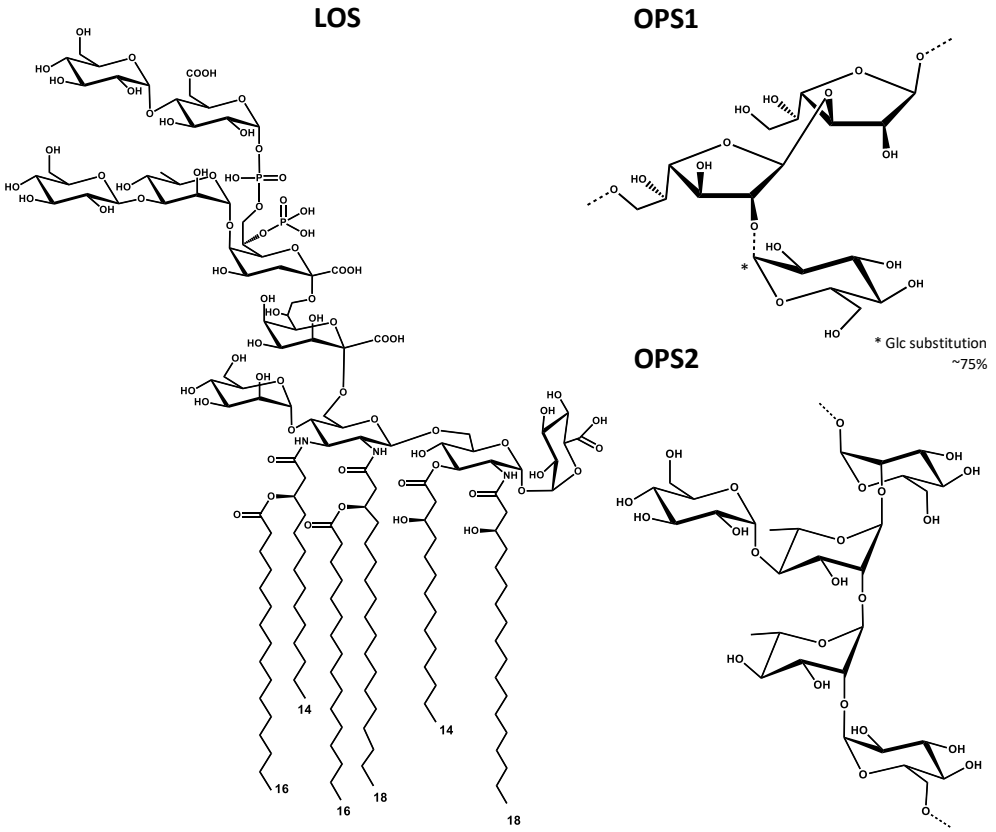

Figure 1. Structure of *Acetobacter pasteurianus* CIP103108 LOS and OPSs

oligosaccharide and the O-polysaccharide, whose presence defy the smooth LPS form, whereas molecules devoid the last domain are characterized as rough LPS (or Lipooligosaccharide, LOS). LPSs are crucial for bacterial survival, contributing significantly to the integrity and stability of the OM and protecting the bacterium from the external milieu stress factors. More interestingly, the LPS (or more precisely the lipid A) is classified as a PAMP (Pathogen Associated Molecular Pattern), recognized by the immune system upon binding to a receptorial complex formed by a transmembrane protein belonging to the Toll-like receptors family (TLRs) and by a small secreted protein, the MD-2. The event activates the defence systems and stimulates production of cytokines, being generally beneficial for the host, as it helps to combat invading microorganisms. Unfortunately, overstimulation of the immune system may lead to fatal effects as life-threading septic shock. Nonetheless modifications in the lipid A region influence significantly the immunostimulant properties of the whole molecule, diminishing or even deactivating the immunological potential, and therefore can even lead to inhibition of signaling triggered by the "agonist" LPS. Thus, the search of LPS exhibiting inhibitory activity is a high important and interesting topic and is the main aim of the presented work.

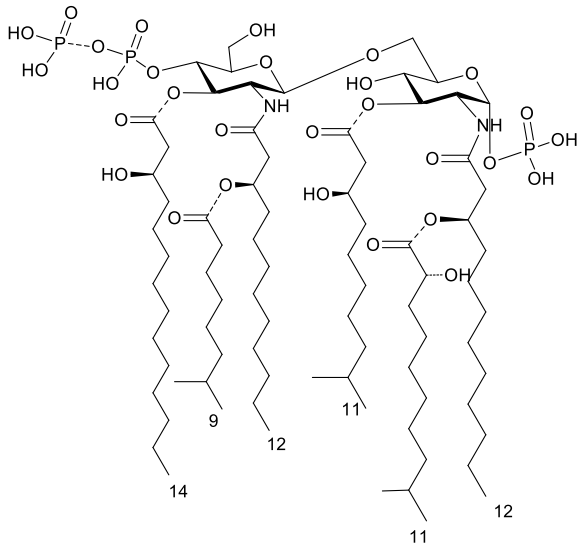

Figure 2 Structure of *Endozoicomonas* sp. HEX311 lipid A

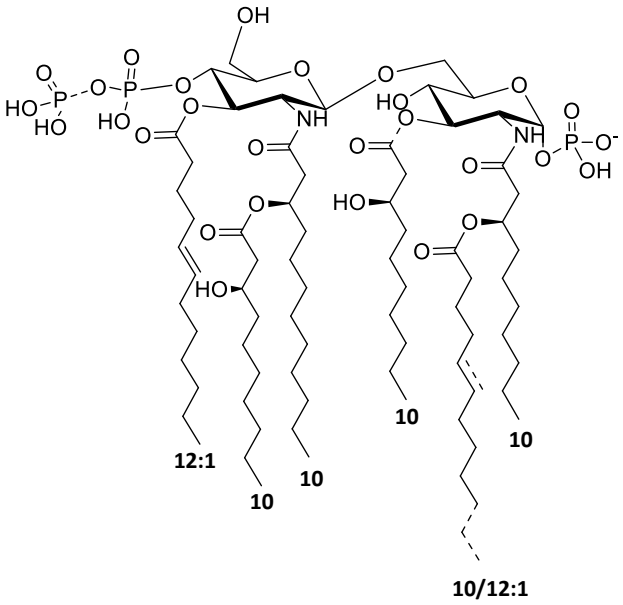

Figure 3 Structure of *Phaeobacter gallaeciensis* BS107 lipid A

The LPS here characterized were isolated from non- human pathogen bacteria derived from different environments. The work includes structural elucidation of the LPS domains of different Gram-negative bacteria, basing on a combination of extensive chemical composition analysis, NMR spectroscopy, and MALDI-TOF MS and MS^2. The structural assays showed particular features of the lipid As derived from an acetic acid bacterium, *Acetobacter pasteurianus* CIP103108 (Figure 1), a sponge symbiont *Endozoicomonas* sp. HEX311 (Figure 2) and a marine bacterium, *Phaeobacter gallaeciensis* BS107 (Figure 3). Moreover, interesting immunostimulatory features were shown for lipid As from *A. pasteurianus* and *P. gallaeciensis* upon assays performed with HEK298 cells and Monocytes-derived Macrophages (MoMs).

A Gram-negative bacterium, the ethanologenic *Zymomonas mobilis* was shown to lack LPS in the outer membrane. Interestingly, by means of DOSY-NMR and DLS analyses it was proven that *Zymomonas mobilis* exopolysaccharide (Figure 4) played a role in the high ethanolic environment tolerance mechanism. A part of this work is focused on interaction studies of two different lipopolysaccharides with the MD-2, a lipid binding protein, pivotal in the innate LPS recognition system and part of the receptorial complex responsible for the recognition of the LPS,

namely the TLR4/MD2 complex. The study was performed applying number of DOSY-NMR studies and Cryo-EM.

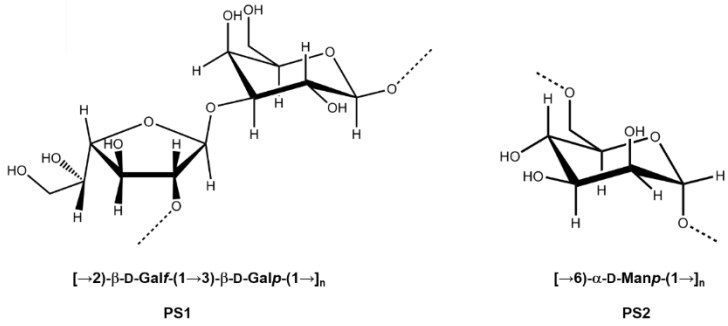

Figure 4 Structure of *Zymomonas mobilis* EPS

The author of the present PhD thesis acknowledges: Prof. Alba Silipo, Prof. Antonio Molinaro, Dr. Flaviana Di Lorenzo, Dr. Roberta Marchetti, Dr. Katarzyna Anna Duda, Prof. Jesús Jiménez Barbero, Dr. Helena Coelho, Dr. Sandra Delgado, Prof. Francesco Peri, Dr. Fabio Alessandro Facchini, Prof. Gerardino D'Errico, Dr. Antonio Fabozzi, Prof. Maria-Lina Bernardini, Dr. Luigi Lembo Fazio for the scientific support.

Abbreviations

AA Acetylated Alditols
Ac_2O Acetic Anhydride
AI Allergy Immunotherapy
AP-1 Activator protein 1
BMDM Bone Marrow-Derived Macrophages
BSTFA *O-bis*-(trimethylsilyl)trifluoroacetamide
CARS Anti-Inflammatory Response Syndrome
CD14 Cluster Differentiation Antigen 14
CMC Critical Micellization Concentration
COSY Correlation Spectroscopy
CPS Capsular Polysaccharide
CXCL-8 Interleukin 8
DAMP Damage Associated Molecular Patterns
DHB 2,5-dihydroxybenzoic acid
DLS Dynamic Light Scattering
DMEM Dulbecco's Modified Eagle's medium
DMSO Dimethyl Sulfoxide
DMSP Dimethylsulfoniopropionate
DOC-PAGE Sodium Deoxycholate-Polyacrylamide Gel Electrophoresis
DOSY Diffusion-Ordered Spectroscopy
DQF-COSY Double Quantum Filter Correlation Spectroscopy
EI-MS Electron Impact Mass Spectrometry
EPS Exopolysaccharide
ESI Electrospray Ionization
FA Fatty Acid
FAB Fast Atom Bombardment
FAME Fatty Acid Methyl Ester
FBS Fetal Bovine Serum
FCB Flexibacter-Cytophaga-Bacteroides
GC Gas Chromatography
GSL Glycosphingolipid
HEK Human Embryonic Kidney [cells]
HMBC Heteronuclear Multiple Bond Correlation spectra
HSQC Heteronuclear Single Quantum Coherence
IgE Immunoglobulin E
IgG Immunoglobulin G
IL Interleukin
IMAC Metal Affinity Chromatography
Kdo 3-deoxy-D-manno-oct-2-ulopyranosonic acid
Ko D-glycero-D-talo-oct-2-ulopyranosonic acid
LBP LPS Binding Protein
LC Liquid Chromatography
LOS Lipooligosaccharide
LPS Lipopolysaccharide
LTA Lipoteichoic acid
MALDI MS Matrix Associated Laser Desorption Ionisation Mass Spectrometry
MD-2 Myeloid Differentiation Protein-2
MeOH Methanol
MGA Acetylated *O*-methyl Glycosides
MHC Major Histocompability Complex
MoMs Monocytes-Derived Macrophages
MPEG Macrophage Expressed Protein
MPL® Monophosphoryl Lipid A®
MS Mass Spectrometry
MS^2 Tandem Mass Spectrometry
MyD88 Myeloid Differentiation Factor
NF-kB Nuclear Factor Kappa-Light-Chain-Enhancer Of Activated B Cells
NMR Nuclear Magnetic Resonance Spectroscopy
NOE Nuclear Overhauser effect
NOESY Nuclear Overhauser Enhancement Spectroscopy

OM Outer Membrane
OPS O-polysaccharide
OS Oligosaccharide
PAMP Pathogen Associated Molecular Pattern
PCP Petroleum/Chloroform/Phenol Extraction
PFG Pulsed Field Gradient
PGN Peptidoglycan
PMAA Partially Methylated Alditol Acetates
pNPP *para*-Nitrophenylphosphate
PRR Pathogen Recognition Receptor
PS Polysaccharide
Pyr Pyridine
R-LPS Rough Type Lipopolysaccharide
ROESY Rotating Frame Overhauser Enhancement Spectroscopy
SDS-PAGE Sodium Dodecyl Sulfate –Polyacrylamide Gel Electrophoresis
SEAP Secreted Embryotic Alkaline Phosphatase
SEC Size Exclusion Chromatography
S-LPS Smooth Type Lipopolysaccharide
SLS Static Light Scattering
STD Saturation Transfer Difference
TDA Tropodithietic Acid
TEM Transmission Electron Microscopy
TFA Trifluoroacetic Acid
Th T-Helper Cell
TLR Toll-Like Receptor
TNF-α Tumor Necrosis Factor α
TOCSY Total Correlation Spectroscopy
TOF Time Of Flight
VLCFA Very Long Chain Fatty Acids
WT Wild Type
WTA Wall Teichoic Acid

INDEX

SECTION I: Introduction

SECTION II: Structural, immunological and functional characterization of bacterial cell wall components

SECTION III: Experimental section

SECTION I

Introduction

Chapter I

Gram negative bacteria

1.1. The prokaryotes

The prokaryotes are a group of simple, unicellular organisms, divided into two distinct domains, namely *Archea* and *Bacteria*. The term *Prokaryota* originates from two Greek words, πρό (*pro*) “before" and κάρυον (*karyon*) "nut or kernel", as they were the first organisms found on Earth, present billions of years prior any organism of the third, *Eucaryota* domain (Campbell, 2000). This fact leads to the logical conclusion that the Prokaryotes are rather simple organisms, with cells organised in a different fashion in comparison to *Eucarya* (Figure 1.1). The first noticeable difference is lack of a membrane enclosed nucleus in case of Prokaryotes. Therefore, unlike *Eucarya*, the genetic material is kept inside a nucleoid. Moreover, they lack numerous membrane-locked organelles. Therefore, Prokaryotes are known to form cells of a small size in range 1 -10 μm, around ten-fold smaller than Eukaryotes (10-100 μm).

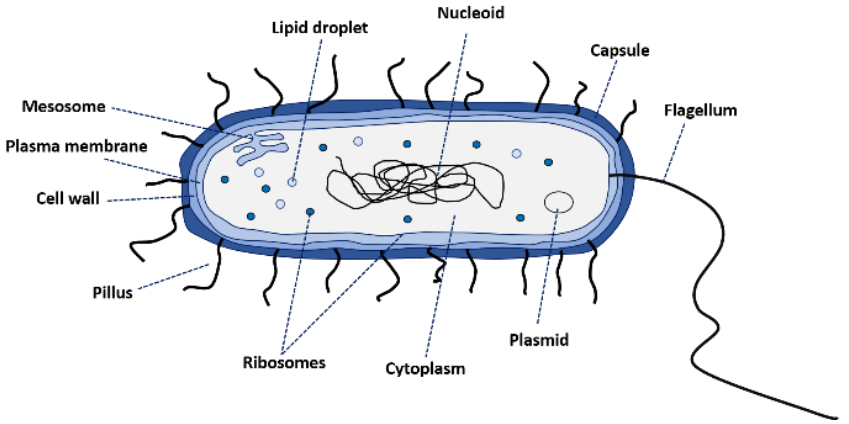

Figure 1.1 Prokaryotic cell scheme

Despite the simplicity, the Prokaryotes create a highly diverse group of microorganisms, widespread on Earth and present in all types of environment, including rivers, oceans, soils, also in conditions considered as “extreme” like hydrothermal vents, hypersaline, highly acidic or basic environments. Furthermore, those organisms are being found interacting with all kinds of organisms, including plants and animals, involved in both, symbiotic and pathogenic interactions and are important decomposers, being crucial element of different elements cycle (Whitman, 1998; Di Lorenzo, 2017a).

Bacteria are a group of prokaryotic unicellular microorganisms that differ from Eukaryotes for their simple cellular organization. The *bacteria* domain includes a heterogenious group of organisms, diverse in terms of cell structure, size or shape (Yang, 2016). Most of them are single-celled but some are organized in multicellular forms consisting of numerous cells that constitute distinctive cell morphologies (coccus, bacillus, spirillum, filamentous) and create distinct colonies visible by light microscopy when grown on petri plates (Raven & Johnson, 2001). Further division can be made basing on the cell wall structure, in particular, Gram-positive bacteria, possessing a thick cell wall between which the dye-iodine complex is trapped, respond to the crystal-violet forming a purple stain, whereas the Gram-negative bacteria possess a thinner, less layered envelope and the dye can be washed out easily (Staley, 2007).

As for the *Archea* domain, it represents a group of mostly extremophilic and non-human pathogen organism, phylogenetically different form Bacteria.

1.2. The cell envelope

Bacterial cell is covered by a multi-layered and complex structure referred to as cell envelope. Unlike many higher organisms, in order to survive, bacteria had to evolve this type of structures to protect themselves from unfavourable conditions of the outer milieu. As stated previously, basing on fundamental differences in the cell wall structure, two main groups can be distinguished- **Gram-positive bacteria and Gram-negative bacteria** (Figure 1.2).

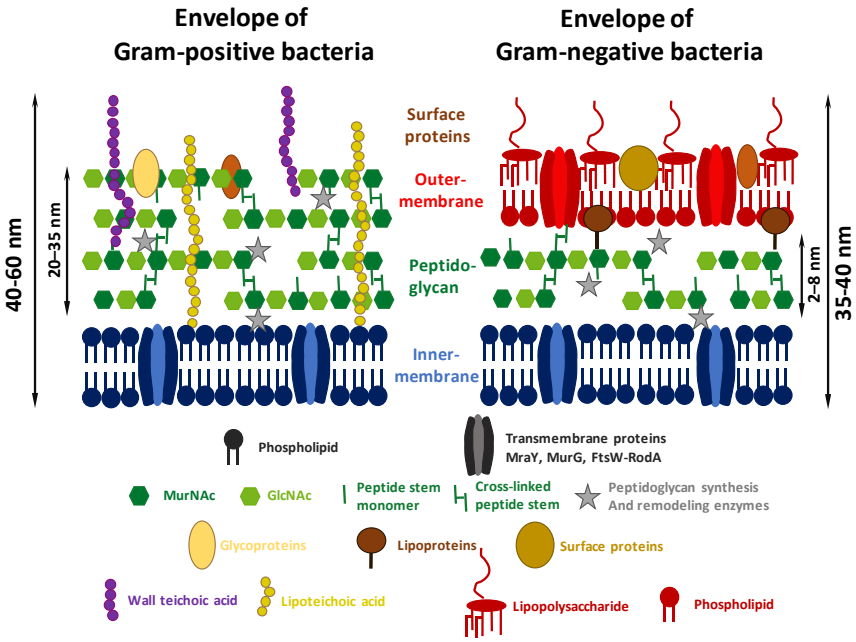

Figure 1.2 Structure of Gram-positive and Gram-negative cell envelope

Despite numerous differences in the envelope architecture, common features are evident (Figure 1.2), as the presence of an inner cytoplasmatic membrane, possessing integral proteins and surrounded by the cell envelope. Thus, a layer of peptidoglycan (or so-called murein) is present, whose main function is providing the structural strength to the cell wall. The murein is built of repeating units of β-(1→4) N-acetylglucosamine (GlcNAc) and N-acetylmuramic acid cross linked at position 3 by short peptide chains containing three to five amino acids with alternating L and D-amino acids. The peptide chain contributes to the formation of a 3D mesh-like structure of the polymer (Tytgat & Lebeer, 2014). Although peptidoglycan is present in both, Gram-positive and negative bacteria, it possesses several structural differences among both groups (Figure 1.3). Firstly, the third position of the oligopeptide in case of Gram-positive is occupied by lysine while in case of Gram-negative species by meso-diaminopimelic acid is present. Furthermore, the peptidoglycan layer in Gram positive bacteria is significantly thicker (30-100 nm) than the one found in Gram-negative (couple nanometres). Gram-positive bacterial murein layer possess specific immersed glycolipids, namely lipoteichoic acid (LTA) and wall teichoic acid (WTA) (Vollmer, 2008, Tytgat & Lebeer, 2014).

In addition to the PGN layer, the Gram-negative cell wall also contains an asymmetric bilayer called the outer membrane (OM) which "coats " the bacterium and faces into the external environment. The OM is constituted from the inner part mainly of phospholipids, whereas the external leaflet is covered up to 75% by a glycolipid known as the lipopolysaccharide (LPS) (Alexander & Rietschel, 2001).

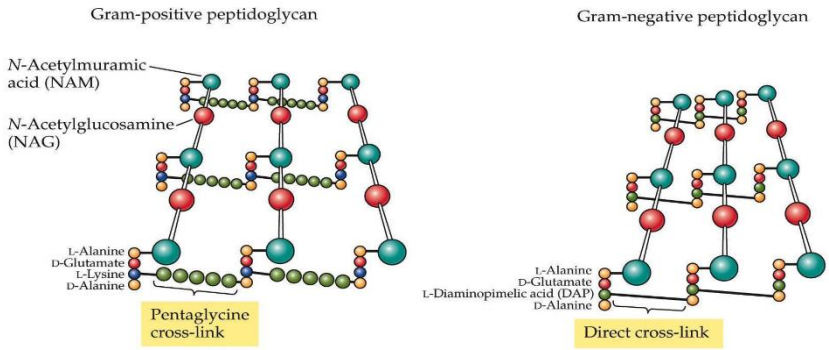

Figure 1.3 Structure of Gram-negative and Gram-positive peptidoglycan (Staley, 2007).

As the LPS are highly-charged, the Gram-negative cell wall has an overall negative charge. The chemical structure of these macromolecules is unique to specific bacterial strain (e.g. sub-species) and is responsible for many of their biological properties. Bacteria can be further covered by glycans, namely capsular polysaccharides (CPS) or exopolysaccharides (EPS).The complexity of all these macromolecules leads to infinite possibilities of structural and functional diversity (Tytgat & Lebeer, 2014).

1.3. The Lipopolysaccharides (LPS)

The lipopolysaccharides (Figure 1.4) are glycoconjugates found on the external leaflet of the outer membrane of Gram-negative bacteria, covering around 75% of the cell surface and greatly contributing to the structural integrity and to the protection of the bacterial cell envelope. These amphiphilic macromolecules play significant role in bacterial survival. They contribute to the membrane integrity, fluidity and permeability upon electrostatic interactions of negatively charged groups with divalent metal ions (Ca^{2+} or Mg^{2+}). They help to resist hydrophobic and hydrophilic antibiotics, and as the most exposed bacterial

components, play a key role in mediating host-bacterium interactions like recognition, colonization or adhesion, virulence, but also tolerance for commensal bacteria and symbiosis (Raetz, 1990; Silipo, 2010, Molinaro, 2015).

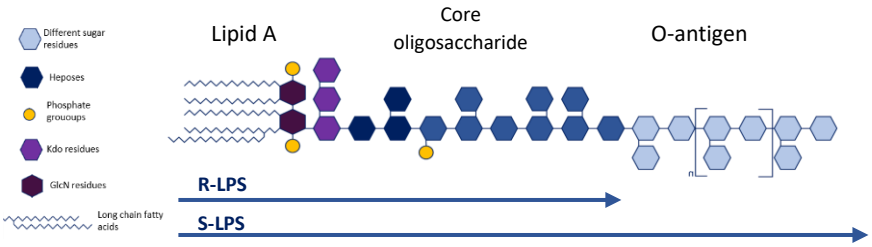

Figure 1.4 Scheme of the structure of LPS

All known lipopolysaccharides possess highly conserved architecture, characterized by presence of three chemically, biologically, biosynthetically and genetically distinct domains including the lipid A, core oligosaccharide and O-polysaccharide. The glycolipid portion, named the **lipid A** is covalently linked to a hydrophilic portion formed by the core oligosaccharide (**core OS**) and a hydrophilic hetero-polysaccharide called **O-polysaccharide chain or O-chain** (Holst, 1996; Alexander & Rietschel, 2001). The presence of a complete LPS, the smooth-type LPS (S-LPS) provides a smooth aspect to the bacterial colonies; bacteria can also synthesize lipooligosaccharide (LOS) if the O-chain is absent and are also termed rough type-LPS (R-LPS) because of a rough morphology of the bacterial colonies. The LPSs structures present a significant variability, where composition of all domains may change among species or even bacterial strains. The LPS by itself is not present as single conserved compound, but as a mixture of molecules varying in terms of molecular mass (e.g. presence of different number of repeating units of O-antigen) and slight compositional variations (e.g. different acylation pattern of the lipid A) (Raetz, 1990; Raetz & Whitfield, 2002).

The LPSs were discovered in the late nineteenth century, by demonstrating that heat killed cholera (*Vibrio cholerae*) bacteria were still toxic, therefore the molecule was named endotoxin (Holst, 1996). During years the LPS was widely studied and its functions and impact on the human body well defined. Nowadays it is well known that the lipopolysaccharides, with their most potent immunologically active site,

the lipid A, are considered as pathogen associated molecular patterns (PAMPs), recognized by specific pathogen recognition receptor (PRR), the toll-like receptor 4 (TLR4) upon binding the LPS with the key protein, myeloid differentiation 2 (MD-2) (Park & Lee, 2013). This binding event is crucial to activate the innate immune response and will be widely discussed in further part of the work (see 1.3.7).

1.3.1. Lipid A, structure and functions

The lipid A is the most inner portion of the LPS, represents the most conserved part of the lipopolysaccharide and anchors the whole molecule to the external leaflet of the OM through hydrophobic and electrostatic interactions with the phospholipid layer. Its general structure consists of a disaccharide backbone formed by a β-(1→6) D-glucosamine backbone, phosphorylated at position 1 of the proximal α-D-GlcN (GlcN I) and position 4 of distal β-D-GlcN (GlcN II) and acylated at position 2 and 3 by so called "primary" fatty acids, in turn further acylated at hydroxyl position with "secondary" fatty acids, usually not hydroxylated and with different length (Molinaro, 2015).

The first complete chemical structure of the lipid A derived from *E. coli* and *S. enterica* were elucidated in 1983. The lipid A from *E. coli* is

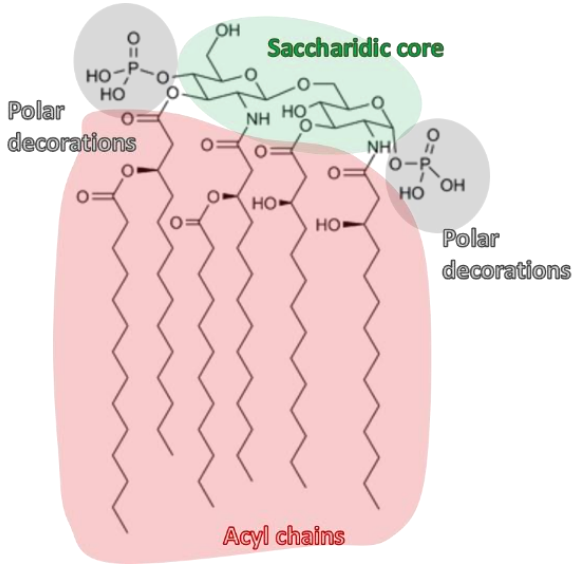

Figure 1.5. General structure of the lipid A

composed by a disaccharide backbone [P→4-β-D-Glc*p*N-(1→6)-β-D-Glc*p*N-1→P] acylated at position 2 and 3 of both Glc*p*Ns and carrying at position 2 and 3 of both Glc*p*Ns as primary fatty acids four 14:0 (3-OH) (Figure 1.5). The primary fatty acids located on the distal Glc*p*N (GlcNII) were both esterified at their hydroxy group by two secondary fatty acids; the amine linked 14:0 (3-OH) was esterified by a 12:0; the ester linked 14:0 (3-OH) by a 14:0 (Figure 1.5). This hexa-acylated lipid A possesses a symmetric (4+2) distribution of the acyl chains.

Even though the lipid A remains the most conserved domain of the LPS, different modifications can be present among different bacterial species, possibly in every region (Figure 1.6) (Silipo & Molinaro, 2011). The saccharidic skeleton of the lipid A is the less variable part of the moiety. The most common modification is the presence of 2,3-dideoxy-2,3-diamino-glucose (GlcN3N or DAG) in place of glucosamine residues. This particularity is found among a number of strains including members of *Rhizobiaceae* and *Bradyrhizobiaceae*, *Rhodopseudomonas* (Di Lorenzo, 2017b) or *Bradyrhizobium* strains (Komaniecka, 2010; Silipo, 2014). Interestingly, the lipid A isolated from *Camphylobacter jejuni* is found to possess both, GlcN and DAG in the backbone (van Mourik, 2010). Furthermore, some of bacteria are found to carry an "extended" sugar backbone, comprising of more than two sugar residues. The lipid As among *Rhizobiaceae* and *Bradyrhizobiaceae* families are reported to possess a skeleton composed of GlcN or DAG with decoration of mannose and uronic acids like glucosamine (GlcA) or galactosamine (GalA). A GlcpN3N disaccharide backbone has been also identified in *Pseudomonas diminuta*, *Aquifex pyrophilus*, *Leptospira interrogans* (Plötz, 2000; Silipo & Molinaro, 2011). A unique and exceptional lipid A structure identified so far is that of *Rizhobium leguminosarum* and *Rizhobium etli*, characterised by an unusual trisaccharide backbone containing a distal galacturonic acid in β-1,4 linkage to GlcNII which is 1,6 linked to a proximal 2-aminogluconic acid residue.

Further modifications are found in the polar decorations. Despite most of known lipid As are *bis*-phosphorylated, different substitutions are found, as pyrophosphate (PP), phospho- or pyrophospho-etanolamine (P-EtN and PP-EtN), phospho-4-amino-4-deoxy-L-arabinopyranose (P-L-Ara4N, as in *Burkholderia* (De Soyza, 2008) or *Pseudomonas aeruginosa*.) Moreover, phospho-glucosamine methyl phosphate, phospho-L,D-

glycero-D-*manno*-heptose has been found linked to both glycoside and non-glycoside phosphates isolated from several species of lipid A.

The acyl chains constitute, together with the polar heads, the most variable component. The heterogeneity is found in terms of fatty acid composition and substitution. Lipid A is often constituted by a mixture of species whose carbohydrate backbone is frequently differently acylated. The acyl chains are generally saturated and usually possess an even number of carbon atoms between 10 and 28, nevertheless also 2-deoxy or oxo-fatty acids were reported. Some bacteria, including *Bradyrhizobium, Sinorhizobium* or *Rodopseudomonas* are found to possess Very Long Chain Fatty Acids (VLCFA) of number of carbon atoms up to 32. Secondary fatty acids rarely possess functional groups , while odd numbered secondary acyl chains can be present (Haag, 2011; Silipo, 2014; Di Lorenzo, 2017b). Moreover, a fascinating example of variability is given by the lipid A isolated from *Bradyrhizobium* strains which is found to possess a sterol-like hopanoid domain linked to the VLCFA (Silipo, 2014). Thus, the term lipid A defines more correctly not one molecule but a family of species structurally related but expressing differences in the acylation and in the phoshorylation pattern. Bacteria can dynamically modulate their acylation pattern in response to environmental changes. An example is given by *Yersinia pestis*, which synthetizes hexa- or tetra-acylated lipid A dependently from the bacterial growth temperature. (Montminy, 2006; Telepnev, 2009).

The acyl chain composition and distribution are strictly connected with the 3D shape of the lipid A (Figure 1.7.). Asymmetric hexaacylated lipid A species are known to adopt a cone-like structure with a tilt up to 50°. In contrast, hypo-acylated and/or symmetric molecules tend to adopt a cylindrical shape with a tilt up to 15° (Seydel, 1993, 2000).

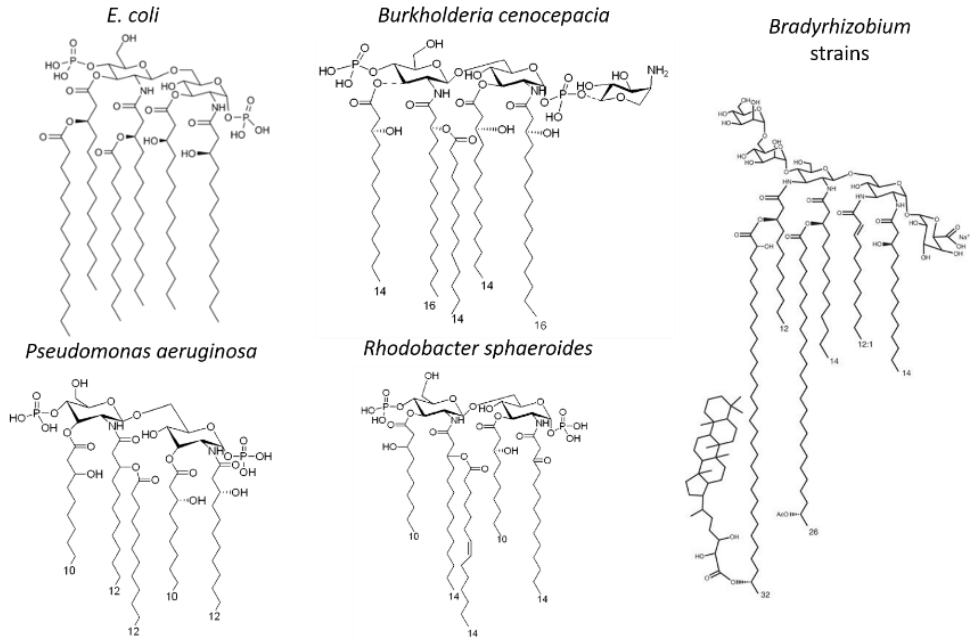

Figure 1.6 Variability of lipid A structures

The lipid A is highly functionalized domain and plays a key role in bacterial survival. The polar anionic substituents are significantly involved in the stabilization of the membrane, by forming electrostatic interactions with divalent cations (Ca^{2+} and Mg^{2+}) which connect the LPS molecules, reducing the membrane permeability and forming an efficient protective barrier (Silipo & Molinaro, 2011). Moreover, many structural variations strongly contribute to bacterial resistance and protection. As an example, the presence of Ara4N in the lipid A increases significantly the resistance to cationic antimicrobial peptides by shielding the negatively charged residues (Hamad, 2012). Other examples may be found in the fascinating world of extremophiles, where structure of lipid A is strictly connected to harsh conditions of external milieu (Di Lorenzo, 2017a).

Finally, the lipid A plays a pivotal role in inflammation provoked by Gram-negative bacteria. The domain is recognized by the human innate immune system by binding to a specific TLR4/MD-2 receptorial complex. Immunostimulant activities of the lipid A are described widely further in Chapter 1.7. and 1.8.

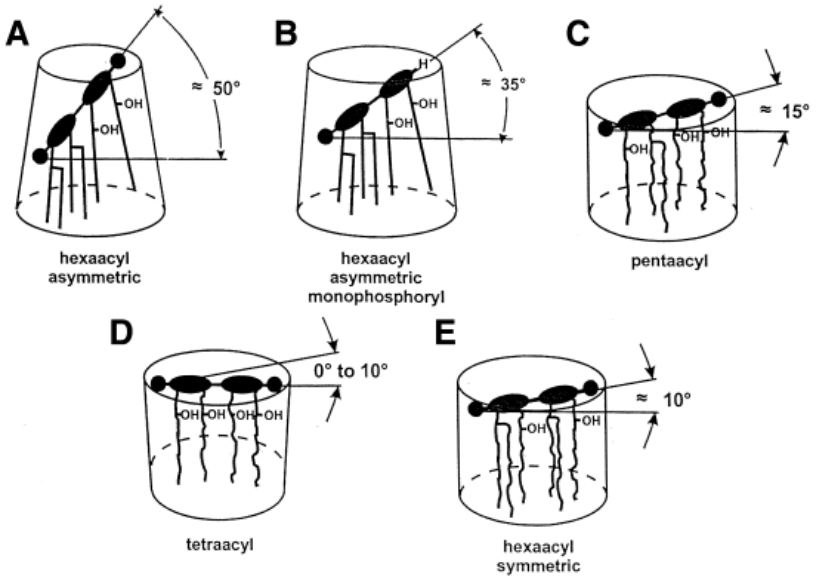

Figure 1.7 Intrinsic conformations of asymmetric hexa acylated lipid A (A), less active monophosporyl lipid A ® (B), and showing low activity, inactive or antagonistic penta- (C) and tetra acylated lipid A (D) and symmetric hexa-acylated lipid A (E) (Seydel, 2000).

1.3.2. Core oligosaccharide structure and functions

The lipid A is covalently connected to the core oligosaccharide. This part is composed by different monosaccharide units, up to 15, in either linear or branched architecture, frequently possessing non-carbohydrate components, which can be present in a non-stoichiometric fashion (Holst, 2011). The core can be further divided into two regions, namely inner core and outer core (Figure 1.8).

The inner core, which is proximal to the lipid A, is structurally less variable and contains peculiar monosaccharides like heptose (L-*glycero*-D-*manno*-heptose and D-*glycero*-D-*manno*-heptose) and 3-deoxy-D-manno-oct-2-ulopyranosonic acid (Kdo), a monose marker for all Gram-negative bacteria that connects the core oligosaccharide to lipid A backbone trhough the non-reducing GlcNII (Silipo & Molinaro, 2010). Furthermore, other ulosonic acids can be also found, like like D-glycero-D-talo-oct-2-ulopyranosonic acid (Ko) in *Burkholderia*, *Acinetobacter*, *Yersinia* or *Serratia* species (Isshiki, 2003; Holst, 2011) or 8-amino-3,8-dideoxy-α-D-manno-oct-2-ulopyranosonic acid (Kdo8N) like in case of *Shewanella* strains (Vinogradov, 2003, 2004). Negatively charged substituents are

often present, as they are involved in the formation of electrostatic interactions with divalent cations, significantly reducing the permeability of the membrane, enhancing the stability and providing resistance to antibiotic compounds and antimicrobial peptides. The most common negative substituents include phosphate (P), pyrophosphate (PP), pyrophosphoryl-2-amino-ethanol (PPEtN), phospho-arabinosamine (PAra4N), uronic acids (often Gal*p*A). On the other side, positively charged groups also might be present, including 2-amino-ethanol (EtN), Ara4N, GlcN, which can substitute cations and interact with the phosphate groups bringing the LPS molecules together and blocking the entrance of positively charged molecules. The outer core, that in case of R-LPS is the most exposed part of the molecule, is characterized by higher structural variability then the inner core, and is mainly composed of common hexoses including Glc*p*, Glc*p*N, Gal*p* and Gal*p*N (Silipo & Molinaro, 2010). However, some particularities in this region can be also found, as *Shewanella oneidensis* MR-1 with a novel type of glycosidic linkage involving an open chain acetal linkage of a GlcN present as non-cyclic carbonyl form (Figure 1.9) (Vinogradov, 2003).

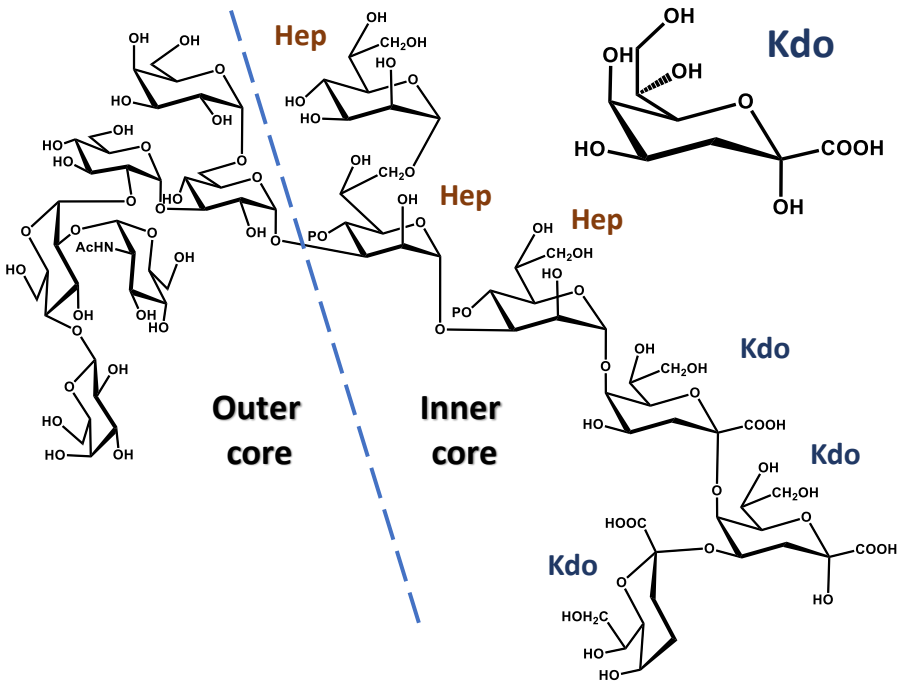

Figure 1.8. Structure of the core OS of *E. coli*. Indicated inner and outer core, Kdo and heptoses (Hep). On the top right α-Kdo*p* residue.

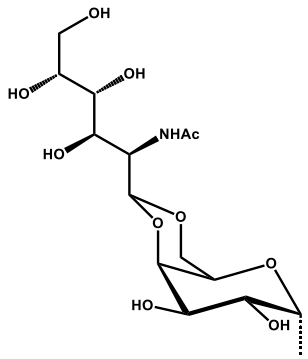

Figure 1.9. 2-acetamido-2-deoxy-D-galactose (N-acetylgalactosamine, GalNAco) in an open-chain form, linked as cyclic acetal to O-4 and O-6 of D-galactopyranose in *Shewanella oneidensis* MR-1 core OS.

1.3.3. O-antigen structure and functions

The O-antigen (also called O-polysaccharide, OPS) is the outermost domain of lipopolysaccharides. The OPS is characterized by high structural diversity, which may occur not only between species, but also between bacterial strains (Raetz & Whitfield, 2002). The domain is made of number of repeating oligosaccharide units containing two to eight monosaccharide residues, the repeating unit can be homopolymeric or heteropolymeric, linear or branched. The addition of non-carbohydrate substituents like phosphate, amino acids, acetyl or formamide groups, often present in non-stoichiometric amount, can be also present. (Knirel, 2011).

Therefore, the O-antigen structure characterizes the serological specificity of the organism. The number of the serogroup are various, while e.g. *E. coli* produces ~170 serotypes (Stenutz, 2006), *S. enterica* is known to form only 46 serogroups (Popoff, 2003).

1.4 Exopolysaccharides

The cell wall polysaccharides or exopolysaccharides are a big group of glycans, present at the surface of bacterial cell wall forming kind of a "coat" around the bacterium. They can either form a biofilm or a capsule covering the cell surface. Predominantly the exopolysaccharides are

represented by large polymers with average molecular weight 1×10^5 to 3×10^5 Da, composed of different number of monosaccharide residues in the repeating unit (commonly up to 10), often carrying negative charge at physiological pH, nonetheless neutral macromolecules are also present. Not infrequently substituents of non-saccharidic nature are present, like ketal-linked pyruvate, acetate groups, succinic acid or inorganic residues such as phosphate or sulphate (Poli, 2010). The arrangement of monosaccharides strongly influences the physical properties of the molecule. Furthermore, the structures of EPS vary significantly and a vast number of different structures was reported. A mixture of polysaccharides (Ates, 2015; Kwon, 1994) can be also produced.

The EPSs play a pivotal role in the biofilm development, making up a matrix for this type of formation. Biofilms represent a living micro-environment for microbes, trapping water, ions and soluble products and enabling biochemical contacts between bacteria and surrounding cells. The exopolysaccharides can be attached either physically to the cell wall or remain associated with it, forming a capsule. Therefore, secreted polysaccharide remains loosely bound to the cellular surface. The EPS play highly important biological roles, are known to carry a significant protective task, shielding the bacterium against unfavourable environmental conditions as high or low temperatures, extreme acidity, UV radiation, heavy metals. In case of high salinity or variations of the pH, the polysaccharide viscosity does not change significantly, and the high stability of the polymer assures protection to the bacterial cell. The EPS can also play a key role in reduction of water loss and subsequently assist in rehydration enhancing the water uptake.

Moreover, the EPSs also are highly involved in host-microbe interaction, includin both, symbiotic and pathogenic interactions with animals and including adhesion or immunomodulation. Finally, some of the EPSs found their industrial applications. The examples can be given by xanthan, dextran, gellan and curdlan produced by *Xanthomonas campestris*, lactic acid bacteria, *Pseudomonas elodea* and *Alcaligenes faecalis*, respectively (Mollakhalili & Mohammadifar, 2015; Nwodo, 2012).

1.5. Other glycolipids

The lipopolysaccharides are strictly connected with Gram-negative bacteria, being a preserved component of their cell wall. Nonetheless it was reported that some organisms are devoid of the LPS on the outer leaflet of the cell wall. An interesting example is given by bacteria from the genus *Sphingomonas*, known to possess other type of glycoconjugate on their outer membrane, the Glycosphingolipids (GSL). Similarly to the LPS, GSLs possess an amphiphilic nature as they can be divided into a polar

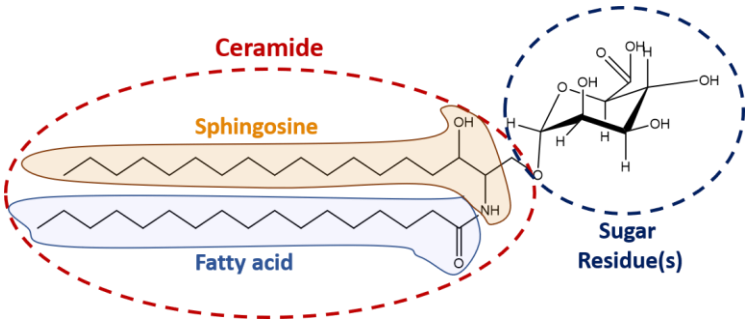

Figure 1.10 General scheme of glycosphingolipids (on the example of GSL-1)

head containing a few monosaccharide units and a hydrophobic tail (Figure 1.10.). The lipophilic part is made up of a ceramide, specific type of lipid, composed of sphingosine and amide - linked fatty acid, whose nature may vary inside and throughout different microbes. A common characteristic is the presence of a negatively charged monosaccharide, glucosamine or neuraminic acid, substituted with the ceramide. In *Sphingomonas paucimobilis* and *Sphingomonas capsulatus* the GSL varies not only in terms of ceramide fatty acids, but also the saccharidic part, therefore two molecules are clearly distinguished, the GSL-1 possessing ceramide linked to Glc*p*A and the GSL-4A possessing a tetrasaccharide domain linked to the ceramide (Figure 1.11.) (Kawahara, 2000; Kawasaki, 1994). Interestingly, significant conformational similarities can be noticed comparing *E. coli* Re-LPS and GSL-1 if three molecules are packed together. While in the LPS two Kdo units, two phosphate groups and six fatty acid chains are present, three GSL-1 comprise of three uronic acids and six fatty acid chains. Furthermore, it was shown that in the system of asymmetric lipid bilayers the GSL-1 behaves similarly to LPS for what concerns the channel function of porin, activation of complement and

interaction with polymyxin B. Furthermore, due to the lack of a complicated carbohydrate domain, the GSLs possess small variation of antigenicity (Kawasaki, 1994).

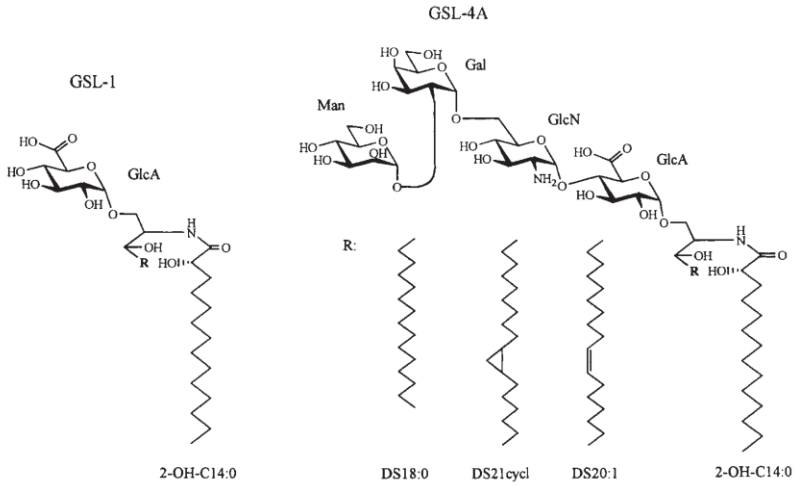

Figure 1.11. Structure of GSL-1 and GSL-4A.

1.6. Innate immunity and adaptive immunity

The immunity is the ability of highly developed organisms to resist infections. Mammals respond to microbe invasion with innate and adaptative immune responses. Specific or adaptative immunity is the acquired capacity to recognize and destroy pathogens or their metabolic compounds. The adaptive immune system is capable to "remember" previously encountered microbes and destroy them just when they attack again. Therefore, using this strategy, the human body can avoid most of infections. Unfortunately, sufficient amount of time is needed to give effective response against invading microbes (Janeway, 2001). Given this, a first line of defence had to be developed and this important role is played by the innate immune system.

Innate immunity relies on recognition of microbial patterns, conserved molecules commonly found in the pathogens, but not found in host organism. Those molecules are known as pathogen associated molecular patterns (PAMPs), and are recognized by specific pattern recognition reseptors, expressed by some of immune system cells. The can be further divided into distinct families (Brubaker, 2015), including

predominantly toll-like receptors (TLRs) or lectins. Skin and any epithelial surface separating the inside of the body with external environment is considered as a part of innate defence and therefore constitute the first barrier protecting human and in general animal body from invading microorganisms. When this is overcame (e.g. orally or by skin damage), innate immunity relies on its specific cells. These includes several types like monocytes and macrophages, neutrophils, eosinophils, basophils, mast cells, NK cells, NKT cells, γδ T cells and dendritic cells. Among all cell players, it is possible to distinguish phagocytes, constituted by macrophages and neutrophils, which are known to express significant variety of cell surface receptors and recognize invading microorganisms. Their phagocytic capabilities rely on ability to induction of actin polymerization upon recognition by the ligand by surface receptors, which lets the membrane to surround the microbe and incorporate it forming a phagosome. The germ gets finally degraded in oxygen-dependent manner, basing on reactive oxygen species or oxygen-independent manner, utilizing lysosomes, specific organelle containing enzymes capable of braking the cell wall of invader. The monocytes and mast cells are afterwards able to release cytokines inducing further immunological responses.

Macrophages also contribute to the adaptive immune system. The adaptive immune system (or also so-called specific immune system) can be further spited into two other groups, namely humoral immunity and cell-mediated immunity. The main cellular players in adaptive immunity are two groups of lymphocytes, namely the T lymphocytes involved in expression of cell-mediated immunity and B-lymphocytes which express humoral immunity. The first step of immune response is antigen-processing by macrophages and dendritic cells followed by presentation to B and T lymphocytes which are recognized by specific receptors expressed on their membrane. Therefore, the binding of the antigens to the receptors provokes activation, proliferation and differentiation into effector cells by a process of clonal selection.

In case of cell mediated immunity, the process involves activation of phagocytes, and T-lymphocytes followed by release of different cytokines. In detail, the cytotoxic T-cells are able to attack the leukocytes presenting the antigenic determinants bounded to proteins of major histocompability complex of class I (MHCI) and combat them.

Furthermore, also T-helper cells play an important role by recognition of the complex formed by the antigen complexed with MHC class II, effecting in release of cytokines which later promotes the activity of macrophages. In contrast, the humoral response involves substances found in the humor (body fluids) and is mediated by molecules such as antibodies, complement proteins and antimicrobial peptides. The process consists of activation of B-cells or plasma cells which later secret antibodies circulating in the bloodstream and all fluids in general, bind to the foreign antigen causing its destruction. Therefore, some the cells undergo a phase differentiation into memory cells, which in future can encounter the new antigen, making the response fester and more effective.

1.7. Basis of TLR4/MD-2 recognition of LPS

One of the key molecules recognized by the innate immune system in case of Gram-negative infection are the lipopolysaccharides. LPS are recognized as Pathogen associated molecular patterns (PAMPs), structurally conserved molecules able to trigger innate immune response by binding to specific Pathogen Recognition Receptors (PRRs) (Medzhitov, 2001; Akira & Kiyoshi, 2004; Molinaro, 2015). In case of LPS, the innate immune response is triggered by binding of the lipid A to a receptorial complex formed by a small secreted protein, MD2 and a specific transmembrane receptor, member of the Toll-Like family, the TLR4 (Lu, 2008). Several proteins are involved in the endotoxin induced signalling pathway. Once in the body, the LPS is extracted and de-aggregated by a serum protein, the LPS binding protein (LBP) and later transferred to a lymphocyte extrinsic membrane glycoprotein, the cluster differentiation antigen 14 (CD14), whose main role is to enhance the sensitivity towards the lipid A, reducing the binging affinity even to picomolar concentrations (Wright, 1990; Tobias, 1995). It is however important to point out that too high concentrations of the LBP and CD14 (soluble and membrane CD14) were demonstrated to inhibit the immune response (Zweigner, 2001; Kitchens, 2001). The myeloid differentiation protein-2 (MD-2) is a small (17kDa) lipid binding protein which plays a pivotal role in the activation process, complexing the N-terminal segment of TLR4 ectodomain. The MD-2 protein possesses two anti-parallel β-sheets which form a hydrophobic pocket accommodating the lipid A (Shimazu, 1999; Kim, 2007; Park, 2009), or more precisely, the acyl chains of the domain.

Thereafter, the appropriate acylation pattern inducing conformational change in the protein is a requirement for the dimerization of the TLR4/MD-2 receptorial complex (Park, 2009; Ohto, 2012). The MD-2 itself is able to bind the LPS and discriminate different lipid As, therefore TLR4, in absence of MD-2, does not recognise the ligand (Shimazu, 1999; Kim, 2007; Park, 2009). The heterodimer formation further induces dimerization of intracellular TIR domains initiating the signaling (Fig 1.8) (Jin & Lee, 2008). TLR4 is the only TLR that is able to transduct the signal through two pathways, namely, utilizing either MyD88 or TRIF adapter. This finally leads to activation of transcription factors like NF-kB or AP-1 from MyD88 and the IFN-β (Figure 1.12.).

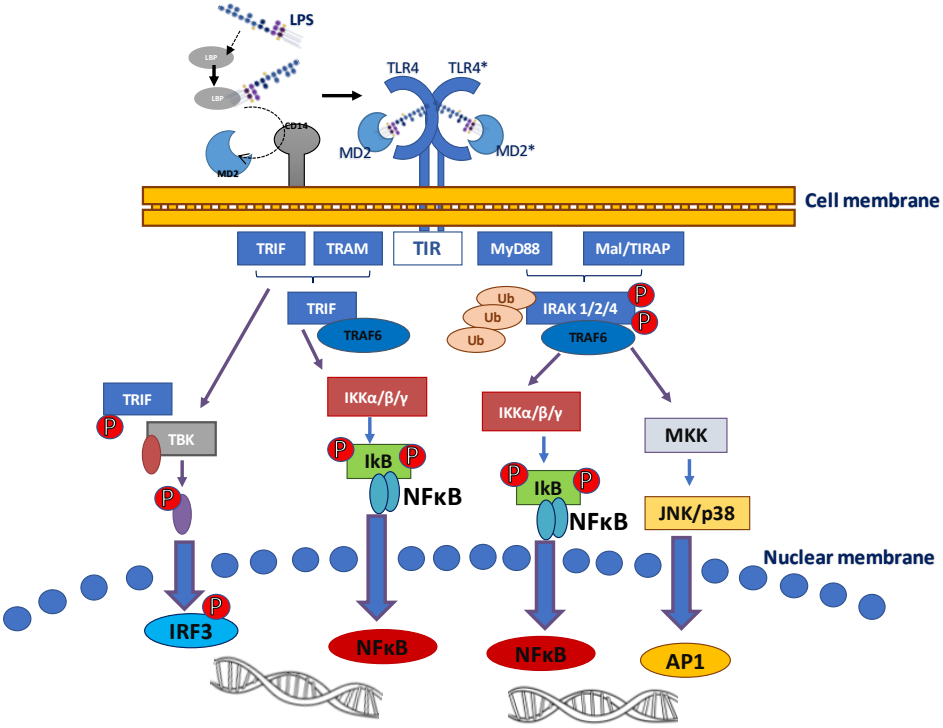

Figure 1.12. Model of LPS signalling

1.8. Modulation of TLR4/MD-2 signalling

The hexa-acylated, asymmetric (4+2) lipid A of *E. coli* LPS is considered as the most potent TLR4/MD-2 agonist. The capacity of various endotoxin to induce or antagonise the synthesis of cytokine and of other

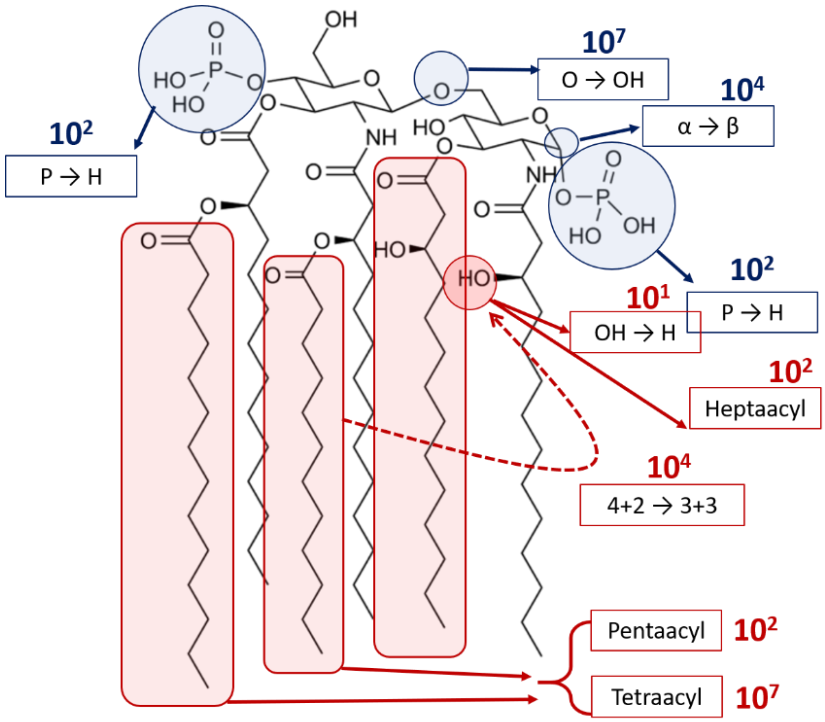

Figure 1.13. Lipid A structure-activity relationship. Indicated chemical changes of the *E. coli* lipid A and factor by which the structure is less active. Blue indications refer to modifications in the polar region, whereas indicated in red – hydrophobic region.

effector molecules is strictly correlated to the primary structure. Structural variations can strongly affect the lipid A potential to induce the TLR4/MD-2 mediated immunological response (Figure 1.13.).

Many structural features including predominantly the number and nature of the acyl chains are considered to modulate the effect upon binding. Lipid A possessing a *bis*-phosphorylated disaccharide backbone with an asymmetric (4+2) distribution of six acyl residues, of which four saturated primary 3-hydroxylated and two secondary non-hydroxylated acyl residues generally of 12-14 carbon atoms in length (as in the case of *E. coli* lipid A, Figure 1.13), represents the most stimulatory agonist

structure for innate immunity in human. Structural variations respect to *E. coli* hexa-acylated lipid A can correspond to less or not agonist active species. *Hypo*-acylated lipid As or symmetrical (3+3) hexa-acylated lipid A, adopting a cylindrical shape (Chapter 1.3.1) are known to act as anatagonists or weak agonists. Furthermore, the activity depends also on the number of phosphate groups, the presence of other decorations or variation in the acylation pattern (Rietschel, 1994; Fox, 2010; Molinaro, 2015).

These strong structure-activity correlation results in the fine tuning of the "agonist properties" of the Lipid A, and results in creation of molecules possessing low immunostimulant properties. A fascinating example is given by Monophosphoryl lipid A® (MPL ®) (Figure 1.14.), which consists of *Salmonella minnesota* lipid A lacking (R)-3-hydroxytetradecanoyl group and the 1-phosphate which possesses low immunostimulatory activities and therefore is used as an anticancer vaccine adjuvant (Cluff, 2010) (see Chapter 1.9). Further modifications in the structure can lead to complete disappearance of the toxic properties and even inhibition of the TLR4/MD-2 activation.

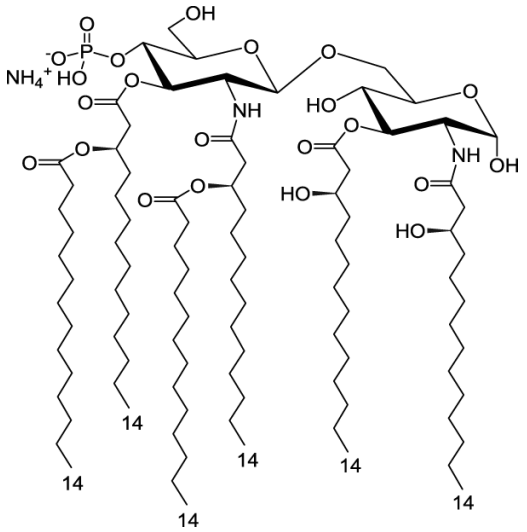

Figure 1.14 The MPL® structure

A well-known TLR4/MD-2 antagonist is a tetra-acylated *E. coli* bio-synthetic precursor, the lipid IVa (Figure 1.15). It was shown that the lipid IVa is able to compete with the toxic LPS for the interaction with the

human TLR4/MD-2, can operate as “antagonist” reducing or, in a dose-dependent manner, completely inhibiting the inflammatory cascade induced by strongly endotoxic lipid A species. Importantly, the molecule acts as a weak agonist in murine TLR4/MD-2 (Saitoh, 2004). Other interesting examples of antagonist lipid A were found in *Rhodobacter capsulatus* (Loppnow, 1990) or *Rhodobacter sphaeroides* (Anwar, 2015) whose structure was an inspiration in antiseptic drug designment (Kim, 2007).

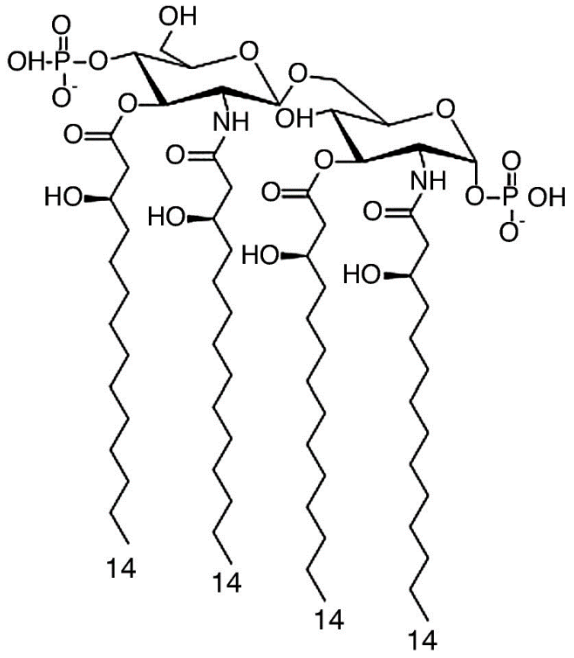

Figure 1.15. Structure of the lipid IVa

1.9 LPS in sepsis and as vaccine adjuvant

The LPS induced activation of innate immune system through the TLR4/MD-2 complex is a beneficial event for the host, which provides a successful first line of defence. However, overstimulation of the system leads to serious, life-threatening effects.

Sepsis is a condition, based on the overwhelmed response of the innate immune system. It is considered as the primary death cause sourcing from infection, especially when not properly treated or

recognized (Singer, 2016). Agonist LPS/lipid A species are able to trigger powerful immune response through TLR4/MD-2 receptor complex, therefore inflammation takes place. When the concentration of the LPS in the body reached high values, systemic inflammatory response syndrome (SIRS) arises. Moreover, as a response to inflammation a contradictory reaction effecting in production of anti-inflammatory cytokines, named Compensatory Anti-Inflammatory Response Syndrome (CARS) occurs. This leads to severe organ dysfunction and finally life-threatening septic shock. Sepsis remains one of the main death reasons among developed countries, furthermore, in the beginning of the century, 45% - 60% of sepsis cases were caused by Gram-negative bacteria (Bone, 1996; McCormick, 2001). Therefore, high demand on new treatment strategies leaded to development of different approaches towards combating the septic cascade. An inspiring example is given by Eritoran (Figure 1.16), antispectic molecule based on a non-toxic lipid A isolated from *Rhodobacter capsulatus*. The drug has shown a significant decrease of TNF-α and IL-6 levels in a randomized controlled trial on individuals challenged with endotoxin. Finally, Eritoran reached phase III of clinical trials (Peri, 2011).

A further lipid A analogue possessing notable applications is the MPL®. The MPL® is a dephosphorylated lipid A obtained from *Salmonalla minnesota* R595, which due to removal of the phosphate groups presents significantly lower toxicity in comparison to the native *Salmonalla minnesota* lipid A (Figure 1.14). This made the compound a promising vaccine adjuvant, administered to various subjects in clinical trials, including allergen immunotherapy.

Allergy is a pathology of the immune system, characterized by a hypersensivity to a substance termed as an allergen which in normal condition is harmless. When the person is sensitized the T helper type 2 cells (Th2) type response, characterized by production of IgE antibodies by B-cells is obtained, which further leads to allergy reaction. The treatment includes allergy immunotherapy (AI) which is based on building immunological tolerance by the patient. After the treatment, immunological system of the patient is modified, therefore instead of IgE release, IgG antibodies which are unable to cause allergic reaction are produced by Th1 pathway. The immunotherapy includes use of pro-Th1

adjuvants, which tend to act as pro-inflammatory agents, being able to trigger immune response.

The agents being possible to use are TLR4/MD-2 ligands, represented by the monophosphoryl lipid A®. Interestingly the tests of MPL® as adjuvant in murine model was successful promoting Th-1 directed responses (Wheeler, 2001; Larsen, 2016). The MPL® is nowadays used in a therapeutic pollen-allergy vaccine, Polinex Quatro®. It is important to point out, that the primary clinical development of the MPL® was concentrated on the potential use of the agent in cancer therapy. For instance, the MPL® is used as an adjuvant in a licensed anticancer vaccine, Melacine® (Fox, 2010). Furthermore, the monophosphoryl lipid A® is also found as a constituent of prophylactic vaccines, including GlaxoSmithKline's (GSK) Fendrix® Cervarix® against hepatitis B and human papilloma virus (HPV) respectively (Fox, 2010). Finally, the MPL® was also combined with other immunostimulants in various adjuvant systems which are in clinical development. For instance, the MPL® in a combination with the saponin QS21 in a liposomal formulation is used as a component of a malaria vaccine which reached phase 3 clinical trials (Lell, 2009). Following the success of the monophosphoryl lipid A® several lipid A based agents are being evaluated for clinical use, like the glucopyranosyl lipid A (GLA), synthetic MPL® derivatives or other *E. coli* lipid A derivatives (Fox, 2010).

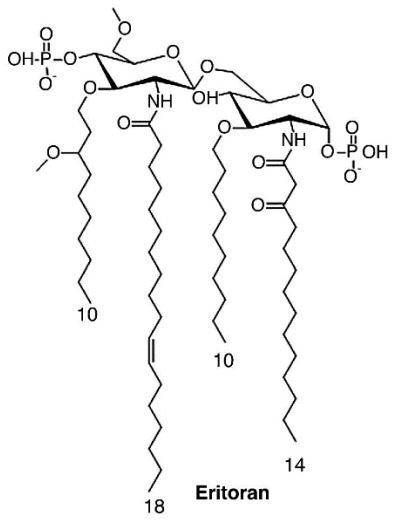

Figure 1.16 Chemical structure of Eritoran.

Aims

The TLR4/MD-2 receptorial complex is a target correlated with broad spectrum of modern-day disorders which still lack specific pharmacological treatment. These include autoimmune disorders, chronic inflammations, asthma, allergies, infectious and central nervous system diseases, and cancer. Thus, throughout last years many efforts were made to find novel, natural or synthetic TLR4/MD-2modulators.

An inspiring example is given by Eritoran, synthetic and well tolerated by humans lipid A mimetic, which acts as TLR4/MD-2 inhibitor. Successfully, the drug reached phase III clinical trials as an antisepsis agent. An inspiration to create such molecule were two natural lipid As isolated from *Rhodobacter sphaeroides* and *R. capsulatus*, phototrophic bacteria found in freshwater or marine environments, which showed agonist activity towards the TLR4/MD-2. On the other hand, compounds able to trigger low immunological response, like the lipid A analogue, MPL® found their role as used nowadays vaccine adjuvants in allergy and cancer therapy or disease prevention. In this context, structural and immunological characterization of the LPS isolated from human non-pathogenic or symbiotic bacteria became an inspiring source of novel, potential TLR4/MD-2 agonists and antagonists. The LPS derived from such bacteria are expected to not induce significant activation of human innate immune system or, even inhibit the signalling caused by agonist LPS. Thus, the main aim of presented work is structural and immunological characterization of new TLR4/MD-2 modulators. An additional goal is to characterize structures and functions of other cell wall glycoconjugates or glycans of these bacteria.

References:

Akira S., Kiyoshi K. (2004) Toll-like receptor signalling, Nature Reviews Immunology, 4, 499–511

Alexander C., Rietschel E.T. (2001) Bacterial lipopolysaccharides and innate immunity. *J. Endotoxin Res.,* 7, 167-202.

Anwar M.A., Panneerselvam S., Shah M., Choi S. (2015) Insights into the species-specific TLR4 signaling mechanism in response to *Rhodobacter sphaeroides* lipid A detection. *Sci. Rep. 5,* e7657.

Ates O. (2015) Systems biology of microbial exopolysaccharides production. *Front. Bioeng. Biotechnol. 3,* e200.

Bone R.C. (1996) The sepsis syndrome. Definition and general approach to management. *Clin. Chest. Med. 17(2),* 175-181.

Brubaker S.W., Bonham K.S., Zanoni I., Kagan J.C. (2015) Innate immune pattern recognition: a cell biological perspective. *Annu. Rev. Immunol. 33,* 257-290.

Campbell N. (2000) Biology: Concepts & Connections. 4th edition. Pearson Education, San Francisco.

Cluff C.W. (2010) Monophosphoryl lipid A (MPL) as an adjuvant for anti-cancer vaccines: clinical results. *Adv. Exp. Med. Biol*. 667, 111-123.

De Soyza A., Silipo A., Lanzetta R., Govan J.R., Molinaro A. (2008) Chemical and biological features of *Burkholderia cepacia* complex lipopolysaccharides. *Innate. Immun. 14,* 127-144.

Di Lorenzo F., Billod J.-M., Martín-Santamaría S., Silipo A., Molinaro A. (2017a) Gram-Negative Extremophile Lipopolysaccharides: Promising Source of Inspiration for a New Generation of Endotoxin Antagonists. *Eur. J. Org. Chem.* 4055-4073.

Di Lorenzo F., Palmigiano A., Al Bitar-Nehme S., Sturiale L., Duda K.A., Gully D., Lanzetta R., Giraud E., Garozzo D., Bernardini M.L., Molinaro A., Silipo A. (2017b) The Lipid A from *Rhodopseudomonas palustris* Strain BisA53 LPS Possesses a Unique Structure and Low Immunostimulant Properties. *Chem. Eur. J. 23,* 3637-3647.

Fox C.B., Friede M., Reed S.G., Ireton G.C. (2010) Synthetic and Natural TLR4 Agonists as Safe and Effective Vaccine Adjuvants. In Sub-cellular biochemistry 53.

Endotoxins: Structure, Function and Recognition (Eds. Wang X., Quinn P.J.). Springer, Dordecht, Heidelberg, London, New York, pp 303 – 322.

Haag A.F., Wehmeier S., Muszyński A., Kerscher B., Fletcher V., Berry S.H., Hold G.L., Carlson R.W., Ferguson G.P. (2011) Biochemical characterization of *Sinorhizobium meliloti* mutants reveals gene products involved in the biosynthesis of the unusual lipid A very long-chain fatty acid. *J. Biol. Chem. 286(20),* 17455-17466.

Hamad M.A., Di Lorenzo F., Molinaro A., Valvano M.A. (2012) Aminoarabinose is essential for lipopolysaccharide export and intrinsic antimicrobial peptide resistance in *Burkholderia cenocepacia*. *Mol. Microbiol. 85(5),* 962-974.

Holst O., Ulmer A.J., Brade H., Flad H.D., Rietschel E.T. (1996) Biochemistry and cell biology of bacterial endotoxins. *FEMS Immunol. Med. Microbial. 16,* 83-104.

Holst, O. (2011) Structure of the lipopolysaccharide core region. In Bacterial Lipopolysaccharides (Eds. Knirel Y.A., Valvano M.A.). Springer-Verlag, Vienna, Austria, pp 21-39.

Isshiki Y., Zähringer U., Kawahara K. (2003) Structure of the core oligosaccharide with a characteristic D-glycero-α-D-talo-oct-2-ulosylonate-(2→4)-3-deoxy-D-manno-oct-2-ulosonate [α -Ko-(2→4)-Kdo] disaccharide in the lipopolysaccharide of *Burkholderia cepacia*. *Carbohydr. Res. 338,* 2659–2666.

Janeway C.A. Jr, Travers P., Walport M., Shlomchik M.J (2001) Immunobiology 5th edition. Garland Science, New York.

Jin M.S., Lee J.O. (2008) Structures of the toll-like receptor family and its ligand complexes. *Immunity 29(2),* 182-191.

Kawahara K., Moll H., Knirel Y.A., Seydel U., Zähringer U. (2000) Structural analysis of two glycosphingolipids from the lipopolysaccharide-lacking bacterium *Sphingomonas capsulate*. *Eur. J. Biochem. 267(6),* 1837-1846.

Kawasaki S., Moriguchi R., Sekiya K., Nakai T., Ono E., Kume K., Kawahara K. (1994) The Cell Envelope Structure of the Lipopolysaccharide-Lacking Gram-Negative Bacterium *Sphingomonas paucimobilis*. *J. Bacteriol.* 176(2), 284-290.

Kim H.M., Park B.S., Kim J.I., Kim S.E., Lee J., Oh S.C., Enkhbayar P., Matsushima N., Lee H., Yoo O.J., Lee J.O. (2007) Crystal structure of the TLR4-MD-2 complex with bound endotoxin antagonist Eritoran. *Cell. 130(5),* 906-917.

Kitchens R.L., Thompson P.A., Viriyakosol S., O'Keefe G.E., Munford R.S. (2001) Plasma CD14 decreases monocyte responses to LPS by transferring cell-bound LPS to plasma lipoproteins. *J. Clin. Invest. 108,* 485-493.

Knirel Y.A. (2011) Structure of O-Antigens. In Bacterial Lipopolysaccharides (Eds. Knirel Y. A., Valvano M. A.). Springer-Verlag, Vienna, Austria pp 41-116.

Kwon K. J., Park K. J., Kim J. D., Kong J. Y., Kong I. S. (1994) Isolation of two different polysaccharides from halophilic *Zoogloea* sp. *Biotechnol. Lett. 16(8),* 783–788.

Larsen J.N., Broge L., Jacobi H. (2016) Allergy immunotherapy: the future of allergy treatment. *Drug Discov. Today. 21(1),* 26-37.

Lell, B., Agnandji, S., von Glasenapp, I., Haertle, S., Oyakhiromen, S., Issifou, S., Vekemans, J., Leach, A., Lievens, M., Dubois, M.C., Demoitie, M.A., Carter, T., Villafana, T., Ballou, W.R., Cohen, J., Kremsner, P.G. (2009) A randomized trial assessing the safety and immunogenicity of AS01 and AS02 adjuvanted RTS,S malaria vaccine candidates in children in Gabon. PLoS ONE, 4, e7611.

Loppnow H., Libby P., Freudenberg M., Krauss J.H., Weckesser J., Mayer H. (1990) Cytokine induction by lipopolysaccharide (LPS) corresponds to lethal toxicity and is inhibited by nontoxic *Rhodobacter capsulatus* LPS*. Infect. Immun. 58 (11),* 3743–3750.

Lu Y.-C., Yeh W.-C., Ohashi P.S. (2008) LPS/TLR4 signal transduction pathway. *Cytokine. 42(2),* 145-151.

McCormick J.K., Yarwoo J.M., Schlievert P.M. (2001) Toxic shock syndrome and bacterial superantigens: an update. *Annu. Rev. Microbiol. 55*, 77–104.

Medzhitov R. (2001) Toll-like receptors and innate immunity. Nature Reviews Immunology, 1, 135–145.

Molinaro A., Holst O., Di Lorenzo F., Callaghan M., Nurisso A., D'Errico G., Zamyatina A., Peri F., Berisio R., Jerala R., Jiménez-Barbero J., Silipo A., Martín-Santamaría S. (2015) Chemistry of Lipid A: At the Heart of Innate Immunity. *Chem. Eur. J. 21,* 500-519.

Mollakhalili Meybodi N., Mohammadifar M. A. (2015) Microbial exopolysaccharides: A review of their function and application in food sciences. *J. Food Qual. Hazards Control. 2(4),* 112–117.

Montminy S.W., Khan N., McGrath S., Walkowicz M.J., Sharp F., Conlon J.E., Fukase K., Kusumoto S., Sweet C., Miyake K., Akira S., Cotter R.J., Goguen J.D., Lien E. (2006) Virulence factors of *Yersinia pestis* are overcome by a strong lipopolysaccharide response. *Nat. Immunol. 7,* 1066-1073.

Nwodo U.U., Green E., Okoh A.I. (2012) Bacterial exopolysaccharides: Functionality and prospects. *Int. J. Mol. Sci. 13(11),* 14002-14015.

Ohto U., Fukase K., Miyake K., Shimizu T. (2012) Structural basis of species-specific endotoxin sensing by innate immune receptor TLR4/MD-2. *Proc. Natl. Acad. Sci. 109,* 7421-7426.

Park B.S., Lee J.O. (2013) Recognition of lipopolysaccharide pattern by TLR4 complexes. *Exp. Mol. Med. 45,* e66.

Park B.S., Song D.H., Kim H.M., Choi B.S., Lee H., Lee J.O. (2009) The structural basis of lipopolysaccharide recognition by the TLR4-MD-2 complex. *Nature. 458,* 1191-1195.

Peri F, Piazza M, Calabrese V, Cighetti R. (2011) Modulation of Lipopolysaccharide Signalling Through TLR4 Agonists and Antagonists. In Bacterial Lipopolysaccharides (Eds. Knirel Y. A., Valvano M. A.). Springer Verlag, Vienna, Austria pp 389-416.

Plötz B.M., Lindner B., Stetter K.O., Holst O. (2000) Characterization of a novel lipid A containing D-galacturonic acid that replaces phosphate residues. The structure of the lipid a of the lipopolysaccharide from the hyperthermophilic bacterium *Aquifex pyrophilus*. *J. Biol. Chem*. 275(15), 11222-11228.

Poli A., Anzelmo G., Nicolaus B. (2010) Bacterial exopolysaccharides from extreme marine habitats: production, characterization and biological activities. *Mar. Drugs. 8(6),* 1779-1802.

Popoff M.Y., Bockemuhl J., Gheesling L.L. (2003) Supplement 2001 (no. 45) to the Kauffmann-White scheme. *Res. Microbiol. 154,* 173–174.

Raetz C.R. (1990) Biochemistry of endotoxins. *Annu. Rev. Biochem. 59,* 129-170.

Raetz C.R., Whitfield C. (2002) Lipopolysaccharide endotoxins. *Annu. Rev. Biochem. 71,* 635–700.

Raven P.H., Johnson G.B. (2011) Biology 9th Edition, Chapter 34 (Ed.: McGraw Hill).

Rietschel E.T., Krikae T., Schade F.U., Mamat U., Schmidt G., Loppnow H., Ulmer A.J., Zahringer U., Seydel U., Di Padova F., Schreier M., Brade H. (1994) Bacterial endotoxin: molecular relationships of structure to activity and function. *FASEB J. 8,* 217-225.

Saitoh S., Akashi S., Yamada T., Tanimura N., Kobayashi M., Konno K., Matsumoto F., Fukase K., Kusumoto S., Nagai Y., Kusumoto Y., Kosugi A., Miyake K. (2004) Lipid A antagonist, lipid IVa, is distinct from lipid A in interaction with Toll-like receptor 4 (TLR4)-MD-2 and ligand-induced TLR4 oligomerization. *Int. Immunol. 16(7),* 961-969.

Seydel U., Labischinski H., Kastowsky M., Brandenburg K. (1993) Phase behavior, supramolecular structure, and molecular conformation of lipopolysaccharide. *Immunobiology. 187(3-5),* 191–211.

Seydel U., Oikawa M., Fukase K., Kusumoto S., Brandenburg K. (2000) Intrinsic conformation of lipid A is responsible for agonistic and antagonistic activity. *Eur. J. Biochem. 267,* 3032-3039.

Shimazu R., Akashi S., Ogata H., Nagai Y., Fukudome K., Miyake K., Kimoto M. (1999) MD-2, a molecule that confers lipopolysaccharide responsiveness on toll-like receptor 4. *J. Exp. Med. 189,* 1777-1782.

Silipo A., De Castro C., Lanzetta R., Parrilli M., Molinaro M. (2010) Lipopolysaccharides. In Prokaryotic cell wall compounds structure and biochemistry (Eds. Konig, H., Herald, C., Varma, A.). Springer-Verlag, Berlin, Germany, pp 133–154.

Silipo A., Molinaro A. (2010) The Diversity of the Core Oligosaccharide. In Sub-cellular biochemistry 53. Endotoxins: Structure, Function and Recognition (Eds. Wang X., Quinn P.J.). Springer, Dordecht, Heidelberg, London, New York, pp. 69-99.

Silipo A., Molinaro A. (2011) Lipid A Structure. In Bacterial Lipopolysaccharides (Eds. Knirel Y.A., Valvano M.A). Springer-Verlag, Vienna, Austria, pp. 1-20.

Silipo A., Vitiello G., Gully D., Sturiale L., Chaintreuil C., Fardoux J., Gargani D., Lee H.I., Kulkarni G., Busset N., Marchetti R., Palmigiano A., Moll H., Engel R., Lanzetta R., Paduano L., Parrilli M., Chang W.S., Holst O., Newman D.K., Garozzo D., D'Errico G., Giraud E., Molinaro A. (2014) Covalently linked hopanoid-lipid A improves outer-membrane resistance of a Bradyrhizobium symbiont of legumes. *Nat. Commun. 5*, e5106.

Singer M., Deutschman C.S., Seymour C.W., Shankar-Hari M., Annane D., Bauer M., Bellomo R., Bernard G.R., Chiche J.D., Coopersmith C.M., Hotchkiss R.S., Levy M.M., Marshall J.C., Martin G.S., Opal S.M., Rubenfeld G.D., van der Poll T., Vincent J.L., Angus D.C. (2016) The Third International Consensus Definitions for Sepsis and Septic Shock (Sepsis-3). *JAMA. 315(8),* 801-810.

Staley J.T., Gunsalus R.P., Lory S., Perry J.J. (2007) Microbial Life 2nd Edition, chapter 4. Sinauer Associates, Inc., Sunderland.

Stenutz R., Weintraub A., Widmalm G. (2006) The structures of Escherichia coli O-polysaccharide antigens. *FEMS Microbiol. Rev. 30,* 382–403.

Telepnev M.V., Klimpel G.R., Haithcoat J., Knirel Y.A., Anisimov A.P., Motin V.L. (2009) Tetraacylated lipopolysaccharide of *Yersinia pestis* can inhibit multiple

Toll-like receptormediated signaling pathways in human dendritic cells. *J. Infect. Dis. 200,* 1694-1702.

Tobias P.S., Soldau K., Gegner J.A., Mintz D., Ulevitch R.J. (1995) Lipopolysaccharide binding protein-mediated complexation of lipopolysaccharide with soluble CD14. J. *Biol. Chem. 270,* 10482-10488.

Tytgat H.L., Lebeer S. (2014) The sweet tooth of bacteria: common themes in bacterial glycoconjugates*. Microbiol. Mol. Biol. Rev. 78(3),* 372-417.

Vinogradov, E., Korenevsky, A., Beveridge, T.J. (2003) The structure of the rough-type lipooligosaccharide from Shewanella oneidensis MR-1, containing 8-amino-8-deoxy-Kdo and an open-chain form of 2-acetamido-2-deoxy-D-galactose. *Carbohydr. Res. 338,* 1991–1997.

Vinogradov, E., Korenevsky, A., Beveridge, T.J. (2004) The structure of the core region of the lipopolysaccharide from Shewanella algae BrY, containing 8-amino-3,8-dideoxy-D-manno-oct-2-ulosonic acid. *Carbohydr. Res. 339,* 737–740.

Vollmer W., Blanot D., de Pedro M.A. (2008) Peptidoglycan structure and architecture. *FEMS Microbiol. Rev. 32,* 149-167.

Wheeler A.W., Marshall J.S., Ulrich J.T. (2001) A Th1-inducing adjuvant, MPL, enhances antibody profiles in experimental animals suggesting it has the potential to improve the efficacy of allergy vaccines. Int. Arch. *Allergy Immunol. 126(2),* 135-139.

Whitman W.B., Coleman D.C., Wiebe W.J. (1998) Prokaryotes: The unseen majority. *PNAS. 95(12),* 6578-6583.

Wright S.D., Ramos R.A., Tobias P.S., Ulevitch R.J., Mathison J.C. (1990) CD14, a receptor for complexes of lipopolysaccharide (LPS) and LPS binding protein. *Science 249,* 1431-1433.

Yang D.C., Blair K.M., Salama N.R. (2016) Staying in Shape: The Impact of Cell Shape on Bacterial Survival in Diverse Environments. *Microbiol. Mol. Biol. Rev. 80 (1),* 187–203.

Zweigner J., Gramm H.J., Singer O.C., Wegscheider K., Schumann R.R. (2001) High concentrations of lipopolysaccharide-binding protein in serum of patients with severe sepsis or septic shock inhibit the lipopolysaccharide response in human monocytes. *Blood, 98,* 3800-3808.

Chapter II

Elucidation of LPS and LOS structure

2.1. Isolation and purification

The first step towards of LPS/LOS structural elucidation is the isolation of components from intact bacterial cells. This goal is achieved using two complementary extraction techniques, which lead to selective isolation of the R-LPS and S-LPS, obviously basing on differences in hydrophobic/hydrophilic character of molecule. Although all of the LPSs possess amphiphilic nature, the presence of the O-antigen significantly increases hydrophilic character of the molecule, therefore S-LPS tends to be extracted rather by aqueous solutions, whereas the LOS lacking the OPS is known to possess higher lipophilic character, hence is more likely isolated with low-polar mixtures.

The isolation process often starts with a pre-extraction step, undertaken in order to remove all cell contaminant. This includes washing the intact cell pellet with solvents as water, ethanol and acetone. Then, the sample undergoes R-LPS specific extraction with petroleum-chloroform-phenol (PCP) (Galanos, 1969). The protocol includes treatment of the lyophilised cells with solution of petroleum/chloroform/phenol (8:5:2), removal of volatile solvents and precipitation of the LOS with water. Remaining cells undergo hot phenol-water extraction to extract S-LPS. This includes treatment of the pellet with phenol water (1:1) solution at 68°C (Westphal & Jann, 1965). The procedure results in the presence of two separate phases which undergo extensive steps of dialysis. Due to its hydrophilic character, the S-LPS is typically present in the water phase, nonetheless several factors including the length of the O-chain, presence of nonpolar groups and charged monosaccharides can significantly affect the solubility of the LPS in water, hence it can be also found in the phenol phase.

The purification steps include use of enzymes, which hydrolyse coextracted proteins and nucleic acids, followed by extensive dialysis. The LPS is detected by performing the sodium dodecyl sulphate–polyacrylamide gel electrophoresis (SDS-PAGE) or sodium deoxycholate-polyacrylamide gel electrophoresis (DOC-PAGE) electrophoresis followed by silver nitrate staining (Kittelberger & Hilbink, 1993). The presence of S-LPS is unveiled by occurrence of a typical ladder-like pattern in the higher part of the migration lane, observed due to size heterogenicity of the O-antigen, characterized by presence of different number of repeating units;

the LOS shows instead a single band at the lower part of the gel, arising from its low molecular weight. The extracted LPS and LOS undergo further purification steps, like size exclusion chromatography.

2.2 Degradation and derivatization techniques

Once a pure LPS/LOS is obtained, the amphiphilic character of the LPS leading to micelle formation is a main difficulty in terms of the structural investigations. Therefore, several degradation techniques were developed in order to overcome this obstacle.

2.2.1 Degradation techniques

The most commonly used degradation technique relies on highly acid-labile ketosidic linkage between the Kdo and non-reducing GlcN of the lipid A. This is due to the lack of any electron withdrawing group, adjacent to anomeric position of Kdo (it's C-3, as C-2 in case of Kdo) which favours the formation of the reaction intermediate carbocation. Furthermore, during the formation of oxonium ion, a passage from chair into half-chair conformation occurs, which is fastened by presence of non-substituted carbons, and finally the presence of a hydroxyl group in axial position of C-5 causes a steric energy release in the formation of carbocation intermediate.

The hydrolysis is performed in mild acidic conditions, namely acetate buffer at pH 4.4 or 1% acetic acid solution, which is sufficient to selectively cleave the ketosidic linkage. The usage of this technique leads to separation of highly hydrophobic lipid A fraction from the water-soluble saccharide moiety which can be further recovered using liquid-liquid extraction (Blight & Dyer, 1956) or simple centrifugation. The main advantage of this technique is isolation of lipid A and the core OS-O-polysaccharide fractions and high simplicity of the protocol. On the other hand, the main disadvantage of the method is formation of microheterogenicity of the reducing Kdo residue (formation of α and β, furanose and pyranose forms) hindering the NMR analysis of the core OS and removal of other highly acid-labile substituents or hydrolysis of other ketosidic linkages if present.

Therefore, alkaline treatment is also widely used. The method comprises of two steps leading to the full de-acylation of LPS/LOS. First, a mild hydrazinolysis in anhydrous conditions is performed in order to remove the ester linked fatty-acids. The reaction is followed with strong alkaline hydrolysis (4M KOH) that leads to deletion of the amide-linked fatty acids. It is worth to point out that both, mild acidic hydrolysis and full-deacylation techniques can be used complementary, thereby the possible presence and position of acid- and base-labile constituents can be easily determined.

2.2.2. Derivatization techniques

Chemical analyses are necessary to obtain important preliminary information about primary structure of poly/oligosaccharides in terms of chemical composition of the molecule (sugar residues and fatty acids), including the absolute configuration of the monosaccharides and their linkage. Volatile, non-polar derivatives are produced which undergo analysis with gas chromatography coupled with mass spectrometry (GC-MS). The main derivatization used in LPS, glycolipid, carbohydrate and lipid analysis are described below.

Acetylated methyl glycosides

One of the most important method providing significant preliminary information is conversion of polysaccharides into acetylated *O*-methyl glycosides (MGA). The molecule undergoes solvolysis (methanolysis) with anhydrous HCl/MeOH solution, leading to formation of *O*-methyl glycoside of each monosaccharide present in the molecule. The second step includes acetylation with anhydrous acetic anhydride (Ac_2O) in pyridine (Pyr) which leads to formation of per-acetylated methyl glycosides, analysable using GC-MS (Figure 2.1). The products are identified on the basis of retention time from the GC analysis and fragmentation pattern from electron impact MS (EI-MS).

The method provides a fast and reliable method for preliminary LPS composition analysis. It is important to point out that the acidic methanolysis leads to formation of a mixture glycosides which can differ in the terms of ring size and configuration at the anomeric centre (α and β; pyranose and furanose form), nonetheless it does not significantly

influence the analysis. The acetylated *O*-methyl glycosides are then injected to GC and identified by comparison with standard or to GC-MS and identified by the fragmentation pattern and the retention time.

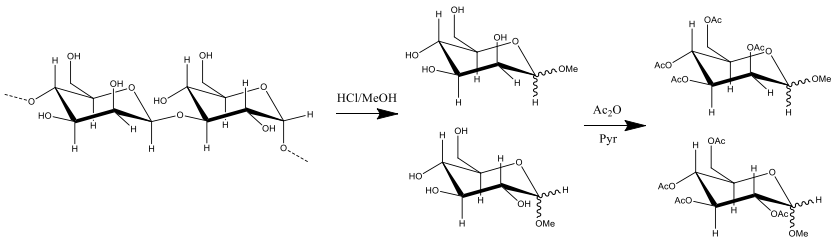

Figure 2.1 Scheme of the reactions taking place during derivatization of a glycan into the corresponding Acetylated Methyl Glycosides (MGA)

Acetylated alditols

Another technique widely used to characterize the sugar composition includes derivation of sugar residues into acetylated alditols (AA). In this protocol the poly/oligosaccharide is hydrolyzed with trifluoroacetic acid followed by reduction of monosaccharides with $NaBH_4$ and acetylationforming an alditol corresponding to every monosaccharide. Finally, the products are acetylated with Ac_2O and Pyr and injected to GC (Figure 2.2). The identification of each monosaccharide undergoes by comparison with standards. Derivatization to acetylated alditols provides a single peak of each monosaccharide, hence the technique can be effectively used to quantify all residues using an internal standard.

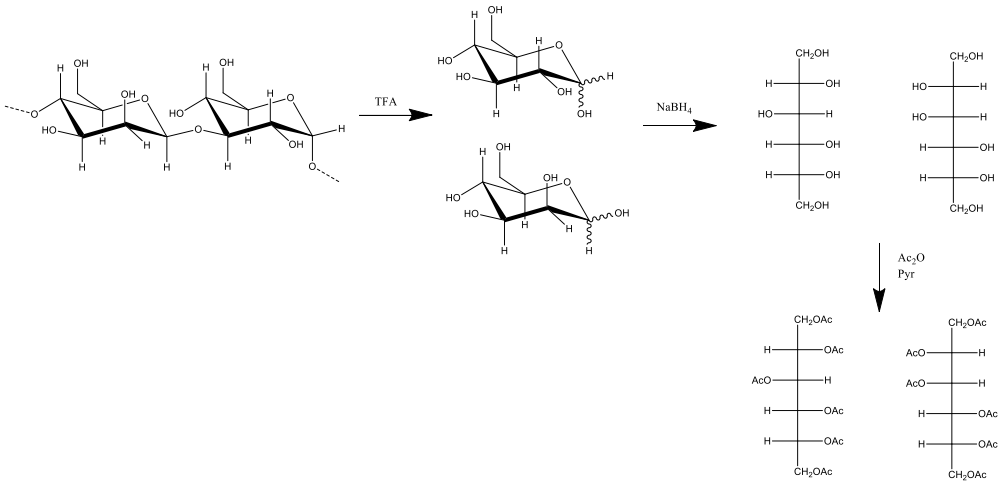

Figure 2.2 Scheme of the reactions taking place during derivatization of a glycan into the corresponding Acetylated Alditol (AA)

Octyl/buthyl glycosides

Derivatization with enantiomerically pure 2-(+)-octanol or 2-(-)-butanol is used to identify the absolute configuration of monosaccharides. They are derivatized as peracetylated 2-(+)-octyl-glycosides and injected to GC-MS and compared with standards of known absolute configuration. The comparison of retention time of the "unknown" acetyl 2-(+)-octyl glycoside (or acetyl 2-(-)-octyl/buthyl glycoside) with one of corresponding racemically pure standard of either D or L 2-(+)-octyl glycoside (or acetyl 2-(-)-octyl/buthyl glycoside if used) and 2-(±)-octyl glycoside (Leontein & Lönngren, 1978) allow the identification of the absolute configuration of the unknown monosaccharide.

Partially methylated alditol acetates

Derivatization of the polysaccharide into partially methylated alditol acetates (PMAA) yields in information on substitution of every monosaccharide and the ring size. This procedure consists in a complete methylation of polysaccharide and successive hydrolysis, reduction with $NaBD_4$, and acetylation (Figure 2.3). The products are separated on a GC column, whereas the analysis of EI-MS spectra provides all information needed to assign the structure of derivatization products. The fragmentation patterns are highly specific to all acetyl and methoxy

groups (Figure 2.3). This is due to selective cleavage of the bond where methyloxy group is engaged, maintaining the positive charge because of resonance effects (Ciucanu & Kerek, 1984). The position of the acetyl groups in the fragments accounts for the attachment point or for the position of ciclyzation of the pyranose or furanose ring. The methyl groups correspond to free positions, not involved in linkages. The reduction of the carbonilic function with sodium borodeuteride discriminates the fragments originated from the reduced position (even masses) form those originated from the last position (odd masses).

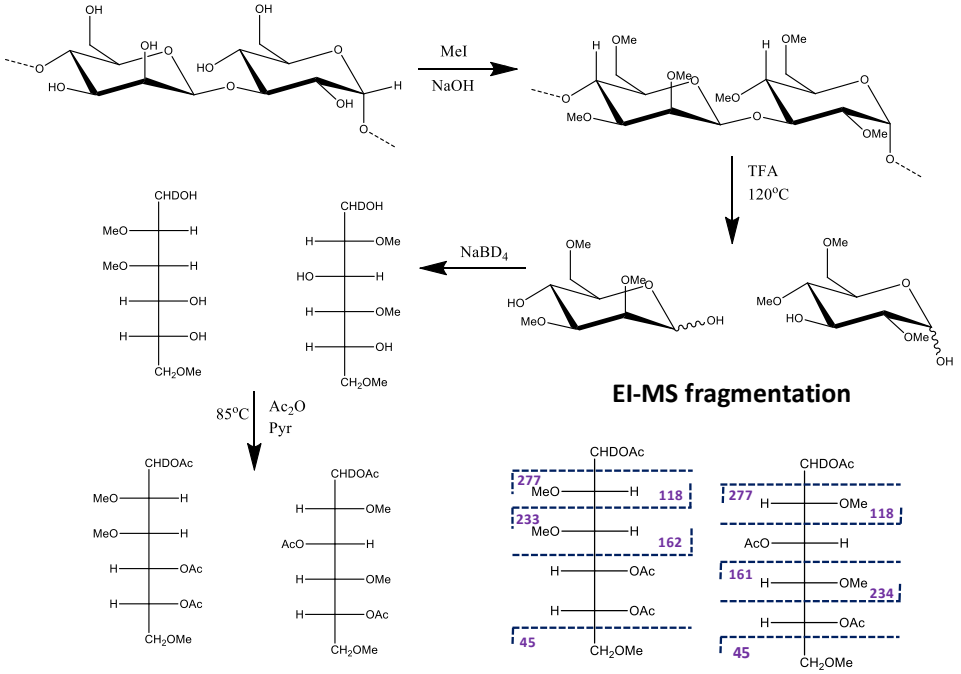

Figure 2.3 Scheme of the reactions taking place during derivatization of a glycan into the corresponding Partially Methylated Alditol Acetates (PMAA). At the bottom an example of primary ions obtained with EI-MS fragmentation.

Fatty acid analysis

The fatty acids composition can be determined by producing fatty acid methyl esters. The sample is treated with HCl, therefore neutralised with NaOH and further treated in highly alkaline conditions. Liberated fatty acids are extracted with chloroform from the solution driven into acidic (pH = 3) environment. Further step is methylation with use of diazomethane and analysis of the products with GC-MS. The quantification is possible using internal standard method. Selectively *O*-

linked fatty acid can be liberated using alkaline treatment, permitting calculation of the quantity of *N*-linked and *O*-linked acyl chains. Moreover, absolute configuration of fatty acids can be further elucidated using method developed by Rietschel (1976).

2.3 Spectral techniques in LPS structural elucidation

The final structural assignments of all LPS components, EPS and any type of glycolipids is performed using a combination of other spectral methods including Nuclear Magnetic Resonance Spectroscopy (NMR) and mass spectrometry, namely Matrix Associated Laser Desorption Ionisation – Time Of Flight (MALDI-TOF), electrospray (ESI-MS) and tandem mass spectrometry (MS^2). Application of these techniques is key in determining the structure of a polysaccharide and the lipid A (and other glycolipids).

2.3.1 Nuclear magnetic resonance

The liquid state NMR is a powerful tool in the field of structural elucidation of carbohydrates, providing information on native samples, not reachable with use of other techniques. This includes type, configuration and ring size of the monosaccharides, their sequence including the branching points and substitutions of other, non-carbohydrate substituents. The NMR study of carbohydrate includes observation of different nuclei, including ^{1}H; ^{13}C and ^{31}P. The analysis includes characterization of mono-dimensional so as bi-dimensional, homo- and heteronuclear spectra.

A typical monodimensional ^{1}H NMR spectrum consists of three distinguishable regions, including:

- Anomeric proton signal region 5.5 – 4.5 ppm
- Ring proton signals 4.5 – 3.0 ppm
- Deoxy and acetyl proton signals 2.5 – 1.0 ppm

Therefore, also ^{13}C NMR spectrum consists of different regions, including:

- Anomeric carbon signals – 110 – 90 ppm
- Ring carbon signals – 90 – 60 ppm
- Nitrogen linked carbon signals 60 – 45 ppm

- Aliphatic methylene carbon signals - ~ 30 ppm
- Methylene carbon of 6-deoxy sugars – 20 – 15 ppm

Full structural characterization comprises use of bi-dimensional techniques. The key step is assignment of all ^{1}H and ^{13}C chemical shifts; characterization of spin systems and assignation of all proton signal among them is done on the basis of Total Correlation Spectroscopy (TOCSY) and Correlation Spectroscopy (COSY). Furthermore, assignment of ^{13}C resonances is done using Heteronuclear Single Quantum Coherence (HSQC spectra). As for the anomeric configuration, α-configured pyranose sugar residues resonate up-field at 5.6 – 4.9 ppm, whereas those involved in β-glycosidic linkage at 4.7 – 4.3 ppm. On the other hand, carbon resonances possess high chemical shifts in case of β anomers (105 – 103 ppm) and low chemical shift in case of α-anomers (101 – 95 ppm). Furthermore, key is the use of $^{3}J_{H,H}$ couplings following the Karpulus law. The coupling constants between vicinal protons is correlated to the dihedral angle, hence high $^{3}J_{H,H}$ (8 – 10 Hz) are diagnostic for trans-diaxial orientation of the protons whereas low $^{3}J_{H,H}$ (<4 Hz) is characteristic for equatorial/axial orientation. Heteronuclear coupling constants between anomeric proton and carbon $^{1}J_{C1,H1}$ are also fundamental in the definition of the anomeric configuration. In pyranose rings, $^{1}J_{C1,H1}$ above 170 Hz corresponds to α-anomers, whereas $^{1}J_{C1,H1}$ below 170 Hz is characteristic for β-anomers.

Other meaningful parameter in designation of the configuration are *intra*-residual NOE contacts, assigned on the basis of Nuclear Overhauser Enhancement Spectroscopy (NOESY) and Rotating Frame Overhauser Enhancement Spectroscopy (ROESY), experiments that correlate spacially close protons. Strong NOE correlations between H1, H3 and H5 are diagnostic for β-*gluco*-configuration, whereas for α-*gluco*-configuration the only NOE contact is between H1 and H2. Observation of NOE is also a very useful tool in designation of monosaccharide sequence. Presence of *inter*-residual correlations of the anomeric position with neighborhood protons are indicative for presence of glycosidic bond.

The positions of glycosidations are characterized by strong downfield shift in carbon resonance up to 10 ppm for involved nuclei and 1 – 2 ppm upfield for adjacent carbon nuclei. Finally, long range *inter*-residual correlations found on the Heteronuclear Multiple Bond Correlation

spectra ($^{1}H^{13}C$ HMBC) are used to undeniably characterize the nuclei involved in binding. It is also worth to mention that strong HMBC correlations of H1/C1 with C5/H5 are diagnostic for pyranose ring, whereas strong contacts between H1/C1 and C4/H4 for furanose residues. If present, the phosphorylation site is determined by $^{1}H^{31}P$ HSQC spectra.

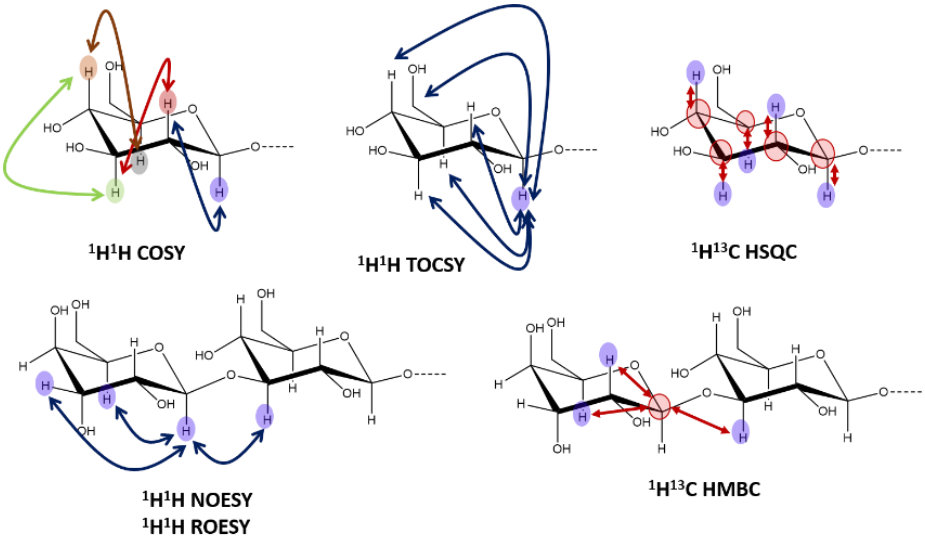

Figure 2.4. Schematic representation of nuclei involved in the main NMR techniques used in carbodydrate analysis. Arrows indicate observed correlations

2.3.2. Mass spectrometry

Mass spectrometry has become a powerful complementary method for structural analysis of lipopolysaccharides and lipooligosaccharides especially with the development of soft ionization techniques like MALDI (Matrix Assisted Laser Desorption Ionisation), ESI (ElectroSpray Ionisation), and the fragment analysis in MS^2 experiments. The MALDI and ESI techniques show high sensitivity also at relatively high molecular mass and provides good spectra of intact molecular ions of lipopolysaccharides.

Oligo/polysaccharide analysis

The use of mild MS techniques brings an invaluable, additional information, to the analysis of 1D and 2D NMR spectra. Usually, for

carbohydrates, MALDI- and ESI MS spectra are performed in negative ion mode, due to the presence of the hydroxyl groups that can lose a proton and acquire a negative charge; nevertheless, spectra in positive ion mode are also performed. The use of MALDI-TOF spectrometry gives a clear view on the presence of various glycoforms and their composition along with presence of non-saccharidic substituents. Furthermore, the use of MS^2 experiments permits us to obtain further important information on residue sequence and positions of non-carbohydrate substituents. General scheme of fragments obtained applying MS^2 on saccharides is presented on figure 2.5 (Domon & Costello, 1988; Mechref, 2003; Bauer, 2012).

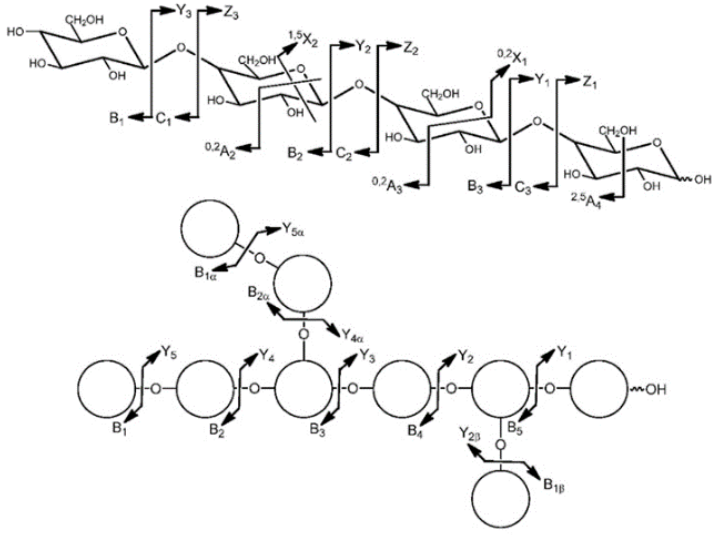

Figure 2.5. Main fragment ions formed applying MS^2 (Bauer, 2012)

MALDI-TOF and MS^2 may be used on any type of oligo/polysaccharide. This makes the technique significantly valuable in core region analysis. Furthermore, also techniques on intact LPS/LOS MALDI-TOF analysis were developed. Treating LOS with MALDI ionization leads to cleavage of labile Kdo linkage, and as a result formation of three groups of peaks on the mass spectrum including lipid A peaks, core OS peaks and intact LOS signals (Sturiale, 2005). The method is of great significance, as it provides a picture of the intact molecule, thus no information is lost by during chemical treatment of the molecule. Moreover, application of this technique to S-LPS analysis can bring

information about molecular weight of the repeating unit due to the molecular weight dispersion characteristic for this type of lipopolysaccharide.

Lipid A analysis

A key approach in structural elucidation is MALDI-TOF and/or ESI-MS along with MS^2 analysis. Analysis of the data gives insights on the lipid A constitution, the number of species and compositional differences between them, and therefore also the distribution of the acyl chains on lipid A skeleton and position of other substituents. Classically the analysis is performed on the lipid A obtained from the mild acid hydrolysis, nonetheless new techniques were developed permitting structural investigations on lipid A microextracted directly from the cell pellet (Larrouy-Maumus, 2016). This gives an opportunity to screen the native molecule features, without applying any chemical modifications. The initial information obtained by MS is composition and distribution of lipid A species, also based on chemical analysis of fatty acid methyl esters (Chapter 2.2.2.).

Further use of tandem mass spectrometry allows us to obtain further structural information based on the fragmentation pattern of the molecule. Positive ion MALDI MS induce cleavage of GlcN backbone, resulting in selective formation of the oxonium ion relative to the non-reducing GlcN unit (Domon & Costello, 1988). Thus, positive ion MALDI carry information significantly helping to elucidate the asymmetric distribution of the acyl chains. The application of mild *O*-deacylation modifications including hydrazinolysis (Holst, 2000) or NH_4OH treatment can be also used for further structural investigation (Silipo, 2002). The ammonium treatment selectively hydrolyse ester linked acyloxyacyl grups, while the amide linked acyloxyacyl groups remain untouched. The spectra are typically recorded in the negative mode, nonetheless also information may be obtained using positive mode.

References:

Bauer S. (2012) Mass Spectrometry for Characterizing Plant Cell Wall Polysaccharides. *Front. Plant. Sci. 3*, 45.

Bligh E.G., Dyer W.J. (1959) A rapid method for total lipid extraction and purification. *Can. J. Biochem. Physiol. 37,* 911-917.

Ciucanu, I., Kerek, F. (1984) A simple and rapid method for the permethylation of carbohydrates. *Carbohydr. Res. 131,* 209–217.

Domon B., Costello C.E. (1988) Structure elucidation of glycosphingolipids and gangliosides using high-performance tandem mass spectrometry. *Biochemistry. 27(5),* 1534-1543.

Galanos C., Luderitz O., Westphal O. (1969) A new method for the extraction of R lipopolysaccharides. *Eur. J. Biochem*. *9*, 245-249.

Holst O. (2000) Deacylation of lipopolysaccharides and isolation of oligosaccharide phosphates. *Methods Mol. Biol. 145,* 345 -353.

Kittelberger R., Hilbink F. (1993) Sensitive silver-staining detection of bacterial lipopolysaccharides in polyacrylamide gels. *J. Biochem. Biophys. Methods*. *26(1),* 81-86.

Larrouy-Maumus G., Clements A., Filloux A., McCarthy R.R., Mostowy S. (2016) Direct detection of lipid A on intact Gram-negative bacteria by MALDI-TOF mass spectrometry. *J. Microbiol. Methods. 120,* 68-71.

Leontein K., Lönngren J. (1978) Determination of the absolute configuration of sugars by Gas-Liquid Chromatography of their acetylated 2-octyl glycosides. *Methods Carbohydr. Chem. 62,* 359-362.

Mechref Y., Novotny M.V., Krishnan C. (2003) Structural Characterization of Oligosaccharides Using Maldi-TOF/TOF Tandem Mass Spectrometry, *Anal. Chem. 75(18),* 4895–4903.

Rietschel E. T. (1976) Absolute configuration of 3-Hydroxy fatty acid present in lipopolysaccharides from various bacterial groups. *Eur. J. Biochem. 64*, 423-428.

Silipo A., Lanzetta R., Amoresano A., Parrilli M., Molinaro A. (2002) Ammonium hydroxide hydrolysis: a valuable support in the MALDI-TOF mass spectrometry analysis of Lipid A fatty acid distribution*. J. Lipid Res. 43,* 2188-2195.

Sturiale L., Garozzo D., Silipo A., Lanzetta R., Parrilli M., Molinaro A. (2005) New conditions for matrix-assisted laser desorption/ionization mass spectrometry of

native bacterial R-type lipopolysaccharides. *Rapid Commun. Mass Spectrom. 19*, 1829-1834.

Westphal O., Jann K. (1965) Bacterial lipopolysaccharides: extraction with phenol-water and further applications of the procedure. *Methods Carbohydr. Chem*. *5*, 83-91.

SECTION II

Structural, immunological and functional characterization of bacterial cell wall components

Chapter III

Acetobacter pasteurianus CIP103108

Premise

Gram-negative bacteria can be found used within human activities as production and processing of traditional foods and beverages, in biotechnology and genetic engineering, in the production of pharmaceuticals (Doyle, 2013). An interesting example is given by a member of *Alphaproteobacteria*, an acetic acid-producing bacterium commonly found associated with plants and plant products and present on sugar-rich substrates such as fruits, flowers and vegetables. The microbe is also commonly involved in the process of wine spoilage during the ageing. The most notable feature of *A. pasteurianus* is its capability to oxidize any alcohol or sugar into the corresponding organic acid, including mostly demanded conversion of ethanol into acetic acid. Moreover, the microbe shows significant resistance to ethanolic environment (Sengun & Karabiyikli, 2011; Yamada & Yukphan, 2008).

Acetobacter pasteurianus is used in the production of fermented foods including kefir or vinegar (Nanda, 2001), but essentially of the Japanese black rice vinegar, *kurozu*, manufactured using a range of microorganisms, including *Aspergillus oryzae,* responsible for saccharification of rice, the sugar fermenting *Saccharomyces cerevisiae* , lactic acid bacteria (Hashimoto, 2017). The consumption of *kurozu* is known to carry significant health benefits including radical scavenging activity (Shimoji, 2002), inhibition of cancer cell proliferation (Nanda, 2004) or the development of colonic aberrant crypt foci (Shimoji, 2003) and it is believed to relieve hypertension (Hashimoto, 2013). Moreover, Hashimoto et al. (2013) reported that freeze-dried *kurozu* is able to stimulate the innate immune system via TLR2 and TLR4 activation, therefore it is hypothesized that some health benefits may derive from bacterial cell components, remaining in the vinegar after the production process. Thus, structural and biological characterization of potential immunoactive bacterial cell envelope compounds such as LPS from *Acetobacter pasteurianus* may shat a light on the health beneficial properties of the vinegar.

3.1 Isolation of the cell wall components

The cell wall components of *Acetobacter pasteurianus* CIP 103108 were isolated applying the hot phenol-water method (Westphal, 1965), preceded by extensive steps of purification with water, ethanol and acetone. The isolated fraction was further purified applying a step of enzymatic digestion followed by extensive dialysis and ultracentrifugation. DOC-PAGE analysis revealed the presence of a mixture of R-type and S-type LPS in the extract. Purification steps, including enzymatic digestion followed by size exclusion chromatography in denaturing conditions, (0,25% DOC) monitored by SDS-PAGE electrophoresis (Figure 3.1.) and ^{1}H NMR (Figure 3.2) allowed to isolate S-type LPS and R-type LPS (Figure 3.2). The lanes corresponding to the eluted fractions showed a clear staining at the higher part of the gel (F2, LPS) whereas the lane corresponding to the last eluted fraction showed exclusive staining at the lower part (F3, LOS). The result was confirmed by

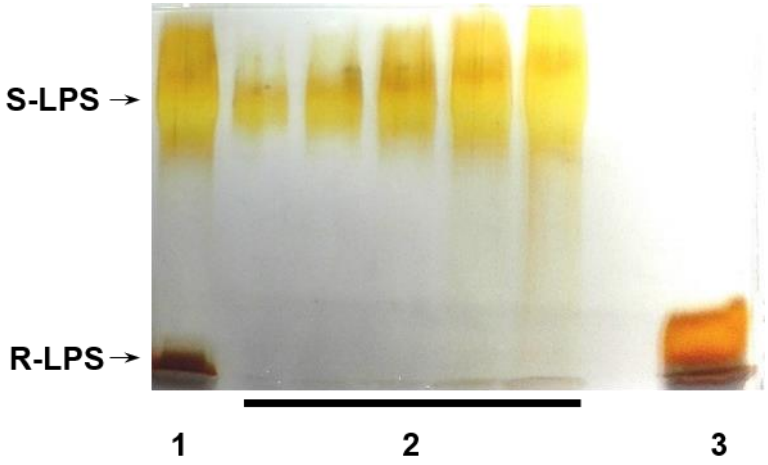

Figure 3.1 Silver-stained SDS-PAGE gel of fraction obtained applying Sephacryl S-200 column under denaturating conditions. 1) Native water phase 2) Fraction “F2” containing S-LPS 3) Fraction “3” containing R-LPS

^{1}H NMR, as they suggested presence of the S-LPS and LOS (R-LPS) separately. Both fractions underwent further structural analyses.

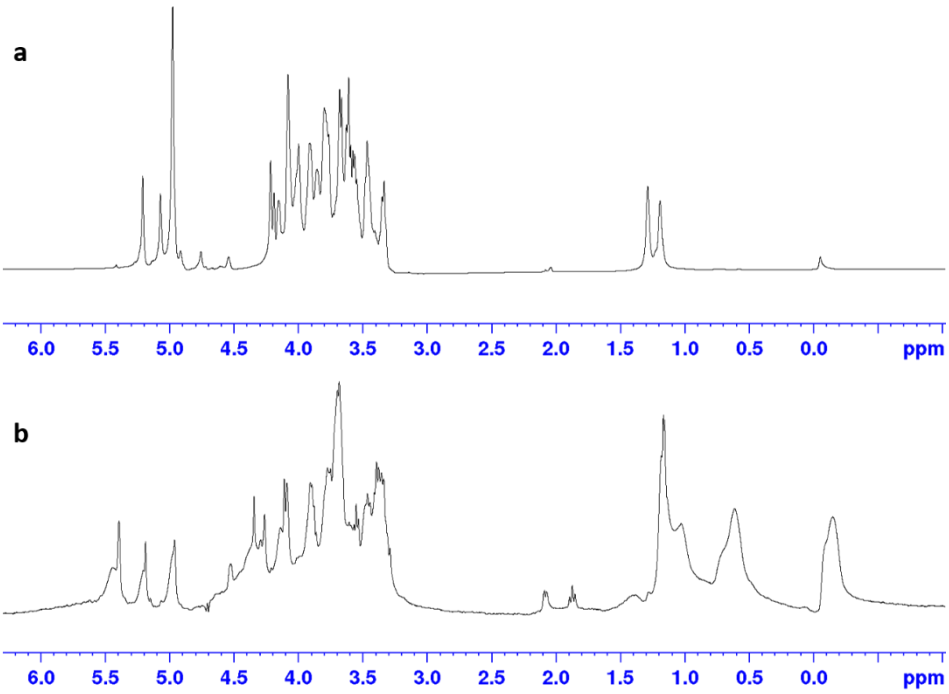

Figure 3.2 ^{1}H NMR spectra of fractions obtained by applying S-200 column in denaturating conditions a) Fraction "2" containing the S-LPS b) Fraction "3" containing R-LPS

3.2. Chemical characterization of *Acetobacter pasteurianus* cell wall components

The fraction containing the S-type LPS underwent extensive steps of qualitative and quantitative analysis. The monosaccharide content was determined on the basis of acetylated *O*-methyl glycoside method and acetylated alditols. The quantity of each neutral sugar and uronic acid was calculated deriving all residues to acetylated alditols and using Xyl as the internal standard. The aminosugars were identified applying strong hydrolysis conditions while the ulosonic acids were identified upon derivatization to acetylated *O*-methyl glycosides and GC-MS analysis. Finally, the absolute configuration was determined with the octyl-glycoside method. The results of full chemical analysis of *A. pasteurianus*

sugar residues is summarized in the Table 3.1. The linkage analysis (Ciucanu & Kerek, 1984) revealed presence of 2,4-disubstituted Rha*p*, 2-substituted Rha*p*, 2-substituted Man*p*, 6-substituted Glc*p*, terminal Glc*p*, 3-substituted Gal*f*, 2,6-disubstituted Gal*f*.

The fatty acids were quantified using 17:0 as a standard and derivatized to fatty acid methyl esters. Selective hydrolysis of *O*-linked acyl chains revealed that only 18:0(3-OH) was attached to the lipid A via amide linkage, whereas 14:0 (3-OH) and 16:0 were linked through ester bound (De Castro, 2010). The detailed composition of the fatty acids is summarized in Table 3.1.

Table 3.1 Composition of the S-LPS fraction

Monosaccharides	**Concentration [nmol/mg]**	
L-rhamnose (Rha)	800	
D-mannose (Man)	103	
D-Glucose (Glc)	1479	
D-Galactose (Gal)	1685	
3-deoxy-D-*manno*-oct-2-ulosonic acid (Kdo)	NQ	
D-*glycero*-D-*talo*-oct-2-ulosonic acid (Ko)	NQ	
D-glucuronic acid (GlcA)	91	
D-glucosamine (GlcN)	NQ	
2,3-diamino-2-3-dideoxy-D-glucose (DAG)	NQ	
Total fatty acids	**Total [nmol/mg]**	**Ester [nmol/mg]**
3OH-14:0	65	11
16:0	89	31
18:0	54	0
3OH-18:0	52	0

NQ – not quantified; tr – trace quantities

The sugar compositional analysis performed on the R-LPS containing fraction revealed presence of Rha, GlcA, Glc, GlcN, DAG, Kdo and Ko. Moreover, the linkage analysis performed with Ciucanu-Kereks

(1984) method unveiled 3-substituted-Rha*p*, terminal-Glc*p*, 5,7,8-substituted Kdo*p* and 8-substituted Ko*p* (Figure 1.3).

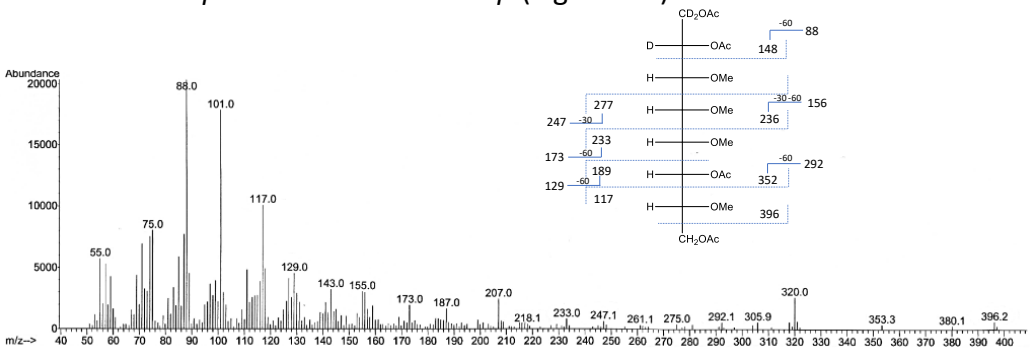

Figure 3.3. The EI-MS fragmentation pattern of 8-substituted-Ko*p* PMAA derivative

3.3 Isolation and purification of the OPS and lipid A.

In order to isolate the O-polysaccharide (OPS) and the lipid A, an aliquot of pure S-LPS underwent mild acidic hydrolysis. The recovery of both fractions was performed using the Blight Dyer extraction (Bligh & Dyer, 1959). The OPS was purified by size exclusion chromatography as the obtained product was heterogenous. As a result, two separate

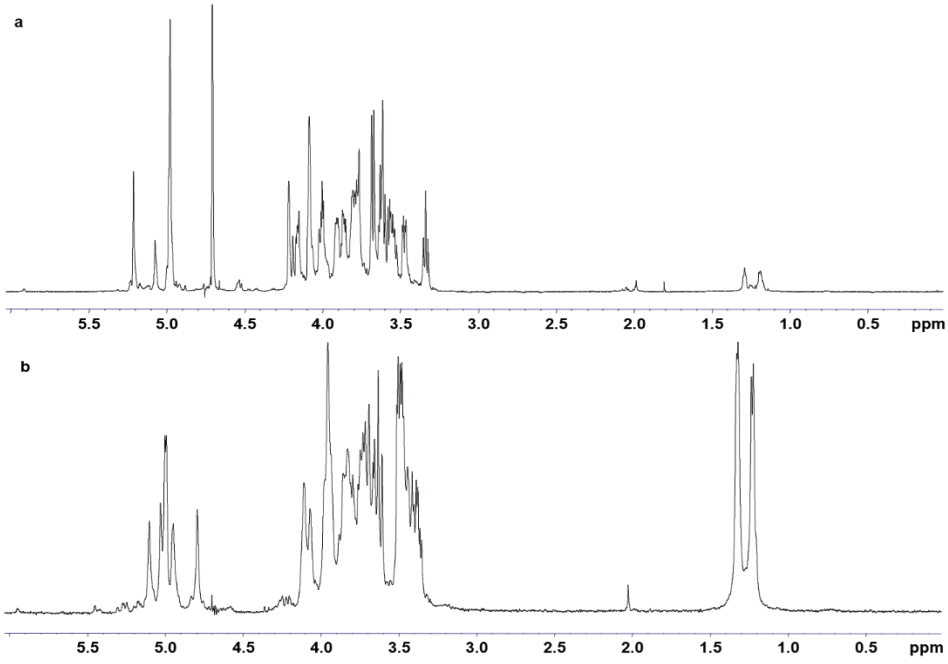

Figure 3.4 ^{1}H NMR spectra of a)**PS1** and b)**PS2**

fractions were obtained whose ^{1}H NMR (Figure 3.4) and compositional analysis clearly indicated presence of two different polysaccharides, abbreviated as **PS1** and **PS2**. Both fractions and the lipid A were characterized as described below.

3.4 Structural characterization of *Acetobacter pasteurianus* CIP103108 OPS

3.4.1. Structural characterization of PS1

The spin systems and monosaccharide sequence were characterized using a combination of 1D and 2D NMR spectra. The anomeric configuration of the monosaccharides was assigned on the basis of the $^{3}J_{H1,H2}$ and $^{1}J_{C1,H1}$ coupling constants and confirmed by the intra-residual NOE contacts; the vicinal $^{3}J_{H,H}$ coupling constants and intra

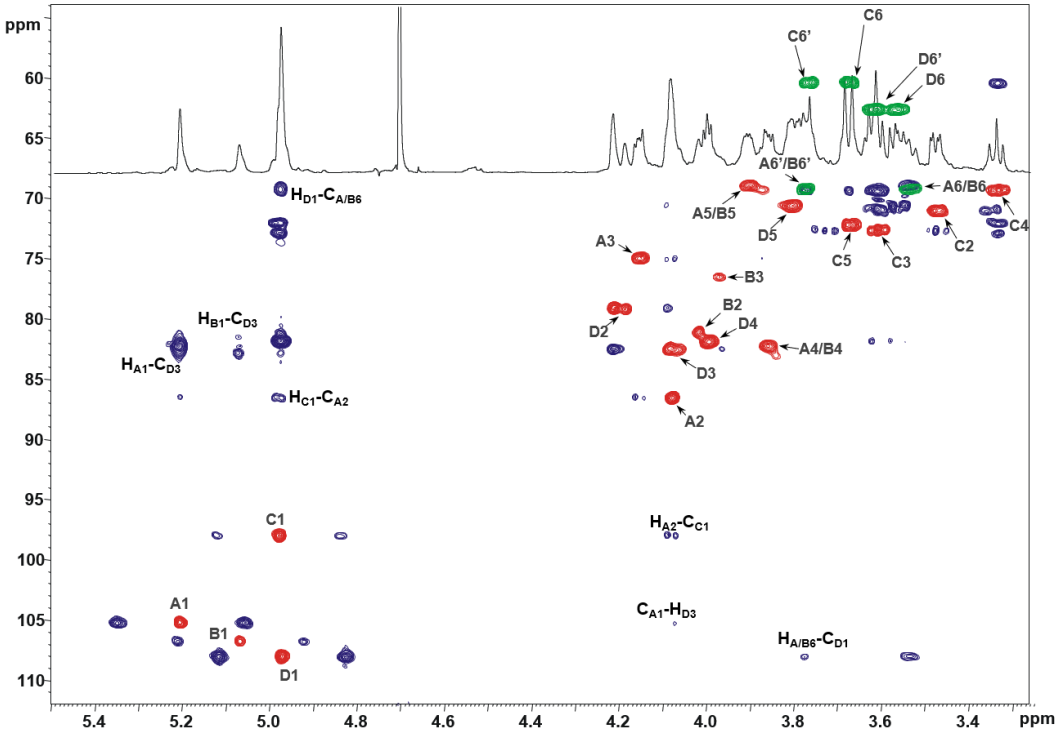

Figure 3.5 Superposed sections of ^{1}H ^{13}C HSQC (red and green) and ^{1}H ^{13}C HMBC (blue) and ^{1}H NMR spectra of **PS1**. The anomeric signals and key *inter*-residual long-range correlations involving sugar residues of **PS1** are indicated. Letters are as found in Table 3.2.

residual NOE contacts revealed the relative configuration of the sugar residues.

The anomeric region of **PS1** revealed the presence of four different anomeric signals (Figure 3.5, Table 3.2). Spin systems **A**, **B** and **D** at 5.21, 5.07 and 4.97 ppm were identified as β-D-Gal*f* units. The downfield shift of all carbon signals, the strong downfield shift of carbon C-4 and the *intra*-residual long-range correlation between positions 1 and 4 found in the HMBC spectrum (Figure 3.5) were diagnostic of a furanose ring (Di Lorenzo, 2014). The β-anomeric configuration was assessed on the basis of ^{13}C chemical shift (Molinaro, 2002). Spin system **C** was identified as an α-D-Glc*p;* its anomeric configuration was assigned on the basis of $^{1}J_{C1,H1}$ (Table 3.2) and the $^{3}J_{H1,H2}$ (< 4 Hz) whereas high $^{3}J_{H3,H4}$ (9.1 Hz) and *intra*-residual NOE connectivity of H-3 and H-5 confirmed the *gluco* configuration.

Table 3.2. Proton (^{1}H) and carbon (^{13}C) (*italic*) chemical shifts of *A. pasteurianus* **PS1**

Residue	1	2	3	4	5	6
A	5.21	4.08	4.15	3.86	3.91	3.53/3.78
2,6-β-D-Gal*f*	*105.2*	*86.6*	*75.0*	*82.3*	*69.0*	*69.3*
	$^{1}J_{C1,H1}$ 172.3 Hz	$^{3}J_{H1,H2}$ 3.4 Hz	$^{3}J_{H2,H3}$ 9.5 Hz	$^{3}J_{H3,H4}$ 9.4 Hz	$^{3}J_{H4,H5}$ 9.4 Hz	
B	5.07	4.02	3.97	3.84	3.86	3.77/3.50
6-β-D-Gal*f*	*106.8*	*81.2*	*76.6*	*82.9*	*69.2*	*69.3*
C	4.98	3.47	3.61	3.34	3.67	3.77/3.67
t-α-D-Glc*p*	*98.1*	*71.1*	*72.7*	*69.4*	*72.3*	*60.4*
D	4.97	4.21	4.09	4.00	3.80	3.62/3.57
3-β-D-Gal*f*	*108.1*	*79.2*	*82.6*	*82.0*	*70.7*	*62.7*

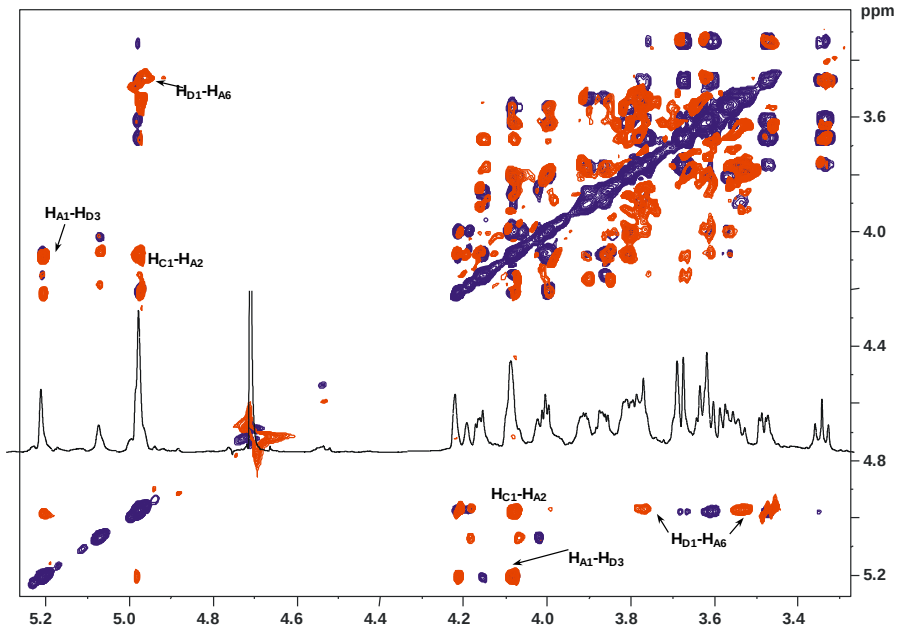

Figure 3.6 Superposed sections of TOCSY (blue) and ROESY (red) and ^{1}H NMR spectra of **PS1**. The key *inter*-residual correlations involving sugar residues of **PS1** are indicated. Letters are as found in Table 3.2.

The downfield shift of carbon resonances suggested glycosylated positions at O-2 and O-6 of **A**, O-6 of **B** and O-3 of **D**. Spin system **C** was characterized as a terminal Glc residue. The *inter*-residual NOE connectivity (Figure 3.6.) along with long-range correlations found on the HMBC spectrum (Figure 3.5) of **A**1/**D**3, **B**1/**D**3, **D**1/**A**6 and **C**1/**A**2 allowed to define the saccharide sequence. Residue **C** was found to be not stoichiometrically linked at position O-2 of the galactofuranose residue **A,** substituted for about 75 %.

A/B **D**

→6)-β-D-Gal*f*-(1→3)- β-D-Gal*f*-(1→

2

↑ **C**

1-α-D-Glc*p** **non-stoichiometric substitution*

3.4.2. Structural characterization of OPS2

The NMR spectrum of **PS2** unveiled the presence of five anomeric signals (Figure 3.7, Table 3.3). Spin systems **A** and **B**, H-1 at 5.10 and 5.03 ppm respectively (Table 3.3), were characterized as α-rhamnopyranose residues. In both cases, correlations of the ring protons with methyl signals were visible from the TOCSY spectrum. The *manno* configuration of both spin systems was assigned on the basis of $^{3}J_{H1,H2}$ and $^{3}J_{H2,H3}$ coupling constants, the α-configuration from *intra*-residual NOE contact of H-1 with H-2 and the chemical shift value of C-5. Analogously, spin systems **C** and **D** were assigned as α-glucopyranose units while spin system **E** was identified as α-mannopyranose.

Table 3.3 Proton (^{1}H) and carbon (^{13}C) (*italic*) chemical shifts of *A. pasteurianus* **PS2**

	Chemical Shift δ (^{1}H/*^{13}C*)					
Unit	**1**	**2**	**3**	**4**	**5**	**6**
A	5.10	4.11	3.97	3.49	3.82	1.32
2,4-α-L-Rha*p*	*100.5*	*78.9*	*68.6*	*81.2*	*68.3*	*16.9*
	$^{1}J_{C1,H1}$ 173.4 Hz	$^{3}J_{H1,H2} < 1$ Hz	$^{3}J_{H2,H3}$ 2.4 Hz	$^{3}J_{H3,H4}$ 9.02 Hz		
B	5.03	4.07	3.84	3.45	3.71	1.22
2-α-L-Rha*p*	*99.9*	*77.3*	*69.6*	*72.0*	*69.6*	*16.6*
	$^{1}J_{C1,H1}$ 172.0 Hz	$^{3}J_{H1,H2} < 1$ Hz	$^{3}J_{H2,H3}$ 3.0 Hz	$^{3}J_{H3,H4}$ 9.5 Hz		
C	5.00	3.49	3.63	3.39	3.94	3.75
t-α-D-Glc*p*	*99.6*	*71.5*	*72.8*	*69.5*	*71.9*	*60.2*
	$^{1}J_{C1,H1}$ 174.4 Hz	$^{3}J_{H1,H2}$ 3.5 Hz	$^{3}J_{H2,H3}$ 9.4 Hz	$^{3}J_{H3,H4}$ 9.5 Hz		
D	4.95	3.50	3.69	3.43	4.10	3.65/3.88
6-α-D-Glc*p*	*98.3*	*71.5*	*72.8*	*69.5*	*70.8*	*66.4*
	$^{1}J_{C1,H1}$ 174.2 Hz	$^{3}J_{H1,H2}$ 2.9 Hz	$^{3}J_{H2,H3}$ 9.5 Hz	$^{3}J_{H3,H4}$ 9.6 Hz		
E	4.80	3.95	3.84	3.38	3.63	3.76
2-α-D-Man*p*	*98.7*	*78.6*	*67.9*	*69.4*	*69.2*	*60.2*
	$^{1}J_{C1,H1}$ 173.2 Hz	$^{3}J_{H1,H2} < 1$ Hz	$^{3}J_{H2,H3}$ 3.5 Hz	$^{3}J_{H3,H4}$ 9.5 Hz		

The downfield shift of carbon resonances identified the glycosylated positions: O-2 and O-4 of **A**, O-2 of **B,** O-6 of **D** and O-2 of **E**. Unit **C** was identified as a terminal residue. The *inter*-residual NOE contacts observed from the ROESY spectrum (Figure3.8) together with the long-range correlations, derived from the HMBC spectrum (Figure 3.7.), between **A**1 with **E**2; **E**1 with **D**6, **D**1 with **B**2; **B**1 with **A**2 so as **C**1 with **A**4 confirmed the following repeating unit for the polysaccharide **PS2**:

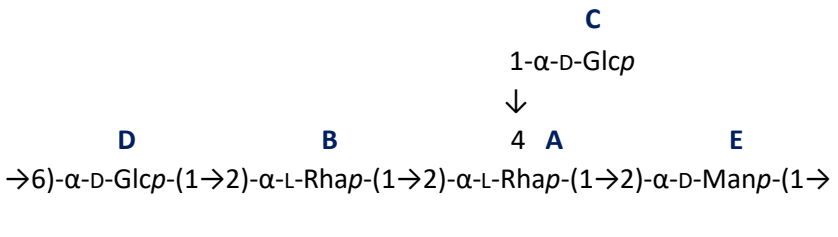

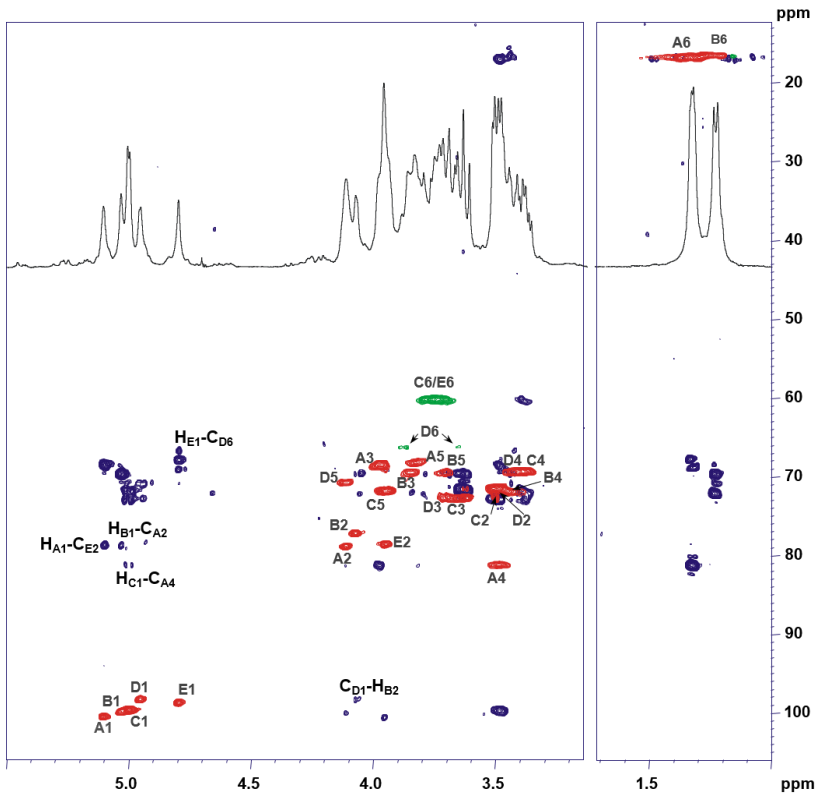

Figure 3.7 Superposed sections of ^{1}H ^{13}C HSQC (red and green) and ^{1}H ^{13}C HMBC (blue) and ^{1}H NMR spectra of **PS2**. The anomeric signals and key *inter*-residual long range correlations involving sugar residues of **PS2** are indicated. Letters are as found in Table 3.3.

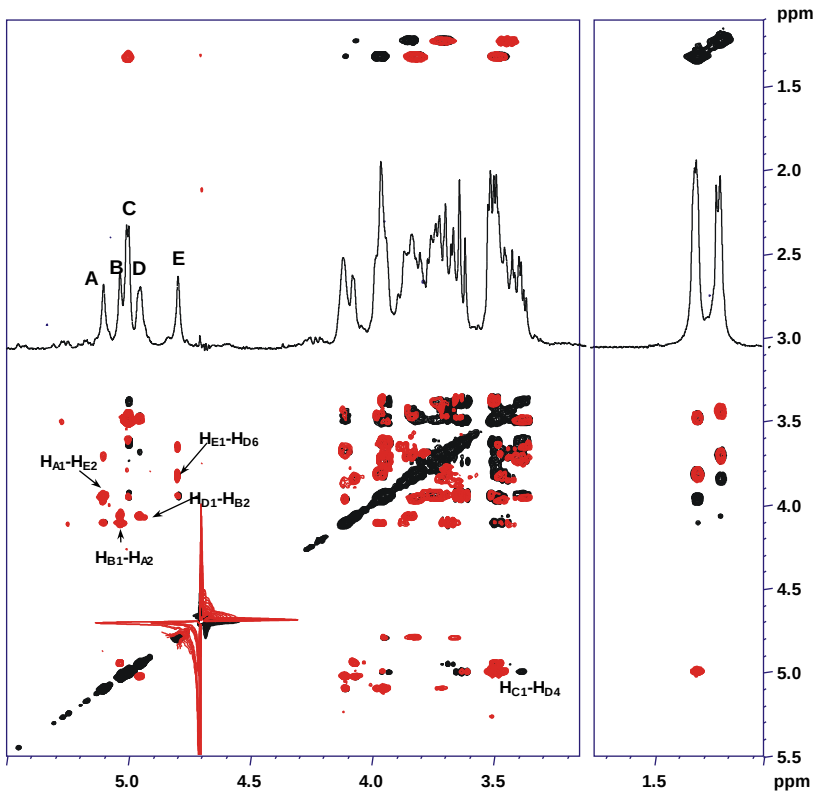

Figure 3.8 Superposed sections of TOCSY (black) and ROESY (red) and ^{1}H NMR spectra of **PS2**. The key *inter*-residual correlations involving sugar residues of **PS2** are indicated. Letters are as found in Table 3.3.

3.5. Structural characterization of the lipid A

A. pasteurianus CIP103108 lipid A structure was investigated by MALDI-MS and MS^2. The negative-ion MALDI MS spectrum (Figure 3.9) revealed the presence of several cluster of peaks in the mass range *m/z* 1543.9 – 2434.7, indicative of lipid A species with a different acylation degree. Each cluster was characterized by the presence of mass differences of 14 amu (-CH_2- unit), attributable to lipid A species differing by the length of their acyl chains (Figure 3.9).

In detail and based on the compositional analysis, cluster of peaks at around *m/z* 2406.7 matched with hexa-acylated lipid A species with a pentasaccharide sugar backbone containing one hexose (identified as Man), one DAG, one GlcN, one acid (identified as GlcA) and one Ko unit and acylated by two 14:0 (3-OH), two 18:0 (3-OH) and two 16:0, in accordance with previously reported structure on *A. pasteurianus* NBRC 3283 lipid A (Hashimoto, 2016). The cluster at *m/z* 2168.4 was assigned to penta-acylated lipid A species made up of two 14:0 (3-OH), two 18:0 (3-OH) and one 16:0, thereafter, tetra-acylated lipid A species at *m/z* 1942.2, devoid of one 14:0 (3-OH) with respect to the species at *m/z* 2168.4, was also identified. Furthermore, tetra-acylated species lacking one hexose and/or Ko units and minor tri-acylated species were also present in the

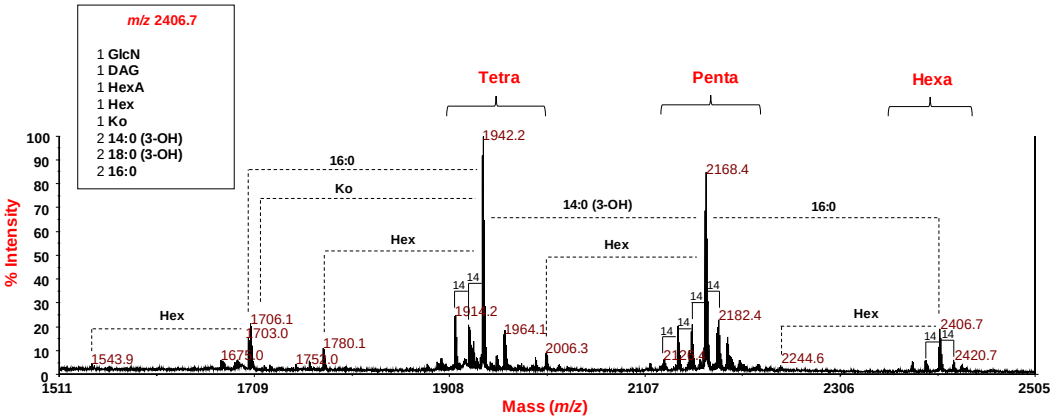

Figure 3.9 Negative ion reflectron MALDI mass spectrum, *A. pasteurianus* CIP103108 lipid A. Various lipid A species are outlined. In the inset, the proposed structural composition of the peak at *m/z* 2406.7 is listed

MALDI spectrum (Figure 3.9).

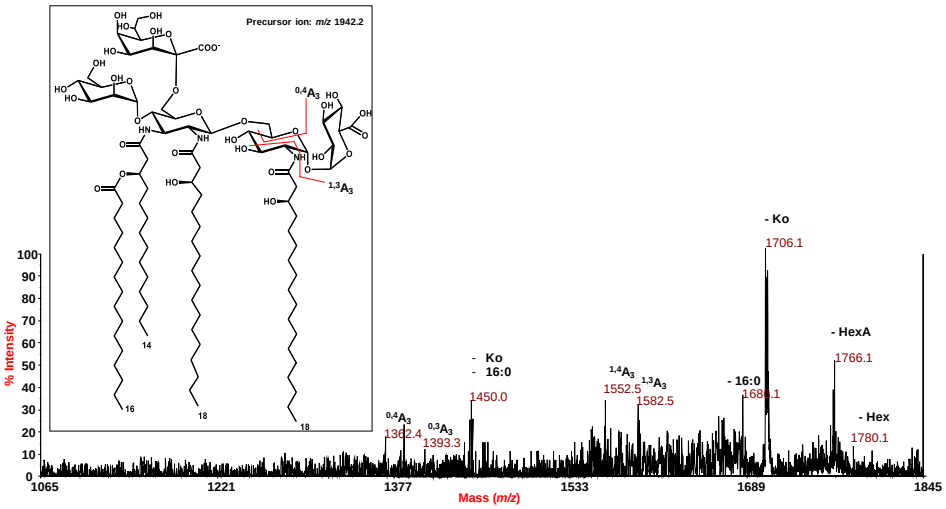

Figure 3.10 Negative-ion MALDI MS^2 spectrum of the tetra-acylated lipid A species at *m/z* 1942.2 from *A. pasteurianus* CIP103108. In the inset, the proposed structure for the tetra-acylated lipid A species matching with the precursor ion at *m/z* 1942.2 is reported showing some of the observed sugar ring fragmentations.

MS^2 experiments were performed in order to characterize the location of the lipid A acyl chains with respect to the saccharide backbone (Sturiale, 2005). The negative-ion MS^2 spectrum of precursor ion *m/z* 1942.2 (Figure 3.10), consistent with a tetra-acylated pentasaccharidic species, showed an intense peak at *m/z* 1706.1 attributed to an ion originated from the loss of Ko residue. Peaks at *m/z* 1766.1 and 1780.1 were assigned to fragments lacking the GlcA and the hexose unit respectively. A lipid A fragment devoid of the 16:0 moiety was attributed to the peak at *m/z* 1686.1. More importantly, peaks originating from the sugar ring fragmentations $^{1,3}A_3$ (*m/z* 1582.5), $^{1,4}A_3$ (*m/z* 1552.5), $^{0,3}A_3$ (*m/z* 1393.3) and $^{0,4}A_3$ (*m/z* 1362.4) were very informative as they clearly demonstrated that the proximal GlcN was decorated by a GlcA and an amide-bound 18:0 (3-OH) moiety whereas the distal DAG was substituted by Ko, hexose and acylated by one 18:0 (3-OH), one 14:0 (3-OH) and one secondary 16:0 fatty acid. Finally, the peak at *m/z* 1450.0 was ascribed to a fragment ion where both Ko and 16:0 were absent.

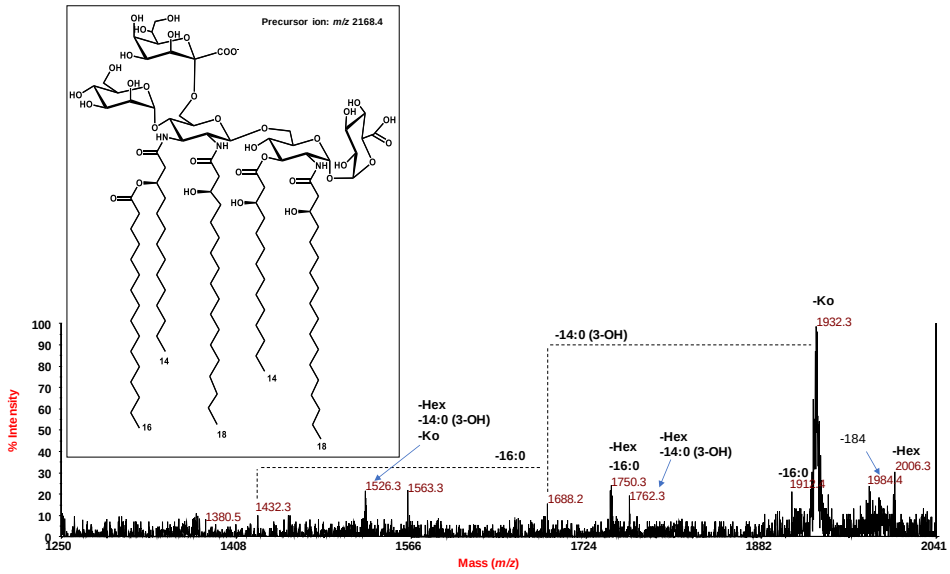

Figure 3.11 Negative-ion MALDI MS^2 spectrum of the penta-acylated lipid A species at *m/z* 2168.4 from *A. pasteurianus* CIP103108. Fragments assignment is reported in the spectrum. In the inset, the proposed structure for the penta-acylated lipid A species assignable to the precursor ion at *m/z* 2168.4.

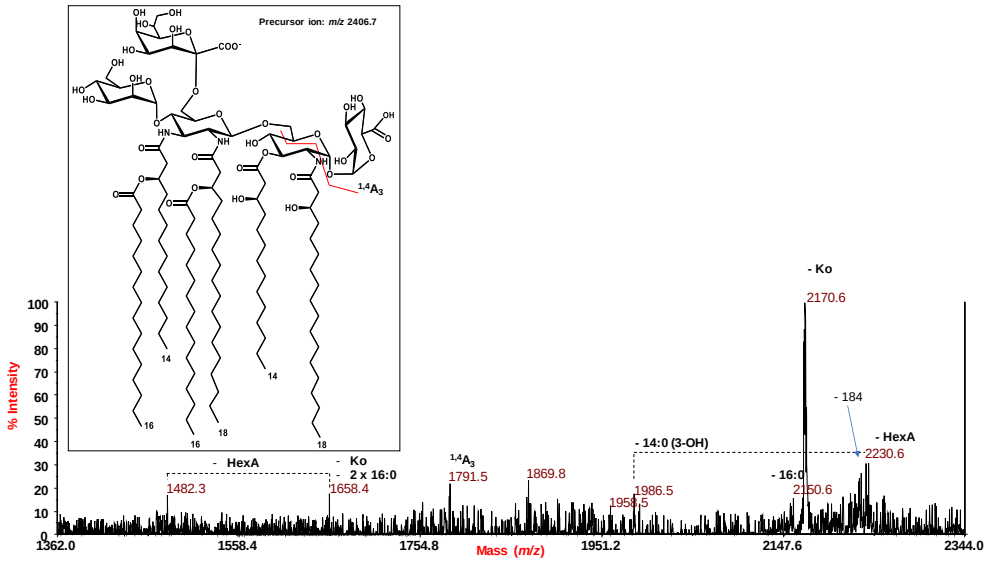

Figure 3.12 Negative-ion MALDI MS^2 spectrum of the hexa-acylated lipid A species at *m/z* 2406.7 from *A. pasteurianus* CIP103108. Fragments assignment is reported in the spectrum. In the inset, the proposed structure for the hexa-acylated lipid A species attributed to the precursor ion at *m/z* 2406.7.

MS^2 experiments conducted on precursor ion at *m/z* 2168.4 (Figure 3.11.) showed an ion peak at *m/z* 1932.3 originating from the loss of Ko unit, as well as from the loss of the hexose at *m/z* 2006.3. Lipid A fragments lacking the Ko and one 14:0 (3-OH) (*m/z* 1688.2) and one 16:0 (m/z 1432.3) were also identified. Moreover, ions originated from the loss of the hexose unit and 16:0 (*m/z* 1750.3) and from the loss of the hexose and one 14:0 (3-OH) (*m/z* 1762.3) were also detected. The absence of an ion originating from the loss of a whole hydroxylated 18:0 or 14:0 bearing a 16:0 suggested that the secondary fatty acid was linked to the acyloxyacyl amides, thus excluding its presence on the proximal GlcN as a substituent of the primary ester-bound 14:0 (3-OH). Furthermore, in support of this hypothesis, a peak was found at *m/z* 1984.4 resulting from the loss of 184 amu arising from the primary *O*-linked 14:0 (3-OH) and promoted by its free 3-OH group. Unfortunately, no ions originating from sugar ring fragmentations were detected. In addition, MS^2 spectrum of precursor ion at *m/z* 2406.7 (Figure 3.12.), relative to a hexa-acylated lipid A species, presented the ion peak derived from the sugar ring fragmentation $^{1,4}A_3$ at *m/z* 1791.5 that was fundamental to further corroborate the location of the 16:0 residues as secondary acyl substituents of the DAG unit.
Therefore, the lipid A and O-chain structure from *A. pasterianus CIP103108* were as reported in Figure 3.13.

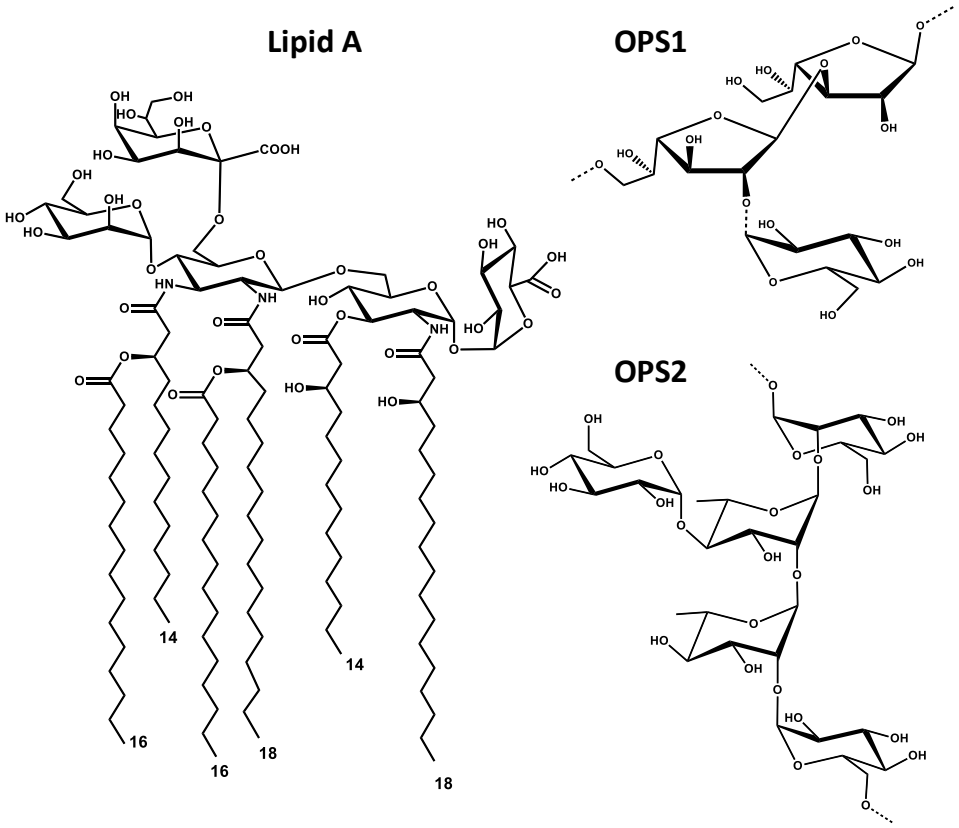

Figure 3.13. Hexa-acylated lipid A and two O-polysaccharides of *Acetobacter pasteurianus* CIP 103108

3.6. Structure of the core region

The partial structure of the core region was identified upon applying NMR on the intact *A. pasteurianus* CIP 103108 LOS. The configuration of each monosaccharide was determined on the basis of $^{3}J_{H,H}$ coupling constants and intra residual NOE contacts, whereas the anomeric configuration was assessed with the $^{3}J_{H1,H2}$ and $^{1}J_{C1,H1}$ coupling constants along with intra-residual NOE connectivity. All sugar residues were present as pyranose rings, according with the ^{13}C chemical shift values and long-range correlations found on the HMBC spectrum between C1/H1 with C5/H5 (C2 with H6 in case of Kdo).

Anomeric region of the intact LOS clearly showed four signals (Table 3.4, Figure 3.14). Spin system **K** was attributed to the Kdo residue on the basis of the diastereotopic methylene proton signals resonating in the high-field region of the ^{1}H NMR spectrum at δ 1.88 (H-3_{ax}) and 2.01 (H-3_{eq}) ppm (Table 3.4); on the basis of the H-3 proton chemical shift it was possible to assign its α-anomeric configuration. Spin system **A** with H-1 at 5.40 ppm was identified as α-Glc*p*. The $^{3}J_{H1,H2}$ value and $^{1}J_{C1,H1}$ = 172 Hz were diagnostic for α anomeric configuration, whereas, high $^{3}J_{H,H}$ of the ring signals were diagnostic for *gluco*-configuration. Spin system **B** (H-1 5.39 ppm) was identified as α-Glc*p*A, the α-gluco configuration was assigned basing on low $^{3}J_{H1,H2}$ and $^{1}J_{C1,H1}$ = 172 Hz. Moreover, the long-range correlation between H4 and H5 with C6 at 175.5 ppm on the $^{1}H^{13}C$ HMBC spectrum was indicative of the uronic acid residue. Spin system **C** with H1 at 5.19 ppm was determined as an α-rhamnopyranose due to the $^{3}J_{H1,H2}$ and $^{3}J_{H2,H3}$ below 3 Hz and the *intra*-residual NOE contact of H-1 only with H-2, whereas the α-anomeric configuration was assigned from on $^{1}J_{C1,H1}$ coupling constant and chemical shift of C5. Moreover, clear correlation of the ring protons with a methyl group observed on the TOCSY spectrum clearly suggested it was a 6-deoxy residue. Spin system **D** (H1 at 4.96 ppm) was identified as β-Glc*p* on behalf of NOE contacts between H-1/H-3 and H-1/H-5, along with $^{1}J_{C1,H1}$ and $^{3}J_{H,H}$ values.

Table 3.4 Proton (^{1}H) and carbon (^{13}C) (*italic*) and phosphorus (^{31}P) chemical shifts of *A. pasteurianus* **core OS**

Residue	^{1}H, ^{13}C and ^{31}P chemical shift values (ppm) of core OS									
	1	**2**	**3**	**3'**	**4**	**5**	**6**	**6'**	**7**	**8**
A	5.40	3.38	3.56		3.34	3.73	3.29	3.73	-	-
t-α-Glc*p*	*98.4*	*71.6*	*73.6*		*69.3*	*69.9*	*61.4*		-	-
$^{1}J_{C1,H1}$ = 174 Hz										
B	5.39	3.54	3.88		3.67	4.08	-	-	-	-
4-α-Glc*p*A1*P*	*94.8*	*71.2*	*73.16*		*76.2*	*73.0*	*175.5*		-	-
$^{1}J_{C1,H1}$ = 176 Hz	*-2.07*	-	-		-	-	-		-	-
C	5.19	4.11	3.77		3.40	3.72	1.16		-	-
3- α-Rha*p*	*100.32*	*66.9*	*75.4*		*70.1*	*69.1*	*16.8*		-	-
$^{1}J_{C1,H1}$ = 171 Hz										
D	4.96	3.45	3.67		3.34	3.90	3.67	3.77	-	-
t-β-Glc*p*	*95.4*	*71.3*	*72.8*		*69.3*	*71.7*	*60.3*		-	-
$^{1}J_{C1,H1}$ = 167 Hz										
K	-	-	2.09	1.88	4.28	4.34	4.07		4.50	4,08
5-α-Kdo*p*7*P*8*P*	*175.0*	-	*33.6*		*66.7*	*74.1*	*67.3*		*75.3*	*67.3*
	-	-	-		-	-	-		*-0.56*	*-2.07*

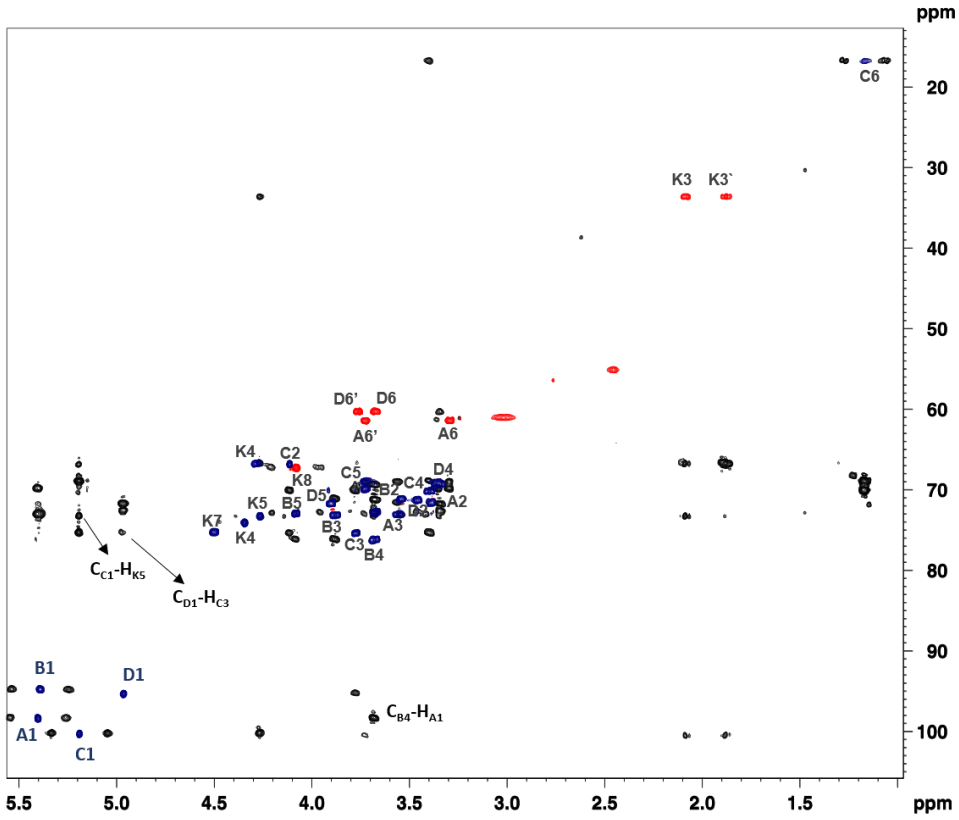

Figure 3.14. Superposed sections of ^{1}H ^{13}C HSQC (blue and red) and ^{1}H ^{13}C HMBC (black) spectra of the **core OS**. The anomeric signals and key *inter*-residual long-range correlations involving sugar residues of **core OS** are indicated. Letters are as found in Table 3.4.

(Figure 3.14.). Low-field shifted carbon signals were pivotal to identify substitution at: O4 of **B**, O3 of **C** and O5 of **K**. Spin systems **A** and **D** were assigned as terminal sugar residues. The primary sequence of the **OS** was inferred by using NOE connectivity attained by the ROESY spectra and by the long-range correlations in the HMBC spectrum. The NOE contact of B_{H4} with A_{H1} along with long range correlation of A_{H1} with B_{C4} were crucial

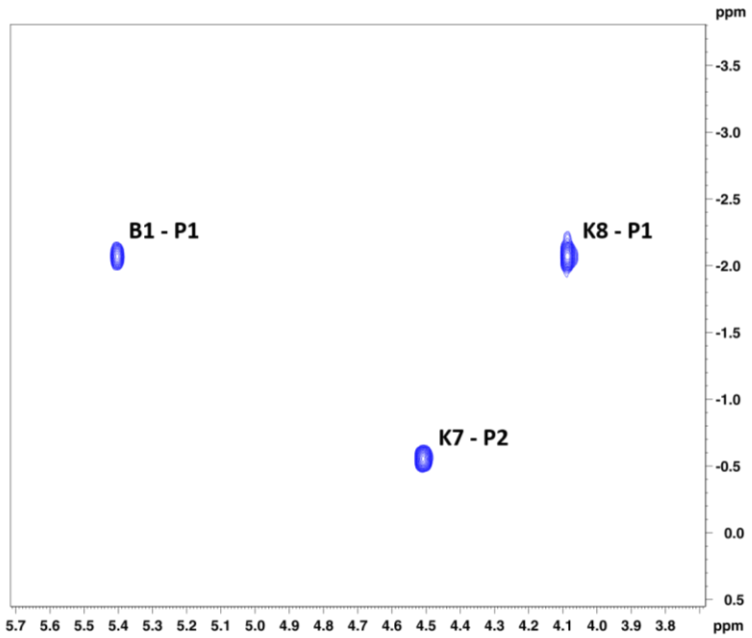

Figure 3.15. Section of ^{1}H ^{31}P HSQC spectrum of the **core OS**. The key correlations involving sugar residues and phosphorus nuclei of the **core OS** are indicated. Letters are as found in Table 3.3.

to identify the linkage between two residues. Furthermore, The NOE contact of D_{H1} with C_{H3} and long-range correlation of D_{H1} with C_{C3} revealed presence of 1-3 linkage between **C** and **D** spin systems. Residue **K** was found substituted at its O-5 position by C_{H1} as evident from the HMBC spectrum and supported by the NOE contact between C_{H1} with $K_{H5.}$ The detection of phosphate groups was done using $^{1}H^{31}P$ HSQC (Figure 3.15.), supported by the low-field shift proton signals at the positions of phosphorylation. Thus, a phosphorus at -2.07 ppm correlated with H-1 of spin system **B** and H-8 of spin system **K**, revealed a presence of phosphodiester bond connecting position 8 of α-Kdo (spin system **K**) and spin system **B** (α-Glc*p*A). A second phosphate group was located at position 7 of Kdo:

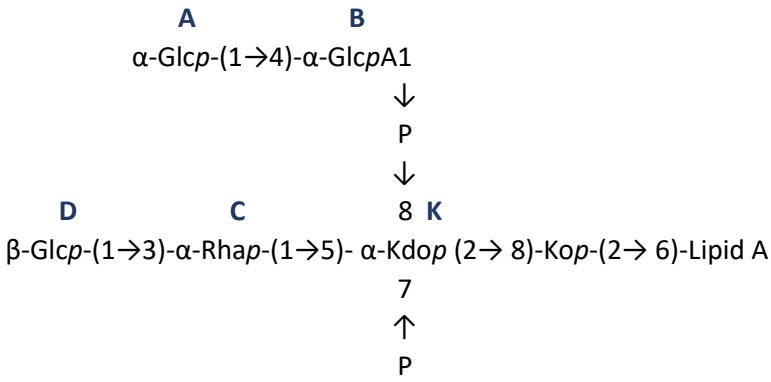

Thereafter, the methylation analysis (Chapter 3.2) unveiled presence of 8-substituted-Ko*p*, strongly suggesting the linkage with the Kdo*p* (**K**). Thus, according to compositional analysis, NMR and MS data the LOS from *A. pasteurianus* CIP103108 (Figure 3.16) possessed the following structure:

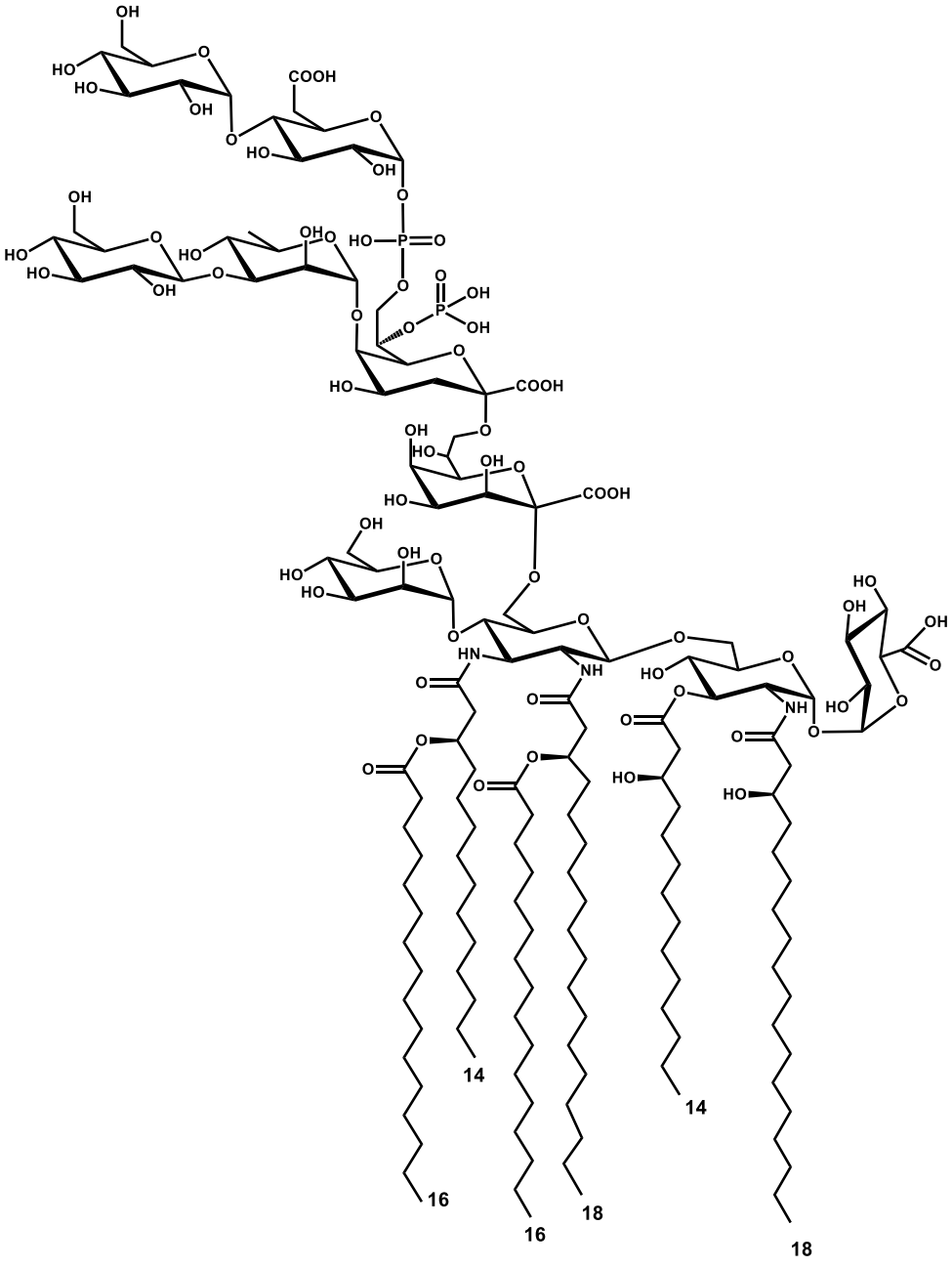

Figure 3.16. The structure of *Acetobacter pasteurianus* CIP 103108 LOS

3.7. Immunological assays

Studies on immunological properties of *A. pasterianus* CIP103108 LPS were performed using HEK-Blue hTLR4 cells. These cells are designed for studying the activation of human TLR4 by monitoring the activation of NF-κB and AP-1 transcription factors. HEK-Blue hTLR4 cells are HEK cells transfected in order to stably express hTLR4, hMD-2 and hCD14 receptor genes and a secreted embryonic alkaline phosphatase (SEAP) reporter gene placed under the control of NF-κB and AP-1. Stimulation with a TLR4 ligand activates NF-κB and AP-1 inducing the production and secretion of SEAP in cells culture medium. Levels of SEAP can be easily determined incubating the enzyme with *para*-nitrophenylphosphate (pNPP). In order to evaluate the capacity of *A. pasteurianus* CIP 103108 LPS to trigger TLR4-

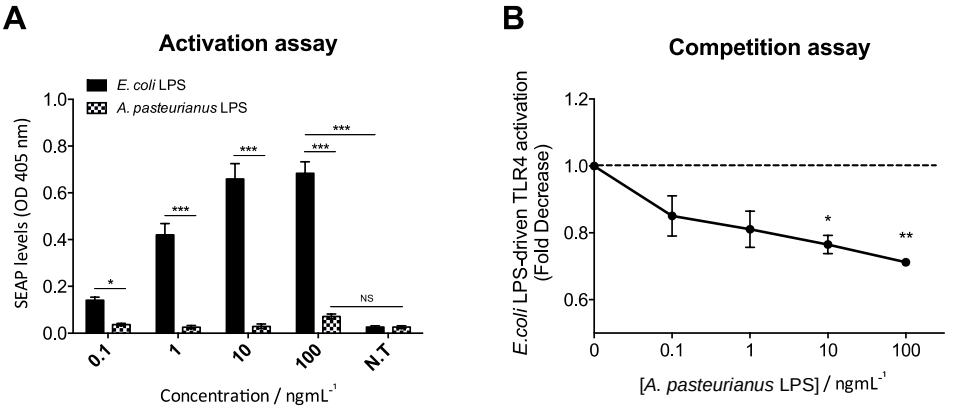

Figure 3.17. Effect of *A. pasteurianus* CIP103108 LPS on TLR4 pathway activation. A) HEK-Blue hTLR4 cells were stimulated with the indicated concentration of *A. pasteurianus* and *E. coli* LPS and incubated for 16 hours. Supernatants were collected and SEAP levels were quantified by pNPP assay as indicator of TLR4 activation. B) Cells were pre-incubated for 30 minutes with the indicated concentrations of *A. pasteurianus* CIP103108 LPS and then stimulated with 1 ng/mL of *E. coli* O55:B5 LPS for 16 hours. Supernatants were collected and SEAP levels quantified as above. For competition assay, data were normalized compared to stimulation with *E. coli* LPS alone and indicated as fold decrease. Results represent the mean percentage ± SEM of at least three independent experiments (NS: not significant, *P<0.05; **P<0.01; ***P<0.001).

mediated signalling (activation assay) cells were exposed to different concentrations (0.1, 1, 10, 100 ng/mL) of this LPS variant for 16 hours. As a positive control *E. coli* O55:B5 LPS was used. As expected, *E. coli* O55:B5 LPS strongly activated TLR4-mediated pathway in a dose-dependent manner. On the contrary, the results obtained revealed that *A. pasteurianus* CIP103108 LPS was incapable to trigger the activation of the same pathway (Figure 3.17.A). Furthermore, the capability of *A. pasteurianus* CIP103108 LPS to interfere with *E. coli* LPS–triggered TLR4-mediated signalling was also evaluated (competition assay). To investigate this aspect, cells were pre-incubated with different concentration of *A. pasteurianus* CIP103108 LPS (0.1, 1, 10, 100 ng/mL) for 30 minutes and then exposed to *E. coli* O55:B5 LPS (1 ng/mL) for 16 hours. Results showed that the pre-incubation with *A. pasteurianus* CIP103108 LPS slightly reduced the capacity of cells to respond to *E. coli* O55:B5 LPS, as demonstrated by the minor activation of the TLR4-mediated pathway (Figure 3.17.B).

3.8. Discussion

The structural and biological investigation performed on *Acetobacter pasteurianus* CIP 103108 LPS has shown many interesting and peculiar features of the biomolecule.

Two novel LPS O-chains were found, **PS1** and **PS2**, both possessing structural analogies with those isolated from other *Acetobacter* strains. The presence of two different O-chains is not considered as a common feature of LPSs, nevertheless this phenomenon was reported among *Burkholderia* species (Vinion-Dubiel, 2003). **PS1** possessed a Gal*f* disaccharide repeating unit carrying a non-stoichiometric Glc substitution; it showed subtle compositional similarities with the O-chains isolated from two *Acetobacter methanolicus* strains, MB58/4 (Grimmecke, 1991) and MB70 (Grimmecke, 1994). Moreover, it was also found that a similar exopolysaccharide was produced by another acidophilic bacterium, *Zymomonas mobilis*, which was proven to have relevance with the outer milieu of bacterium (see Chapter 6.3). The second polysaccharide **PS2** contained a pentasaccharide repeating unit constituted by a tetrasaccharide skeleton containing glucose, mannose and two rhamnose

residues, one of which carrying a terminal glucose as an appendage. A similar O-antigen was reported for *Acetobacter tropicalis* SKU1100 (Ali, 2011), whose backbone also contained two rhamnose residues, although in an α-(1-3) linkage, instead of the α-(1-2) here reported, with one rhamnose further substituted by a glucose residue. Furthermore, other O-polysaccharides possessing structural similarities were also found in *Acetobacter diazotrophicus* PAL5 (Previato, 1997). None of the above structures possessed mannose residues, though for *A. diazotrophicus* PAL5 contained a *manno*-configured sugar.

Recently, Hashimoto et al. (2016) reported about the capability of *A. pasteurianus* NBRC 3283 LPS to remain stable in acidic conditions for long periods and correlated this capability to its unique lipid A structure (see Chapter 1.3.1). Indeed, the authors demonstrated that the LPS was characterized by the occurrence of a D-*glycero*-D-*talo*-oct-2-ulosonic acid (Ko), in place of Kdo, as the first sugar of the core OS, directly linked to the lipid A domain. This was explained with the acid-lability of Kdo that would be degraded in the acid environmental conditions of bacterium life. Thus, the substitution of Kdo with the acid-stable Ko is considered as an adaptation phenomenon necessary for bacterial survival. The presence of Ko has been so far described in the core oligosaccharides from *Burkholderia*, *Acinetobacter, Yersinia*, and *Serratia* species (Holst, 2011), although a direct linkage of Ko to the lipid A has so far reported only for *Acinetobacter haemolyticus* (Vinogradov, 1997), in which the Kdo is almost completely replaced by Ko residues. Furthermore, *A. pasteurianus* LPS is devoid of phosphate groups and the lipid A is characterized by tetrasaccharide backbone composed of Man-DAG-GlcN-GlcA. Interestingly, lipid A devoid of phosphate groups and with a similar sugar skeleton were already reported for other plant associated bacteria belonging to the *Alphaproteobacteria* family, as *Rhizobiaceae* and *Bradyrhizobiaceae*. The lipid A isolated from *Rhodopseudomonas palustris* (Di Lorenzo, 2017) possessed nearly the same tetrasaccharide skeleton but with a complete DAG skeleton. *Bradyrhizobium* strains possess instead an α-(1 → 6)-disaccharide linked to the non-reducing DAG (Komaniecka, 2010; Silipo, 2014). Moreover, a DAG-GlcN disaccharide skeleton was previously reported for *Campylobacter jejuni* (van Mourik, 2010) while a DAG backbone has been found in the lipid A of other strains like *Azorhizobium caulinodans* (Choma, 2012), *Phyllobacterium trifolii* (Zamłyńska, 2017), *Leptospira interrogans* (Que-Gewirth, 2004),

Acidithiobacillus ferrooxidans (Sweet, 2004), *Thiobacillus (Yokota, 1987)*, *Bartonella* (Malgorzata-Miller, 2016) and *Brucella* (Casabuono, 2017). The occurrence of this phenomenon is explained by the presence of two enzymes, GnnA and GnnB in the lipid A biosynthesis process which are pivotal for synthesis of UDP-D-Glc*p*N3N from UDP-D-Glc*p*NAc (Sweet, 2004).

Moreover, the structure of the core region was studied applying NMR techniques on the intact LOS sample. The oligosaccharide was composed by one Kdo residue and, interestingly, was phosphorylated at both positions 7 and 8. In detail, a phosphodiester bridge at position 8 connected the Kdo to an α-Glc*p*-(1→4)-α-Glc*p*A disaccharide, reported in the past in the core region of *Arenibacter certesii* KMM 3941^T (Silipo, 2005). *Acetobacter pasteurianus* CIP103108 core is devoid of heptose residues, previously reported in other Alphaproteobacteria, as *Agrobacterium* and Rizhoium strains (Molinaro, 2003; De Castro, 2006a; De Castro, 2006b; Forsberg, 1998) or Gammaproteobacteria, as *Acinetobacter* strains (Vinogradov, 2002; Leone, 2006). Furthermore, the methylation analysis performed on the LOS permitted to observe a derivative corresponding to 8-substituted-Ko*p* disaccharide, corroborating the hypothesis that the Ko residue was linked in the `8 with the Kdo residue.

The lipid A is considered as the centre of toxicity of the LPS. It is well known that this part of the molecule is recognized by the TLR4/MD-2 receptor complex resulting in immunostimulation activity (see Chapter 1.7. and 1.8.). A widely known fact is that hexa-acylated *bis*-phosphorylated lipid A produced by *E. coli* possesses high affinity to TLR4/MD-2 receptor complex, triggering powerful innate immune response. Overstimulation by agonist LPS can deregulate innate immune system signalling, finally effecting in uncontrolled, massive proinflammatory cytokine release. Nevertheless, it was shown that modifications of the lipid A structure can tune and modulate the innate immune response. Within this frame, research and investigation of natural LPS able to inhibit the TLR4/MD-2 dependent signalling is an important and interesting topic (see Chapter 1.8 and 1.9).

The results obtained on TLR4/MD-2 mediated NF-kB activation on *A. pasteurianus* CIP103108 LPS have shown significantly lower response

than *E. coli* O55:B5 LPS. A weak effect of inhibition of the TLR4/MD-2 mediated activation of NF-kB induced by *E. coli* O55:B5 LPS was also observed. The very weak agonist activity may be explained by lipid A structural features as i) the absence of phosphate groups (Rietschel, 1994, Fox, 2010; Molinaro, 2015), ii) the presence of penta-, tetra- and tri-acylated species, besides the hexa-acylated form, iii) the occurrence of a DAG unit (see Chapter 1.8.).

3.9. Interaction studies with MD-2

The lipopolysaccharides are amphiphilic molecules composed of hydrophobic domain, the lipid A and hydrophilic portion, the core oligosaccharide and O-polysaccharide in the S-form. Therefore, this type of molecules is expected to form aggregates in aqueous environment, after reaching the critical *micelle* concentration (CMC) (Santos, 2003). Moreover, at higher concentrations, the lipopolysaccharides show tendency to aggregate in almost spherical, multi-Lamellar or non-Lamellar supramolecular forms depending on the environment (García-Verdugo, 2005). The issue concerning the aggregation of the LPS and whether the large or small aggregates are the biologically active units was still not clarified and is debated in the literature (Schromm, 2007; Mueller, 2004; Gutsmann, 2007).

The behaviour of two lipopolysaccharides, isolated from *Acetobacter pasteurianus* CIP103108 and *Bradyrhizobium BTAi-1 Δshc* (Silipo, 2014) was studied in presence and absence of MD-2. Both LPSs are known to present different affinity to the TLR4/MD-2 receptorial complex. *Bradyrhizobium* LPS is a potent antagonist of the receptorial complex (Lembo-Fazio, 2018), whereas *Acetobacter pasteurianus* LPS shows low activation of the TLR4/MD-2 receptorial complex. MD-2 belongs to the group of lipid binding proteins, and is able to disaggregate the LPS micelles. The behaviour of the LPS aggregates in presence of MD-2 not yet extensively studied, has been here examined.

The NMR became not only a powerful tool in the structural characterization of organic compounds, but also in the detection and characterization of binding events. The ligands-based techniques are centered on the observation of ligand behaviour in the free state and

upon addition of the receptor, the bound sate. In comparison to the receptor-based techniques, they exhibit a range of useful properties, including no limitation of the protein size, they do not require presence of labelled protein, as the resonances of ligand are observed and finally they require small amounts of receptor. Moreover, the techniques are easily applicable in medium low affinity range (Marchetti, 2016).

One of the most used ligand-based methods is the Diffusion Spectroscopy (DOSY). The method relies on changes in ligand diffusion coefficient in absence and presence of the protein. The translational motion of the molecules in solution is known as the self-diffusion, which strictly depends on different physical parameters, including size and shape of the molecule, viscosity and temperature. The diffusion coefficient is described by the Stokes-Einstein equation.

$$D_x = \frac{k_\mathrm{B} T}{6\pi\eta R_\mathrm{h}}$$

The diffusion can be further measured applying pulse field gradient NMR spectroscopy (Lucas, 2004; Marchetti, 2016). The protein and receptor in the free state, obviously, present different diffusion coefficient, as both vary in terms of shape and molecular weight and change upon binding As a result, the small ligand adopts the features of larger receptor, increasing the hydrodynamic radius, changing shape and consequently the transitional diffusion. In case of strong protein-ligand association both possess the same diffusion coefficient, however if fast exchange is present, the diffusion is characterized as an average of free and bound ligand.

3.9.1. Isolation of ligands

The isolation process of *A. pasteurianus* LPS (Figure 3.18) was previously described in Chapter 3.1. In order to isolate the LPS from *Bradyrhizobium BTAi-1 Δshc* (Figure 3.18) the LPS was isolated applying the hot-phenol water method (Westphal & Jann, 1965) and purified as described .

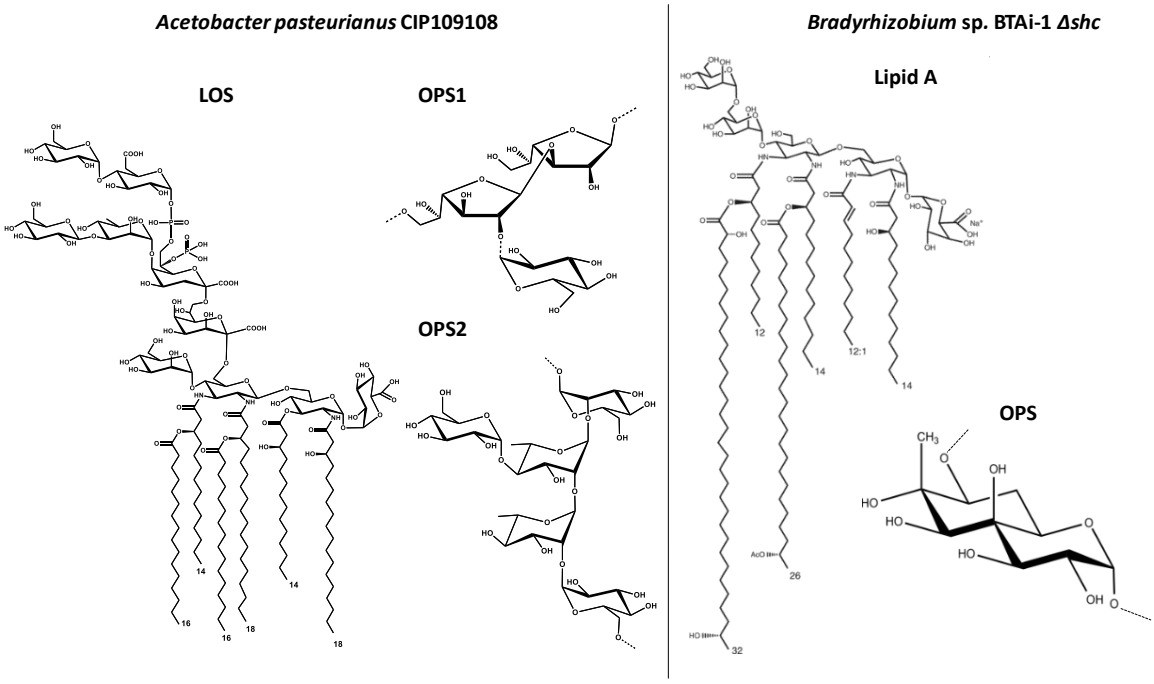

Figure 3.18 Structure of *Acetobacter pasteurianus* CIP103108 and *Bradyrhizobium* BTAi-1 *Δshc* (Silipo, 2014) LPSs

3.9.2. Preparation and purification of recombinant hMD-2

The hMD-2 used in the experiments was expressed by *Pichia pastoris* with the N-terminal *S. cerevisiae* α-MF prepro leader sequence and the C-terminal 6xHis tag as reported (Facchini, 2018).

3.9.3. Effect of MD-2 on *Acetobacter pasteurianus* CIP103108 LPS aggregation

The ^{1}H-NMR spectrum of *Acetobacter pasteurianus* in presence of 60 μM hMD-2 has shown significant decay of signals in the anomeric region (Figure 3.19.) It was not possible to observe any perturbation in the lipid A fatty acid region of the spectrum, as the signals overlaid with those from the hMD-2.

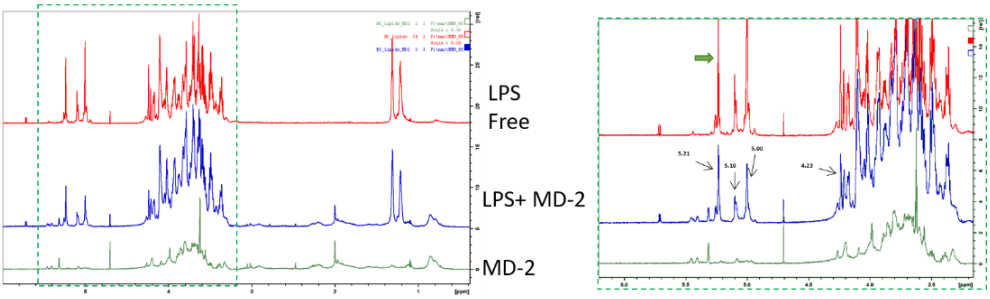

Figure 3.19. ^{1}H-NMR spectra. **Green:** ^{1}H-NMR of 60uM of hMD-2, **Blue:** ^{1}H-NMR of 0.9 mg/mL of LPS from *Acetobacter pasteurianus*; **Red:** ^{1}H-NMR of 0.9 mg/mL of LPS from *Acetobacter pasteurianus* in presence of 60μM of hMD-2; The spectra were acquired in deuterated phosphate buffer at pH 7.5, 298 K, 64 scans.

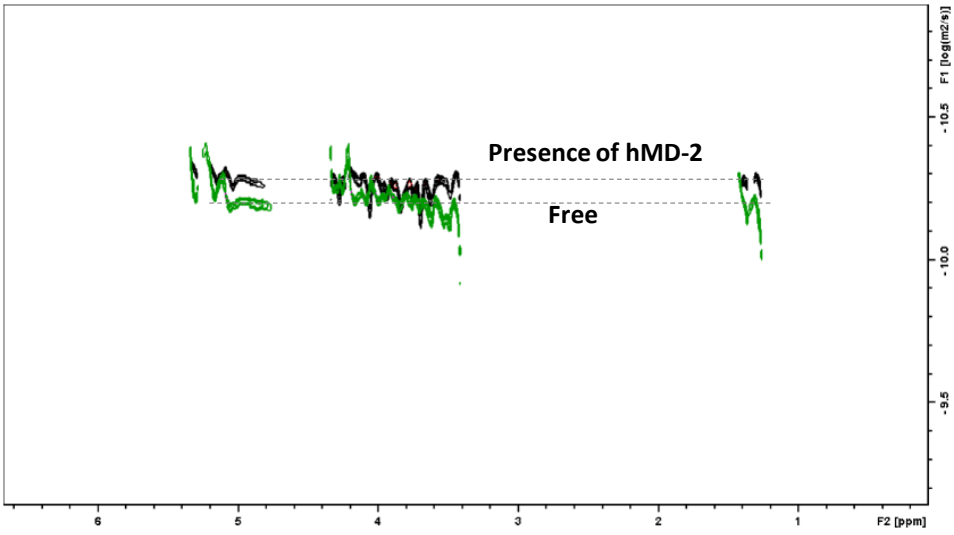

Figure 3.20. DOSY spectrum **Black:** DOSY of 0.9 mg/mL of LPS from *Acetobacter pasteurianus* in presence of 60 μM of hMD-2 **Green :** DOSY of 0.9 mg/mL of *Acetobacter pasteurianus*; The spectra were acquired in deuterated phosphate buffer at pH 7.5, 298 K, 64 scans, 32 points, **Δ (d20) = 300 ms and δ (p30) = 4 ms**

DOSY experiments were performed on free *A. pasteurianus* CIP103108 LPS and upon addition of hMD-2 (Figure 3.20.). Interestingly, a clear decrease of diffusion (Table 3.5) was observed, which can be associated with increased aggregate size or shape change.

Table 3.5. Diffusion coefficient values of *Acetobacter pasteurianus* CIP103108 LPS free and in presence of hMD-2

Sample	**D/m^2s^{-1}**
0.9 mg/mL LPS from *Acetobacter pasteurianus* LPS	$1.06x10^{-11}$
0.9 mg/mL LPS from *Acetobacter pasteurianus* + hMD-2 60 μM	$5.16x10^{-12}$
Difference	**$5.47x10^{-12}$**

The DOSY data were compared with results from the Cryo-TEM. As expected, *A. pasteurianus* LPS formed rather homogeneous aggregates, with circular shape and conserved size distribution near 60 nm. Significant differences were observed upon addition of hMD-2. As presented on Figure 3.21, some of micelles lost their circular form and, moreover, a rather heterogeneous size distribution was clearly observed.

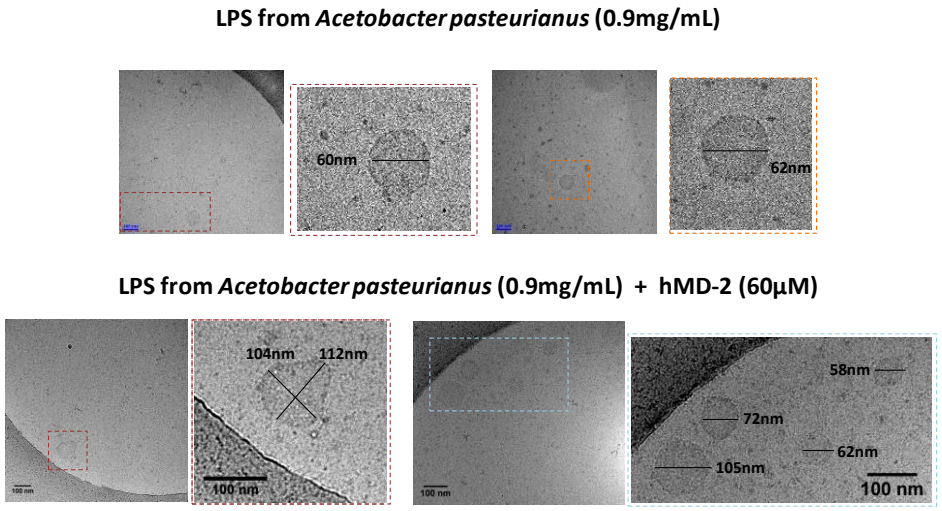

Figure 3.21. Cryogenic Transmission Electron Microscopy (Cryo-TEM) of LPS from *Acetobacter pasteurianus* (0.9mg/mL) nominal magnification of 40,000 X (0.26 nm/pixel).

3.9.4. Effect of MD-2 on *Bradyrhizobium* BTAi-1 Δshc LPS aggregation

Obtained data were further confronted with studies performed on *Bradyrhizobium BTAi-1 Δshc* LPS. The ^{1}H-NMR spectrum registered on the lipopolysaccharide in presence of 60 µM hMD-2 (Figure 3.22) showed clear perturbation of the signals at 2.04 and 1.41 ppm, whose reduction of the intensity and line broadening derived from the changes in the transverse relaxation times, indicative of a binding event. Thereafter, DOSY NMR experiments were performed on *Bradyrhizobium BTAi-1 Δshc* LPS with and without hMD-2 (Figure 3.23.).

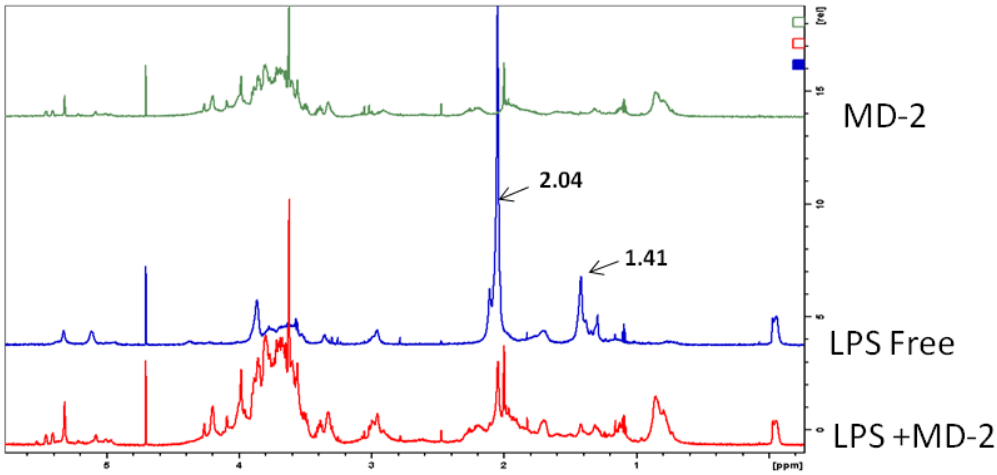

Figure 3.22. ^{1}H-NMR spectra. Green: ^{1}H-NMR of 60µM of hMD-2, **Blue:** ^{1}H-NMR of 0.9 mg/mL of LPS from *Bradyrhizobium BTAi-1 Δshc*; **Red:** ^{1}H-NMR of 0.9 mg/mL of LPS from *Bradyrhizobium BTAi-1 Δshc* in presence of 60µM of hMD-2; The spectra were acquired in deuterated phosphate buffer at pH 7.5, 298 K, 64 scans.

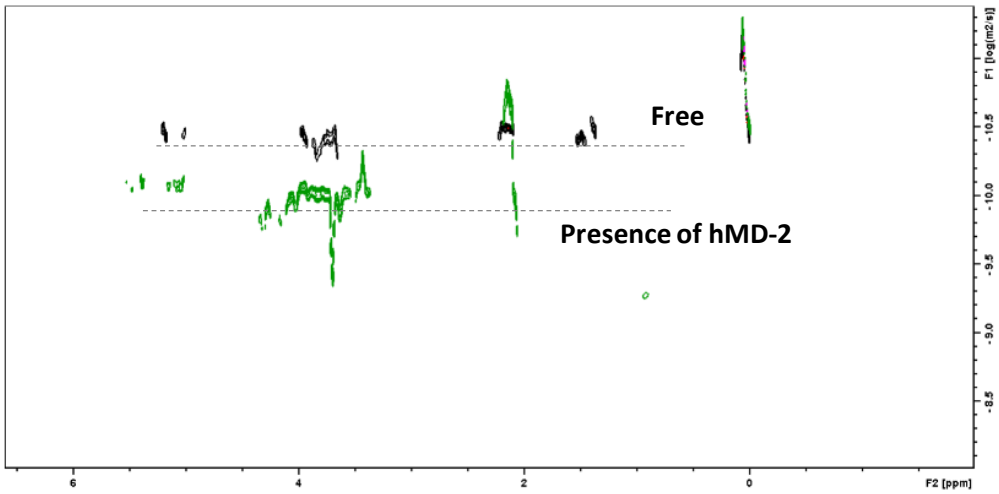

Figure 3.23. DOSY spectrum **Black:** DOSY of 0.9 mg/mL of LPS from *Bradyrhizobium BTAi-1 Δshc* **Green :** DOSY of 0.9 mg/mL of LPS from *Bradyrhizobium BTAi-1 Δshc* in presence of 60 µM of hMD-2; The spectra were acquired in deuterated phosphate buffer at pH 7.5, 298 K, 64 scans, 32 points and **Δ (d20) = 500 ms and δ (p30) = 5 ms.**

Contrairly to LPS from *A. pasteurianus* CIP103108, a significant increase of diffusion coefficient (Table 3.6.) was clearly observed in presence of hMD-2, what suggested disruption of existing aggregates and reorganization of free forms into smaller aggregates after the binding. Similar behaviour was reported in case of a lipid A mimetic, FP7 (Cighetti, 2014). The Cryo-TEM analysis will be performed in order to corroborate the data obtained by DOSY-NMR measurements.

Table 3.6. Diffusion coefficient values of *Bradyrhizobium* BTAi-1 Δshc free and in presence of hMD-2

Sample	D/m^2s^{-1}
0.9 mg/mL LPS from *Bradyrhizobium* BTAi-1 Δshc	$5.781x10^{-12}$
0.9 mg/mL LPS from *Bradyrhizobium* BTAi-1 Δshc + hMD-2 60 μM	$2.09x10^{-11}$
Difference	**$-1.5x10^{-11}$**

3.9.5 Discussion

MD-2 is a lipid binding protein, which plays a key role in activation of innate immune system upon recognition of the Lipid A portion of the lipopolysaccharide (see Chapter 1.7). The binding of LPS lipid A to hMD-2 was studied by means of DOSY NMR and Cryo-TEM. The lipopolysaccharides from *Acetobacter pasteurianus* and *Bradyrhizobium BTAi-1 Δshc* clearly interacted with MD2, as evident changes in the intensity of some ^1H signals upon addition of the protein were observed, which probably arised from the changes in the transverse properties of the ligand. Interestingly, the DOSY experiments showed opposite behaviour of both lipopolysaccharides. The diffusion coefficient of *Bradyrhizobium BTAi-1 Δshc* LPS in presence of the MD-2 significantly decreased. This suggests a reorganization of the aggregates which finally resulted in the formation of smaller aggregates, than the LPS by itself. This behavior was previously reported for a lipid A analogue, FP7 (Cighetti, 2014). The result is also in agreement with studies on *Salmonella minnesota Re595* with LPS-binding Protein (LBP) and bactericidal/permeability-increasing protein (BPI), in which the authors reported strong disaggregation of micelles upon addition of the protein. It is worth to add that the LBP is also involved in the recognition pathway

of LPS by innate immune system, which was proven to amplify the signaling at a certain concentration (Tobias, 1997).

Contrarily, the LPS from *A. pasteurianus* possessed lower diffusion coefficient upond addition of MD-2, which arises from reduction of mobility, likey due to changes in the particle shape or increase of its size. Indeed, this hypothesis was supported by the data obtained from Cryo-TEM, where changes of the shape and increase of particle size was observed.

Finally, it was also possible to compare the aggregation of both LPS in aqueous solution using DOSY experiments. The diffusion coefficient of *Acetobacter pasteurianus* was shown to have nearly 40% lower value than *Bradyrhizobium*.

References:

Ali I.A.I., Akakabe Y., Moonmangmee S., Deeraksa A., Matsutani M., Yakushi T., Yamada M., Matsushita K. (2011) Structural characterization of pellicle polysaccharides of *Acetobacter tropicalis* SKU1100 wild type and mutant strains. C*arbohyd. Polym. 86(2),* 1000-1006.

Bligh E.G., Dyer W.J. (1959) A rapid method of total lipid extraction and purification. *Can. J. Biochem. Phys. 37(8),* 911-917.

Casabuono A.C., Czibener C., Del Giudice C.M.G., Valguarnera E., Ugalde J.E., Couto A.S. (2017) New Features in the Lipid A Structure of *Brucella suis* and *Brucella abortus* Lipopolysaccharide. *J. Am. Soc. Mass Spectrom. 28(12),* 2716-2723.

Choma A., Komaniecka I., Turska-Szewczuk A., Danikiewicz W., Spolnik G. (2012) Structure of lipid A from a stem-nodulating bacterium *Azorhizobium caulinodans*. *Carbohyd. Res. 352,* 126-136.

Cighetti R., Ciaramelli C., Sestito S.E., Zanoni I., Kubik Ł., Ardá-Freire A., Calabrese V., Granucci F., Jerala R., Martín-Santamaría S., Jiménez-Barbero J., Peri F. (2014) Modulation of CD14 and TLR4·MD-2 activities by a synthetic lipid A mimetic. *Chembiochem. 15(2),* 250-258.

Ciucanu I., Kerek F. (1984) A simple and rapid method for the permethylation of carbohydrates. *Carbohydr. Res. 131,* 209–217.

De Castro C., Carannante A., Lanzetta R., Lindner B., Nunziata R., Parrilli, M., Holst O. (2006a) Structural characterisation of the core oligosaccharides isolated from the lipooligosaccharide fraction of *Agrobacterium tumefaciens* A1. *Chem. Eur. J. 12(17),* 4668-4674.

De Castro C., Carannante A., Lanzetta R., Liparoti V., Molinaro A., Parrilli M. (2006b) Core oligosaccharide structure from the highly phytopathogenic *Agrobacterium tumefaciens* TT111 and conformational analysis of the putative rhamnan epitope. *Glycobiology 16(12),* 1272-1280.

De Castro C., Parrilli M., Holst O., Molinaro A. (2010) Microbe-associated molecular patterns in innate immunity: extraction and chemical analysis of gram-negative bacterial lipopolysaccharides. *Methods Enzymol. 480,* 89-115.

Di Lorenzo F., Paciello I., Fazio L.L., Albuquerque L., Sturiale L., Da Costa M.S., Lanzetta R., Parrilli M., Garozzo D., Bernardini M.L., Silipo A., Molinaro A. (2014) Thermophiles as potential source of novel endotoxin antagonists: the

full structure and bioactivity of the lipo-oligosaccharide from *Thermomonas hydrothermalis. Chembiochem. 15(14),* 2146-2155.

Di Lorenzo F., Palmigiano A., Al Bitar-Nehme S., Sturiale L., Duda K.A., Gully D., Lanzetta R., Giraud E., Garozzo D., Bernardini M.L., Molinaro A., Silipo A. (2017) The Lipid A from *Rhodopseudomonas palustris* Strain BisA53 LPS Possesses a Unique Structure and Low Immunostimulant Properties. *Chem. Eur. J. 23,* 3637-3647.

Doyle M.P., Steenson L.R., Meng J. (2013) Bacteria in Food and Beverage Production. In The Prokaryotes (Eds. Rosenberg E., DeLong E.F., Lory S., Stackebrandt E., Thompson F.). Springer, Berlin, Heidelberg, Germany, pp. 241-256.

Facchini F.A., Zaffaroni L., Minotti A., Rapisarda S., Calabrese V., Forcella M., Fusi P., Airoldi C., Ciaramelli C., Billod J.M., Schromm A.B., Braun H., Palmer C., Beyaert R., Lapenta F., Jerala R., Pirianov G., Martin-Santamaria S., Peri F. (2018) Structure-Activity Relationship in Monosaccharide-Based Toll-Like Receptor 4 (TLR4) Antagonists. *J. Med. Chem. 61(7),* 2895-2909.

Forsberg L.S., Carlson R.W.J. (1998) The Structures of the Lipopolysaccharides from Rhizobium etli Strains CE358 and CE359. The complete structure of the core region of R. etli lipopolysaccharides**.** Biol. Chem. 273(5), 2747-2757.

Fox C.B., Friede M., Reed S.G., Ireton G.C. (2010) Synthetic and Natural TLR4 Agonists as Safe and Effective Vaccine Adjuvants. In Sub-cellular biochemistry 53. Endotoxins: Structure, Function and Recognition (Eds. Wang X., Quinn P.J.). Springer, Dordecht, Heidelberg, London, New York, pp 303 - 322

García-Verdugo I., Sánchez-Barbero F., Soldau K., Tobias P.S., Casals C. (2005) Interaction of SP-A (surfactant protein A) with bacterial rough lipopolysaccharide (Re-LPS), and effects of SP-A on the binding of Re-LPS to CD14 and LPS-binding protein. *Biochem. J. 391(Pt 1),* 115-124.

Grimmecke H.D., Knirel Y.A., Shashkov A.S., Kiesel B., Lauk W., Voges M. (1994) Structure of the capsular polysaccharide and the O-side-chain of the lipopolysaccharide from *Acetobacter methanolicus* MB 70, and of oligosaccharides resulting from their degradation by the bacteriophage Acm6. *Carbohyd. Res. 253,* 277-282.

Grimmecke H.D., Mamat U., Lauk W., Shashkov A.S., Knirel Y.A., Vinogradov E.V., Kochetkov N.K. (1991) Structure of the capsular polysaccharide and the O-side-chain of the lipopolysaccharide from *Acetobacter methanolicus* MB

58/4 (IMET 10945), and of oligosaccharides resulting from their degradation by the bacteriophage Acml. *Carbohyd. Res. 220,* 165-172.

Gutsmann T., Schromm A.B., Brandenburg K. (2007) The physicochemistry of endotoxins in relation to bioactivity. *Int. J. Med. Microbiol. 297(5),* 341-352.

Hanuszkiewicz A., Hübner G., Vinogradov E., Lindner B., Brade L., Brade H., Debarry J., Heine H., Holst O. (2008) Structural and immunochemical analysis of the lipopolysaccharide from *Acinetobacter lwoffii* F78 located outside Chlamydiaceae with a Chlamydia-specific lipopolysaccharide epitope. *Chem. Eur. J. 14(33),* 10251-10258.

Hashimoto M., Matsumoto T., Tamura-Nakano M., Ozono M., Hashiguchi S., Suda Y. (2017) Characterization of outer membrane vesicles of *Acetobacter pasteurianus* NBRC3283. *J. Biosci. Bioeng. 125(4),* 425-431.

Hashimoto M., Obara K., Ozono M., Furuyashiki M., Ikeda T., Suda Y., Fukase K., Fujimoto Y., Shigehisa H. (2013) Separation and characterization of the immunostimulatory components in unpolished rice black vinegar (kurozu). *J. Biosci. Bioeng. 116(6),* 688-696.

Hashimoto M., Ozono M., Furuyashiki M., Baba R., Hashiguchi S., Suda Y., Fukase K., Fujimoto Y. (2016) Characterization of a Novel D-*Glycero*-D-*talo*-oct-2-ulosonic acid-substituted Lipid A Moiety in the Lipopolysaccharide Produced by the Acetic Acid Bacterium *Acetobacter pasteurianus* NBRC 3283. *J. Biol. Chem. 291(40),* 21184-21194.

Holst, O. (2011) Structure of the lipopolysaccharide core region. In Bacterial Lipopolysaccharides (Eds. Knirel Y.A., Valvano M.A.). Springer-Verlag, Vienna, Austria, pp 21-39.

Komaniecka I., Choma A., Lindner B., Holst O. (2010) The Structure of a Novel Neutral Lipid A from the Lipopolysaccharide of *Bradyrhizobium elkanii* Containing Three Mannose Units in the Backbone. *Chem. Eur. J. 16,* 2922-2929.

Lembo-Fazio L., Billod J.-M., Di Lorenzo F., Paciello I., Pallach M., Vaz-Francisco S., Holgado A., Beyaert R., Fresno M., Shimoyama A., Lanzetta R., Fukase K., Gully D., Giraud E., Martín-Santamaría S., Bernardini M.-L., Silipo A. (2018) *Bradyrhizobium* Lipid A: Immunological Properties and Molecular Basis of Its Binding to the Myeloid Differentiation Protein-2/Toll-Like Receptor 4 Complex. Front. Immunol. 9, e1888.

Leone S., Molinaro A., Pessione E., Mazzoli R., Giunta C., Sturiale L., Garozzo D., Lanzetta R., Parrilli M. (2006) Structural elucidation of the core-lipid A

backbone from the lipopolysaccharide of *Acinetobacter radioresistens* S13, an organic solvent tolerating Gram-negative bacterium. *Carbohydr. Res. 341,* 582-590.

Lucas L.H., Larive C.K. (2004) Measuring ligand-protein binding using NMR diffusion experiments. *Concepts Magn. Reson. 20A(1),* 24-41.

Malgorzata-Miller G., Heinbockel L., Brandenburg K., van der Meer J.W.M., Netea M.G., Joostena L.A.B. (2016) *Bartonella quintana* lipopolysaccharide (LPS): structure and characteristics of a potent TLR4 antagonist for in-vitro and in-vivo applications. *Sci. Rep. 6,* e34221.

Marchetti R., Perez S., Arda A., Imberty A., Jimenez-Barbero J., Silipo A., Molinaro A. (2016) Rules of Engagement" of Protein-Glycoconjugate Interactions: A Molecular View Achievable by using NMR Spectroscopy and Molecular Modeling. *ChemistryOpen. 5(4),* 274-296.

Molinaro A., De Castro C., Lanzetta R., Parrilli M., Raio A., Zoina A. (2003) Structural elucidation of a novel core ligosaccharide backbone of the lipopolysaccharide from the new bacterial species *Agrobacterium larrymoorei*. *Carbohydr. Res. 338,* 2721-2730.

Molinaro A., Holst O., Di Lorenzo F., Callaghan M., Nurisso A., D'Errico G., Zamyatina A., Peri F., Berisio R., Jerala R., Jiménez-Barbero J., Silipo A., Martín-Santamaría S. (2015) Chemistry of Lipid A: At the Heart of Innate Immunity. *Chem. Eur. J. 21,* 500-519.

Molinaro A., Piscopo V., Lanzetta R., Parrilli M. (2002) Structural determination of the complex exopolysaccharide from the virulent strain of *Cryphonectria parasitica*. *Carbohydr. Res. 337(19),* 1707-1713.

Mueller M., Lindner B., Kusumoto S., Fukase K., Schromm A.B., Seydel U. (2004) Aggregates are the biologically active units of endotoxin. *J. Biol. Chem. 279,* 26307-26313.

Nanda K., Miyoshi N., Nakamura Y., Shimoji Y., Tamura Y., Nishikawa Y., Uenakai K., Kohno H., Tanaka T. (2004) Extract of vinegar "Kurozu" from unpolished rice inhibits the proliferation of human cancer cells. *J. Exp. Clin. Cancer Res. 23(1),* 69-75.

Nanda K., Taniguchi M., Ujike S., Ishihara N., Mori H., Ono H., Murooka Y. (2001) Characterization of acetic acid bacteria in traditional acetic acid fermentation of rice vinegar (komesu) and unpolished rice vinegar (kurosu) produced in Japan. *Appl. Environ. Microbiol. 67,* 986-990.

Previato J.O., Jones C., Stephan M.P., Almeida L.P.A., Mendonça-Previato L. (1997) Structure of the repeating oligosaccharide from the lipopolysaccharide of the nitrogen-fixing bacterium *Acetobacter diazotrophicus* strain PAL 5. *Carbohyd. Res. 298,* 311–318.

Que-Gewirth N.L., Ribeiro A.A., Kalb S.R., Cotter R.J., Bulach D.M., Adler B., Girons I.S., Werts C., Raetz C.R. (2004) A Methylated Phosphate Group and Four Amide-linked Acyl Chains in Leptospira interrogans Lipid A the membrane anchor of an unusual lipopolysaccharide that activates TLR2. *J. Biol. Chem. 279(24),* 25420 -25429.

Rietschel E.T., Krikae T., Schade F.U., Mamat U., Schmidt G., Loppnow H., Ulmer A.J., Zahringer U., Seydel U., Di Padova F., Schreier M., Brade H. (1994) Bacterial endotoxin: molecular relationships of structure to activity and function. *FASEB J. 8,* 217-225.

Santos N.C., Silva A.C., Castanho M.A., Martins-Silva J., Saldanha C. (2003) Evaluation of lipopolysaccharide aggregation by light scattering spectroscopy. *Chembiochem. 4(1),* 96-100.

Schromm A.B., Howe J., Ulmer A.J., Wiesmüller K.-H., Seyberth T., Jung G., Rössle M., Koch M.H.J., T. Gutsmann T., Brandenburg K. J. (2007) Physicochemical and Biological Analysis of Synthetic Bacterial Lipopeptides: validity of the concept of endotoxic conformation. *J. Biol. Chem. 282,* 11030-11037.

Sengun I.Y., Karabiyikli S. (2011) Importance of acetic acid bacteria in food industry. *Food Control. 22(5),* 647-656.

Shimoji Y., Sugie S., Kohno H., Tanaka T., Nanda K., Tamura Y., Nishikawa Y., Hayashi R., Uenakai K., Ohigashi H. (2003) Extract of vinegar "Kurozu" from unpolished rice inhibits the development of colonic aberrant crypt foci induced by azoxymethane. *J. Exp. Clin. Cancer Res., 22(4),* 591-597.

Shimoji Y., Tamura Y., Nakamura Y., Nanda K., Nishidai S., Nishikawa Y., Ishihara N., Uenakai K., Ohigashi H. (2002) Isolation and identification of DPPH radical scavenging compounds in Kurozu (Japanese unpolished rice vinegar). *J. Agric. Food Chem. 50(22),* 6501-6503.

Silipo A., Molinaro A., Nazarenko E.L., Sturiale L., Garozzo D., Gorshkova R.P., Nedashkovskaya O.I., Lanzetta R., Parrilli M. (2005) Structural characterization of the carbohydrate backbone of the lipooligosaccharide of the marine bacterium *Arenibacter certesii* strain KMM 3941(T). *Carbohydr. Res. 340(16),* 2540-2549.

Silipo A., Vitiello G., Gully D., Sturiale L., Chaintreuil C., Fardoux J., Gargani D., Lee H.I., Kulkarni G., Busset N., Marchetti R., Palmigiano A., Moll H., Engel R., Lanzetta R., Paduano L., Parrilli M., Chang W.S., Holst O., Newman D.K., Garozzo D., D'Errico G., Giraud E., Molinaro A. (2014) Covalently linked hopanoid-lipid A improves outer-membrane resistance of a Bradyrhizobium symbiont of legumes. *Nat. Commun. 5,* e5106.

Sturiale L., Garozzo D., Silipo A., Lanzetta R., Parrilli M., Molinaro A. (2005) New conditions for matrix-assisted laser desorption/ionization mass spectrometry of native bacterial R-type lipopolysaccharides. *Rapid Commun. Mass Spectrom. 19*, 1829-1834.

Sweet C.R., Ribeiro A.A., Raetz C.R. (2004) Oxidation and transamination of the 3"-position of UDP-N-acetylglucosamine by enzymes from *Acidithiobacillus ferrooxidans*. Role in the formation of lipid a molecules with four amide-linked acyl chains. *J. Biol. Chem. 279(24),* 25400-25410.

Tobias P.S., Soldau K., Iovine N.M, Elsbach P. Weiss J. (1997) Lipopolysaccharide (LPS)-binding Proteins BPI and LBP Form Different Types of Complexes with LPS. *J. Biol. Chem. 272(30),* 18682-18685.

van Mourik A., Steeghs L., van Laar J., Meiring H.D., Hamstra H.J., van Putten J.P., Wösten M.M. (2010) Altered linkage of hydroxyacyl chains in lipid A of *Campylobacter jejuni* reduces TLR4 activation and antimicrobial resistance. *J. Biol. Chem. 285,* 15828–15836.

Vinion-Dubiel A.D., Goldberg J.B. (2003) Lipopolysaccharide of *Burkholderia cepacia* complex. *J. Endotoxin Res. 9*, 201–213.

Vinogradov E.V., Duus J., Brade H., Holst O. (2002) The structure of the carbohydrate backbone of the Lipopolysaccharide from *Acinetobacter baumannii* strain ATCC 19606. *Eur. J. Biochem. 269,* 422-430.

Vinogradov E.V., Müller-Loennies S., Petersen B.O., Meshkov S., Thomas-Oates J.E., Holst O., Brade H. (1997) Structural investigation of the lipopolysaccharide from *Acinetobacter haemolyticus* strain NCTC 10305 (ATCC 17906, DNA group 4). *Eur. J. Biochem. 247(1),* 82-90.

Westphal O., Jann K. (1965) Bacterial lipopolysaccharides: extraction with phenol-water and further applications of the procedure. *Methods Carbohydr. Chem., 5,* 83–91.

Yamada Y., Yukphan P. (2008) Genera and species in acetic acid bacteria. *Int. J. Food. Microbiol. 125(1*), 15-24.

Yan J., Kline A.D., Mo H., Zartler E.R., Shapiro M.J., (2002) Epitope mapping of ligand-receptor interactions by diffusion NMR. *J. Am. Chem. Soc. 124,* 9984–9985.

Yokota A., Rodriguez M., Yamada Y., Imai K., Borowiak D., Mayer H. (1987) Lipopolysaccharides of *Thiobacillus* species containing lipid A with 2,3-diamino-2,3 dideoxyglucose. *Arch. Microbiol. 149,* 106-111.

Zamłyńska K., Komaniecka I., Zebracki K., Mazur A., Sroka-Bartnicka A., Choma A. (2017) Studies on lipid A isolated from *Phyllobacterium trifolii* PETP02^{T} lipopolysaccharide. *A. Van. Leeuw. J. Microb. 110,* 1413-1433.

Chapter IV

Endozoicomonas sp. HEX 311

Premise

Marine sponges (phylum Porifera) are home for complex and diverse microbial communities, which can make up to 35 % of the sponge biomass (Taylor, 2007; Schmitt, 2012; Hentschel, 2012). Among the 47 phyla found in such marine organisms, some are specifically associated with sponges, creating a phylum known as Poribacteria (Fieseler, 2004; Reveillaud, 2014). The latter can be involved in sponge feeding but also virulence and symbiotism (Böhm, 2001; Lee, 2001; Hadas, 2009). This implies that a mechanism able to recognize and discriminate between pathogens and beneficial bacterial partners is likely present in marine sponges. However, the mechanisms underlying such a fine detection are still obscure. Within this frame, it has been shown that sponges possess an efficient innate immune system resembling the mammalian one, which is able to recognize Gram-positives, through binding to the proteoglycan, and Gram-negatives through recognition of the outer membrane lipopolysaccharide (Wiens, 2005).

Moreover, Wiens et al. (2005) demonstrated that the marine demosponge *Suberites domuncula* recognizes LPS through a transmembrane receptor, named *S. domuncula* LPS Interacting Protein (SLIP), that upon LPS binding and similarly to what happens in mammals, it dimerizes leading to the recruitment of the immune system adaptive protein of the Myeloid Differentiation factor 88 (MyD88). This leads to the activation of specific MAP kinases pathways, resulting in over-expression of the perforin-like protein termed MPEG (macrophage-expressed protein) which has a toxic effect on Gram-negative bacteria. This represents a further confirmation that sponges own the molecular instruments to combat pathogenic microbes.

It is important to underline that *S. domuncula* harbours a large microbioma, including not only opportunistic and pathogenic bacteria, but also commensals such as *Endozoicomonas* sp. HEX311. As a Gram-negative, *Endozoicomonas* sp. HEX311 exhibits LPS on its surface thus it can be recognized by SLIP and consequently can elicit an inflammatory process (Gardères, 2015). On the contrary, *Endozoicomonas* sp. HEX311 is tolerated by the sponge acting as a beneficial symbiont required for healthy host (Neave, 2016). In this context, it was previously reported about structural differences in the lipid A moiety observed between the

S. domuncula commensal *Pseudoalteromonas* sp. 2A and its pathogenic counterpart *Pseudoalteromonas* sp. 1A1 (Di Lorenzo, 2017a). The slightly different structures might be responsible for the diverse biological activity exerted by the two *Pseudoalteromonas* species and further studies are ongoing in order to shed light on this fundamental aspect. Meanwhile, the structural characterization of other sponge-associated commensal LPS may furnish more details on how structural features of LPSs may affect the activation/modulation of the sponge immune system as well as on its role in the establishment of a symbiotic or a pathogenic relationship with the host sponge.

Furthermore, as a potent stimulator of mammalian immune response, noticeable efforts have been made so far to identify natural or ad hoc synthesized lipid A able to interfere or modulate immune/inflammatory responses mediated by toxic lipid A, such as Eritoran (Christ, 1995; Fox, 2010). The latter is a well-tolerated, synthetic lipid A mimetic, acting as a TLR4/MD-2 inhibitor, which reached phase III clinical trials as an antisepsis agent; the model of inspiration for synthesis of such a TLR4/MD-2 antagonist was the lipid A from *Rhodobacter sphaeroides* and *R. capsulatus*, two phototrophic bacteria found in freshwater or marine environments (Christ, 1995) (see Chapter 1.9). In this context, the not human pathogen/human associated nature of *Endozoicomonas* strains, in addition to the still unresolved mechanisms at the basis of sponge-associated LPS immunopotency, render the *Endozoicomonas* sp. HEX311 LPS an intriguing molecule to be investigated both under the structural and immunological point of view.

In this scenario, here is reported the characterization of *Endozoicomonas* sp. HEX311 lipid A structure achieved by merging data that were attained from the fatty acid and sugar compositional analyses performed on pure LPS with information derived from a matrix-assisted laser desorption ionization (MALDI) mass spectrometry (MS) and MS^2 study executed on both the isolated lipid A fraction and on the intact bacterial pellet.

4.1 Isolation

The lipopolysaccharide was extracted from dried cell pellet applying the hot phenol-water protocol (Westphal & Jann, 1965). The

isolated material was purified by means of enzymatic digestion followed by extensive dialysis and ultracentrifugation. The purity and nature of the LPS was determined on the basis of DOC-PAGE electrophoresis followed by silver staining, revealing presence of S-LPS

4.2 Compositional analysis

An aliquot of pure S-LPS underwent monosaccharide and fatty acid compositional study. In details, sugar content investigation (De Castro, 2010) unveiled the presence of L-arabinose (Ara), D-mannose (Man), D-glucose (Glc), D-galactose (Gal), 2-amino-2-deoxy-D-glucose (GlcN), 2-amino-2-deoxy-D-galactose (GalN) and 3-deoxy-D-manno-oct-2-ulosonic acid (Kdo). Linkage analysis (Ciucanu & Kerek, 1984) on intact S-LPS revealed the presence of terminal Ara, terminal, 4-substituted and 6-substituted Man, terminal Gal, terminal and 3-substituted Glc, 6-substituted GlcN, 3-substituted GalN and 5-substituted Kdo. The fatty acid compositional analysis revealed that *Endozoicomonas* sp. HEX311 lipid A was mainly composed of *iso*-2-hydroxyundecanoic acid (*iso*-11:0 (2-OH)), *iso*-(*R*)-3-hydroxyundecanoic acid (*iso*-11:0 (3-OH)), (*R*)-3-hydroxydodecanoic acid (12:0 (3-OH)), (*R*)-3-hydroxytetradecanonic acid (14:0 (3-OH)) and *iso*-nonanoic acid (*iso*-9:0). As minor species, *iso*-2-hydroxynonanoic acid (*iso*-9:0 (2-OH)), *iso*-undecanoic acid (*iso*-11:0) and dodecanoic acid (12:0) were also identified. The absolute configuration of the two 2-OH fatty acids remains to be defined. The calculated percentage of the fatty acids composing the *Endozoicomonas* sp. HEX311 lipid A is reported in Table 4.1.

Table 4.1. Semi-quantitative compositional analysis of *Endozoicomonas* sp. HEX311 fatty acids. The percentage of each residue, attained from integrated areas of the peaks eluted from the GC-MS, is also reported

Component	% of total fatty acids
9:0	16.4
9:0(2-OH)	1.2
11:0	1.8
11:0(2-OH)	14.8
11:0(3-OH)	15.2
12:0	2.0
12:0(3-OH)	32.2

14:0(3-OH)	16.4

4.3 MALDI-TOF and MS^2

The complete structural characterization of *Endozoicomonas* sp. HEX311 lipid A was performed applying extensive MALFI-TOF and MS^2 analysis. In order to cleave the acid-labile α-ketosidic linkage between the Kdo and the lipid A, an aliquot of *Endozoicomonas* sp. HEX311 S-LPS underwent mild acid hydrolysis. The glycolipid fraction was recovered using the Bligh-Dyer extraction (Bligh & Dyer, 1959) and underwent detailed analysis by MALDI and MS^2. Parallel MALDI investigation was executed on the bacterial pellet, following Larrouy-Maumus technique order to obtain structural information on the native, not-treated lipid A (Larrouy-Maumus, 2016).

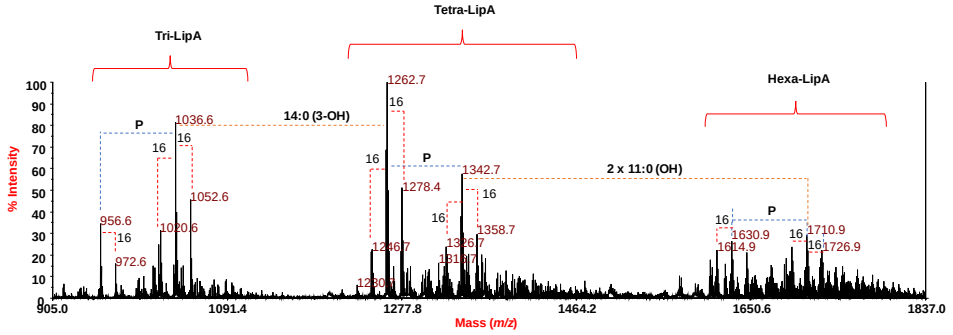

Figure 4.1. Negative ion reflectron MALDI mass spectrum, *Endozoicomonas* sp. HEX311 lipid A. Tri-, tetra and hexa-acylated lipid A species are outlined.

The reflectron MALDI mass spectrum, recorded in negative polarity, executed on the mild acid hydrolysis product is reported in Figure 4.1. The spectrum highlighted, in the range *m/z* 956.6–1726.9, a heterogeneous pattern of peaks relative to deprotonated $[M - H]^-$ lipid A species differing in the nature and number of fatty acid chains and in phosphate content. Three distinct family of peaks around *m/z* 1036.6, 1262.7 and 1710.9 were clearly apparent and matched with tri-, tetra-, and hexa-acylated lipid A species (Figure 4.1). A 16 amu difference (Δ*m/z* = ± 16) found for signals within each cluster was attributed to the loss or the additional presence of an oxygen atom, suggesting the absence or the substitution of hydroxylated fatty acids in both tri-, tetra- and hexa-acylated lipid A forms. Furthermore, differences of 80 amu (Δ*m/z* = 80),

diagnostic for the occurrence of a further phosphate unit were also detected, likely suggesting the presence of a pyrophosphate group decorating the lipid A sugar backbone. In detail and on the basis of fatty acid compositional analysis, the ion at *m/z* 1262.7 was attributed to a *bis*-phosphorylated tetra-acylated lipid A species carrying two units of 12:0 (3-OH), one 14:0 (3-OH) and one *iso*-9:0. The relative lipid A form carrying an additional phosphate group was also assignable to the species at *m/z* 1342.7 (Figure 4.1). A *bis*-phosphorylated tri-acylated lipid A species lacking the 14:0 (3-OH) unit with the respect to species at *m/z* 1262.7 was assigned to the peak at *m/z* 1036.6, whose *mono*-phosphorylated form could be also attributed to the peak at *m/z* 956.6. Finally, the mass range *m/z* 1614.9 - 1726.9 showed a less intense cluster of peaks compatible with *bis*-hexa-acylated lipid A species carrying two 12:0 (3-OH), one 14:0 (3-OH), one *iso*-9:0 and two hydroxylated *iso*-11:0 fatty acid chains (Figure 4.1). Hexa-acylated species decorated by pyrophosphate and phosphate groups were also detected in the above mass range (Figure 4.1). Notably, the negative-ion MALDI mass spectrum, measured on the intact bacterial pellet confirmed the structural characterization attained from the isolated lipid A fraction.

To delineate the detailed structure of *Endozoicomonas* sp. HEX311 lipid A, disclosing the location of the acyl chains and of the phosphate decorations with respect to the glucosamine disaccharide backbone, a

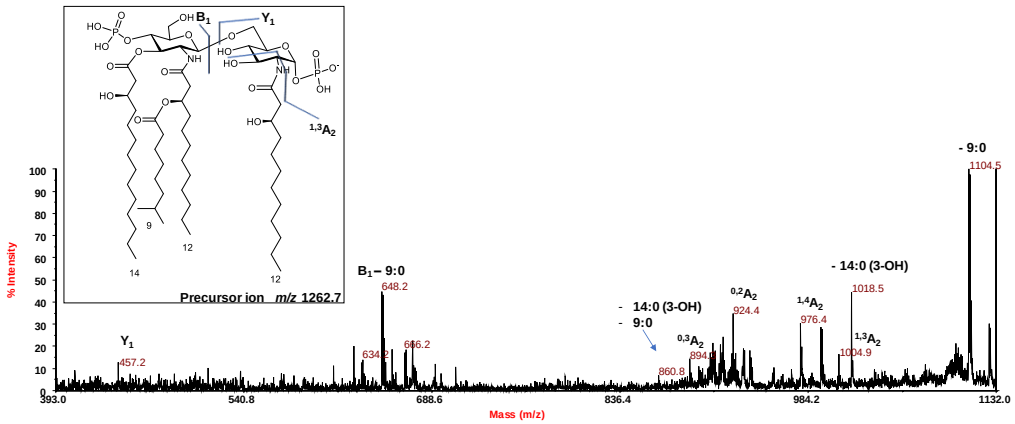

Figure 4.2. Negative-ion MALDI MS^2 spectrum of the tetra-acylated lipid A species at *m/z* 1262.7 from *Endozoicomonas* sp. HEX311. Fragments assignment is reported in the spectrum. In the inset, the proposed structure for the hexa-acylated lipid A species assignable to the precursor ion at *m/z* 1262.7.

negative-ion MS^2 analysis on several peaks was executed. In detail, the MS^2 spectrum of the precursor ion at *m/z* 1262.7 (Figure 4.2), corresponding to a *bis*-phosphorylated tetra-acylated lipid A species, showed two intense peaks at *m/z* 1104.5 and 1018.5 attributed to ions that were derived from the loss of the secondary *iso*-9:0 and the primary 14:0 (3-OH) fatty acids respectively. The observation of both these fragmentations was crucial in terms of the structural characterization. Indeed, the absence of fragments matching with the loss of a whole unit of a hydroxylated fatty acid bearing a secondary acyl substituent in addition to the presence of a fragment originated from a sequential loss of 14:0 (3-OH) and *iso*-9:0 (*m/z* 860.8) from the precursor ion concurred to indicate that the secondary *iso*-9:0 was bound to an *N*-linked primary acyl moiety. Moreover, the observation of several ions originating from sugar ring fragmentations ($^{0,3}A_2$, $^{0,2}A_2$ and $^{1,4}A_2$) (Domon & Costello, 1988), was fundamental to define the nature of the primary fatty acids decorating the non-reducing glucosamine unit (namely, one 14:0 (3-OH) and one 12:0 (3-OH)), and thus to locate the secondary acyl chain *iso*-9:0 only at the non-reducing glucosamine residue. Moreover, the occurrence of the $^{1,3}A_2$ cross-ring fragmentation (*m/z* 1004.9) which takes place only when the hydroxyl group at position 3 of the reducing glucosamine is not substituted, further corroborated the structural hypothesis that the 14:0 (3-OH) was placed at position 3 of the non-reducing glucosamine, and thus

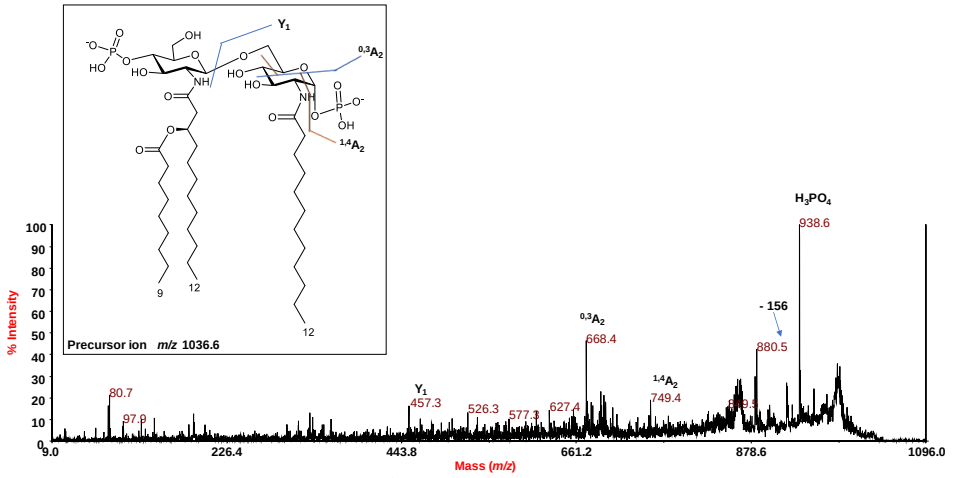

Figure 4.3. Negative-ion MALDI MS^2 spectrum of the hexa-acylated lipid A species at *m/z* 1036.6 from *Endozoicomonas* sp. HEX311. Fragments assignment is reported in the spectrum. In the inset, the proposed structure for the hexa-acylated lipid A species assignable to the precursor ion at *m/z* 1036.6.

that 12:0 (3-OH) and *iso*-9:0 were located at position 2 of the same glucosamine residue as the primary and secondary fatty acids, respectively. Finally, the occurrence of a further important peak originating from the cleavage of the glycosidic linkage (Y_1) at *m/z* 457.2 further confirmed that in the tetra-acylated lipid A form the reducing glucosamine unit only carried one phosphate and one *N*-linked 12:0 (3-OH) unit.

A further confirmation of the structural assessment was obtained by analysing data attained from the negative-ion MS^2 of precursor ion at *m/z* 1036.6 relative to the tri-acylated lipid A species lacking the primary ester-linked 14:0 (3-OH) (Figure 4.3). Indeed, mass spectrum clearly showed cross-ring fragmentations (namely $^{0,3}A_2$ and $^{1,4}A_2$) crucial to locate both the phosphate and the acyl chains.

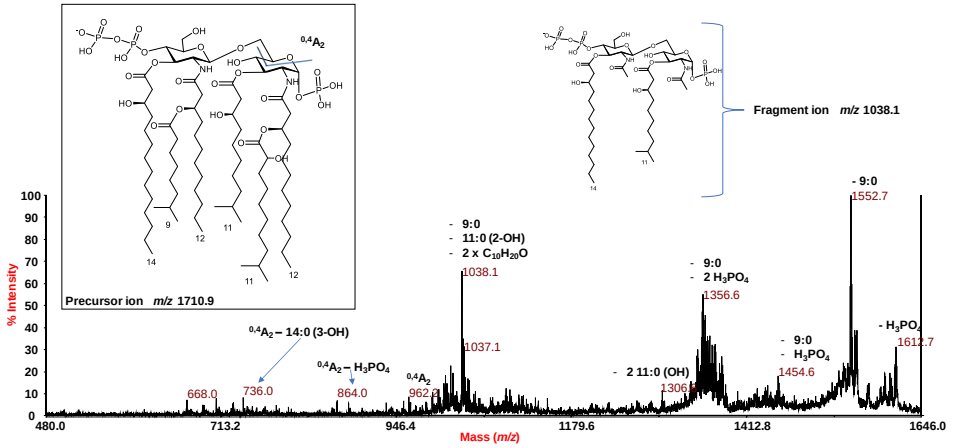

Figure 4.4. Negative-ion MALDI MS^2 spectrum of the hexa-acylated lipid A species at *m/z* 1710.9 from *Endozoicomonas* sp. HEX311. Fragments assignment is reported in the spectrum. In the inset, the proposed structure for the hexa-acylated lipid A species assignable to the precursor ion at *m/z* 1710.9.

The negative-ion MS^2 analysis of precursor ion at *m/z* 1710.9 (Figure 4.4.), corresponding to the hexa-acylated lipid A species carrying the pyrophosphate and the phosphate groups, was fundamental to define the location of the phosphate decorations and of the two hydroxylated *iso*-11:0 acyl moieties with the respect to the disaccharide backbone. In detail, MS^2 spectrum revealed an intense peak at *m/z* 1552.7 attributed to a fragment devoid of the secondary *iso*-9:0 acyl chain; the relative fragments lacking also one and two phosphate units were detected at

m/z 1454.6 and 1356.6. A further intense and important peak, at *m/z* 1038.1, was assigned to a fragment originating from a rearrangement following the loss of the secondary acyl chains. Indeed, the observation of a loss of 672 mass units, matching with the sequential loss of one *iso*-9:0 and one *iso*-11:0 (2-OH) plus 312 mass units, led to the conclusion that after the removal of the secondary fatty acids a rearrangement, promoted by the free 3-OH groups on the 12:0, drove the loss of 156 mass units ($C_{10}H_{20}O$) from each primary *N*-linked acyl chain (Di Lorenzo, 2017c).

Since such a fragmentation occurred only when the *iso*-9:0 and *iso*-11:0 (2-OH) units were absent, it was crucial to establish the location of the latter as a secondary acyl substituent of the primary *N*-linked 12:0 (3-OH) moiety of the reducing glucosamine unit. In support to this hypothesis, other cross-ring fragmentations were observed such as that visible at *m/z* 962.2 attributed to a $^{0,4}A_2$ fragment, whose relatives devoid of one phosphate or one 14:0 (3-OH) units were also detected at *m/z* 864.0 and 736.0 respectively. These fragmentations were also helpful in locating the pyrophosphate group only at the 4' position of the non-reducing glucosamine unit. Finally, at *m/z* 1612.7 a lipid A fragment devoid of one phosphate group was also identified as well as a fragment derived from the sequential loss of both the hydroxylated *iso*-11:0 residues (*m/z* 1306.6). Once again, the absence of a fragment derived for the loss of an entire hydroxylated fatty acid bearing a secondary acyl substituent definitively confirmed the occurrence of the *iso*-11:0 (2-OH) as a secondary fatty acid of the acyloxyamide decorating the reducing glucosamine unit. Similarly, negative-ion MS^2 analysis of precursor ion at *m/z* 1342.7, relative to the tetra-acylated form lacking the two hydroxylated *iso*-11:0 and carrying one pyrophosphate and one phosphate unit, confirmed the above *Endozoicomonas* sp. HEX311 lipid A structural assessment (not shown).

Finally, in order to unambiguously determine the nature and location of the secondary fatty acids, an aliquot of lipid A was *O*-deacylated through ammonium hydroxide hydrolysis (Silipo, 2002). The MALDI mass spectrum, recorded in negative polarity, (Figure 4.5.) of the ammonium-treated lipid A showed (i) the ion at *m/z* 1036.3, which was assigned to a *bis*-phosphorylated tri-acyl residue composed of both the primary *N*-linked 12:0 (3-OH) and the secondary *iso*-9:0 unit, (ii) the ion at *m/z* 896.3, which was explained as the *bis*-phosphorylated di-acyl residue composed only of the *N*-linked primary acyl moieties 12:0 (3-OH) and (iii) a less intense ion at *m/z* 1220.3 matching with a *bis*-phosphorylated tetra-acyl residue built up of the primary amide-bound 12:0 (3-OH) units carrying their respective secondary acyl substituents (Figure 4.6). The occurrence of these peaks further corroborated the nature of the amide-bound fatty acids and the occurrence of *iso*-9:0 and *iso*-11:0 (2-OH) as secondary fatty acids in an acyloxyacyl amide moiety. Thus, combining data on intact LPS and cells with those from the mild acid hydrolysis and ammonium treated products, it was possible to define the *Endozoicomonas* sp. HEX311 S-LPS as expressing a complex blend of lipid A species whose main component with the highest acylation degree is shown in Figure 4.6.

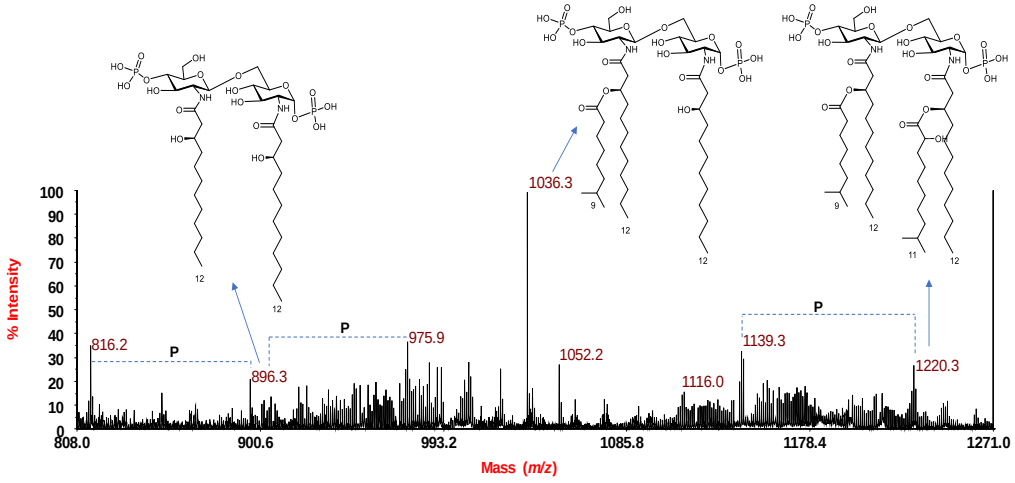

Figure 4.5. Negative ion reflectron MALDI mass spectrum, *Endozoicomonas* sp. HEX311 lipid A obtained from ammonium hydroxide hydrolysis. The proposed structure of the products is reported in the figure.

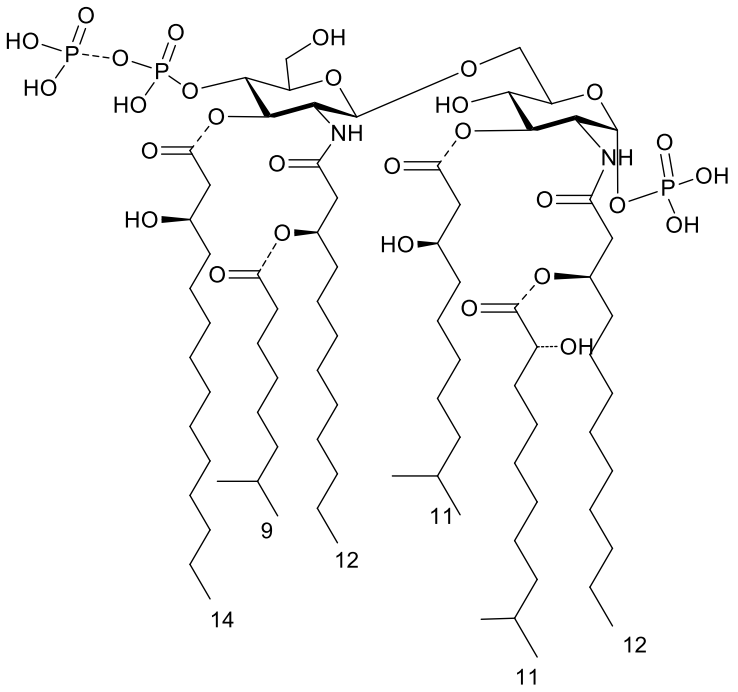

Figure 4.6. The proposed structure of *Endozoicomonas* sp. HEX311 lipid A. The non-stoichiometric substitutions are indicated as dotted lines.

4.4. Discussion

The observed structural features of the *Endozoicomonas* sp. HEX311 lipid A may explain the absence of an immune response by the sponge against the bacterium, thus suggesting that the LPS recognition might be similar to the mammalian one. Indeed, as previously mentioned, marine sponges possess elements resembling the mammalian innate immune system and in mammals one of the properties strongly connected with activation of TLR4/MD-2-dependent immune response is the number, nature and distribution of the acyl chains (Molinaro, 2015). Hypo-acylated lipid As (namely lipid A species expressing less than six acyl chains) often exhibit low immunostimulatory activity. Moreover, a 4+2 symmetry (presenting a “cone” conformation) has been proven to more favourably establish agonist interactions with TLR4/MD-2 complex whereas a 3+3 symmetry (creating a cylindric conformation) showed to reduce the agonist effect of the whole LPS molecule (Molinaro, 2015).

As demonstrated, *Endozoicomonas* sp. HEX 311 lipid A (Figure 4.6) is mainly composed of tetra- and tri- acylated species, that is highly *hypo*-acylated species that might be poorly recognized by the sponge immune system. Moreover, when hexa-acylated forms occur, these present a 3+3 distribution of the acyl chains, which are also typically correlated to a weak immunopotential (Molinaro, 2015; Di Lorenzo, 2017b, 2017c, 2017d, 2018). Therefore, the expression of a lipid A with structural features leading to a weak immunoactivity might be a key requirement to establish a successful symbiosis between the microbe and the sponge. Finally, the *Endozoicomonas* sp. HEX 311 lipid A was found to possess uncommon features such as the odd-numbered fatty acids reported for other marine bacteria including *Shewanella pacifica* KMM 3772 (Silipo, 2005), *Arenibacter certesii* KMM 3941^T (Leone, 2007), *Pseudoalteromonas haloplanktis* ATCC 14393^T (Krasikova, 2003) or *Chryseobacterium scophtalmum* CIP 104199^T (Vorobeva, 2006). The occurrence of both odd-numbered as well as very short acyl chains (*iso*-9:0) might also have a role in the establishment of the symbiotic process as it was previously demonstrated that not only the amount, but also the length of the fatty acids is required for a proper TLR4/MD-2 activation with a minimum length of eight and an optimal length of ten carbon atoms (Stöver, 2004).

In conclusion, all the above described structural features (the occurrence mainly of hypo-acylated species, the 3+3 symmetry of the hexa-acylated forms and the presence of both very short and odd-numbered fatty acids render *Endozoicomonas* sp. HEX 311 lipid A a potential TLR4/MD-2 poor agonist whose immunological properties are also worth being investigated, since they can potentially provide interesting information useful both in the comprehension of the molecular mechanisms underlying the sponge-bacterium interaction process but also under the future perspective of the development of derivative compounds with an immunomodulatory action on the immune system (see Chapter 1.3.1 and 1.8.).

References:

Bligh E.G., Dyer W.J. (1959) A rapid method of total lipid extraction and purification. *Can. J. Biochem. Phys. 37,* 911-917.

Böhm M., Hentschel U., Friedrich A., Fieseler L., Steffen R., Gamulin V., Müller I.M., Müller W.E.G. (2001) Molecular response of the sponge *Suberites domuncula* to bacterial infection. *Mar. Biol. 139,* 1037-1045.

Ciucanu I., Kerek F. (1984) A simple and rapid method for the permethylation of carbohydrates. *Carbohydr. Res. 131,* 209-217.

Di Lorenzo F. (2017a) The lipopolysaccharide lipid A structure from the marine sponge-associated bacterium *Pseudoalteromonas* sp. 2A. *Antonie Leeuwenhoek 110,* 1401-1412.

Di Lorenzo F., Billod J.-M., Martín-Santamaría S., Silipo A., Molinaro A. (2017b) Gram-negative extremophile lipopolysaccharides: promising source of inspiration for a new generation of endotoxin antagonists. Eur. *J. Org. Chem.,* 4055-4073.

Di Lorenzo F., Palmigiano A., Al Bitar-Nehme S., Sturiale L., Duda K.A., Gully D., Lanzetta R., Giraud E., Garozzo D., Bernardini M.L., Molinaro A., Silipo A. (2017c) The Lipid A from *Rhodopseudomonas palustris* Strain BisA53 LPS Possesses a Unique Structure and Low Immunostimulant Properties. *Chem. Eur. J. 23,* 3637-3647.

Di Lorenzo F., Palmigiano A., Albitar-Nehme S., Pallach M., Kokoulin Nadezhda M., Romanenko K.L., Bernardini M.-L., Garozzo D., Molinaro A., Silipo A. (2018) Lipid A Structure and Immunoinhibitory Effect of the Marine Bacterium *Cobetia pacifica* KMM 3879T. *Eur. J. Org. Chem.,* 2707-2716.

Di Lorenzo F., Palmigiano A., Paciello I., Pallach M., Garozzo D., Bernardini M.-L., Cono V., Yakimov M.M., Molinaro A., Silipo A. (2017d) The Deep-Sea Polyextremophile Halobacteroides lacunaris TB21 Rough-Type LPS: Structure and Inhibitory Activity towards Toxic LPS. *Mar. Drugs. 15(7),* e201.

Domon B., Costello C.E. (1988) A systematic nomenclature for carbohydrate fragmentations in FAB-MS/MS spectra of glycoconjugates. *Glycoconj. J. 5,* 397–409.

Fieseler L., Horn M., Wagner M., Hentschel U. (2004) Discovery of the novel candidate phylum "Poribacteria" in marine sponges. *Appl. Environ. Microbiol. 70 (6),* 3724–3732.

Fox C.B., Friede M., Reed S.G., Ireton G.C. (2010) Synthetic and Natural TLR4 Agonists as Safe and Effective Vaccine Adjuvants. In Sub-cellular biochemistry 53. Endotoxins: Structure, Function and Recognition (Eds. Wang X., Quinn P.J.). Springer, Dordecht, Heidelberg, London, New York, pp 303 - 322

Gardères J., Bedoux G., Koutsouveli V., Crequer S., Desriac F., Le Pennec G. (2015) Lipopolysaccharide from commensal and opportunistic bacteria: characterization and response of the immune system of the host sponge *Suberites domuncula*. *Mar. Drugs. 16,* 4985–5006.

Hadas E., Shpigel M., Ilan M. (2009) Particulate organic matter as a food source for a coral reef sponge. *J. Exp. Biol. 212,* 3643–3650.

Hentschel U., Piel J., Degnan S.M., Taylor M.W. (2012) Genomic insights into the marine sponge microbiome. *Nat. Rev. Microbiol. 10,* 641–654.

Krasikova I.N., Kapustina N.V., Isakov, V.V., Gorshkova N.M., Solov'eva, T.F. (2003) Elucidation of structure of lipid A from the marine Gram-negative bacterium *Pseudoalteromonas haloplanktis* ATCC 14393T. *Russ. J. Bioorgan. Chem. 30(4),* 367-373.

Larrouy-Maumus G., Clements A., Filloux A., McCarthy R.R., Mostowy S. (2016) Direct detection of lipid A on intact Gram-negative bacteria by MALDI-TOF mass spectrometry. *J. Microbiol. Methods. 120,* 68-71.

Lee Y.K., Lee J.H., Lee H.K. (2001) Microbial symbiosis in marine sponges. *J. Microbiol. 39,* 254-264.

Leone S., Silipo A., Nazarenko E.L., Lanzetta R., Parrilli M., Molinaro A. (2007) Molecular Structure of Endotoxins from Gram-negative Marine Bacteria: An Update. *Mar. Drugs. 5(3),* 85-112.

Molinaro A., Holst O., Di Lorenzo F., Callaghan M., Nurisso A., D'Errico G., Zamyatina Z., Peri F., Berisio R., Jerala R., Jiménez-Barbero J., Silipo A., Martín-Santamaría S. (2015) Chemistry of Lipid A: At the Heart of Innate Immunity. *Chem. Eur. J., 21,* 500-519.

Neave M.J., Apprill A., Ferrier-Pagès C., Voolstra C.R. (2016) Diversity and function of prevalent symbiotic marine bacteria in the genus Endozoicomonas. *Appl. Microbiol. Biotechnol. 100(19),* 8315-8324.

Reveillaud J., Maignien L., Eren A.M., Huber J.A., Apprill A., Sogin M.L., Vanreusel A. (2014) Host-specificity among abundant and rare taxa in the sponge microbiome. *ISME J. 8,* 1198–1209.

Schmitt S., Tsai P., Bell J., Fromont J., Ilan M., Lindquist N., Perez T., Rodrigo A., Schupp P.J., Vacelet J., Webster N., Hentschel U., Taylor M.W. (2012) Assessing the complex sponge microbiota: Core, variable and species-specific bacterial communities in marine sponges. *ISME J. 6(3),* 564-576.

Silipo A., Lanzetta R., Amoresano A., Parrilli M., Molinaro A. (2002) Ammonium hydroxide hydrolysis: a valuable support in the MALDI-TOF mass spectrometry analysis of Lipid A fatty acid distribution. *J. Lipid Res. 43,* 2188-2195.

Silipo A., Leone S., Molinaro A., Sturiale L., Garozzo D., Nazarenko E.L. Gorshkova R.P., Ivanova E.P., Lanzetta R., Parrilli M. (2005) Complete structural elucidation of a novel lipooligosaccharide from the Outer Membrane of the marine bacterium *Shewanella pacifica*. *Eur. J. Org. Chem. 2005(11),* 2281-2291.

Taylor M.W., Radax R., Steger D., Wagner M. (2007) Sponge-associated microorganisms: Evolution, ecology, and biotechnological potential. *Microbiol. Mol. Biol. Rev. 71,* 295-347.

Vorobeva E.V., Krasikova I.N., Dmitrenok A.S., Isakov V.V., Nedashkovskaya O.I., Solov'eva T.F. (2006) An Unusual Lipid A from a Marine Bacterium *Chryseobacterium scophtalmum* CIP 104199T. *Russ. J. Bioorg. Chem. 32(5),* 485-491.

Westphal O., Jann K. (1965) Bacterial lipopolysaccharides: extraction with phenol-water and further applications of the procedure. *Methods Carbohydr. Chem. 5,* 83–91.

Wiens M., Korzhev M., Krasko A., Thakur N.L., Perović-Ottstadt S., Breter H.J., Ushijima H., Diehl-Seifert B., Müller I.M., Müller W.E.G. (2005) Innate immune defence of the sponge *Suberites domuncula* against bacteria involves a MyD88-dependent signalling pathway. Induction of a perforin-like molecule. *J. Biol. Chem. 280(30),* 27949–27959.

Christ W.J., Asano O., Robidoux A.L.C., Perez M., Wang Y.A., Dubuc G.R. Gavin W.E., Hawkins L.D., McGuinness P.D., Mullarkey M.A., Lewis M.D., Kishi Y., Kawata T., Bristol J.R., Rose J.R., Rossignol D.P., Kobayashi S., Hishinuma L., Kimura A., Asakawa N., Katayama I., Yamatsu I. (1995) E5531, a pure endotoxin antagonist of high potency. Science, 268, 80-83

Stöver A. G. , Da Silva Correia J. , Evans J. T. , Cluff C. W. , Elliott M. W., Jeffery E.W. , Johnson D. A. , Lacy M. J. , Baldridge J. R. , Probst P., Ulevitch R. J., Persing D. H., Hershberg R. M. (2004) Structure-activity relationship of synthetic toll-like receptor 4 agonists, J. Biol. Chem., 279, 4440–4449.

Chapter V

Phaeobacter gallaeciensis BS107 SA/WT

Premise

Over the years marine bacteria became an interesting source of new lipid A structures with interesting immunological properties (Vorobeva, 2006; Maaetoft-Udsen, 2013; Anwar, 2014; Molinaro, 2015). *Phaeobacter gallaeciensis* is a Gram-negative marine bacterium, belonging to the *Roseobacter* clade of α-proteobacteria (Wagner-Döbler 2006), found abundantly in coastal regions of oceans, especially during the algal blooms. They are well known colonizers of both, biotic and abiotic surfaces and are being found interacting with micro- and macro-algae as well as eukaryotes (Buchan, 2005, Slightom, 2009). It was demonstrated that *P. gallaeciensis* is involved in a biphasic interaction with a microscopic algae, *Emiliania huxleyi*. Both, mutualistic and parasitic phases are identified by a group of small molecules. In case of the mutualistic phase, algae are producing dimethylsulfoniopropionate (DMSP), which is used by bacteria as a source of carbon and sulphur. Therefore, the bacteria produce phenylacetic acid, which is a growth promoter for the algae, and an antibiotic - tropodithietic acid (TDA). Thereafter, with the algal growth, *E. huxleyi* starts to produce p-cumaric acid which induces bacteria to synthesise algaecides named roseobacticides A and B, thus the relation changes from a mutualistic into opportunistic parasitism (Seyedsayamdost, 2011; Wang, 2016). *Phaeobacter* spp. became potent aquatic probiotic thanks to the competitive success of these organisms against fish and mollusc pathogens (Thole, 2012; Genard, 2014).

The characterization of the structure and the immunological properties of *P. gallaeciensis* LPS, as a human non-pathogenic bacterium seems promising source of a novel hTLR4/MD-2 modulator. Furthermore, with the aim to assess if the ability of *P. gallaeciensis* to switch from mutualistic into opportunistic parasitism was correlated to changes the cell wall components, the lipid A fractions in mutualistic (WT strain) and pathogenic (SA strain) phase were isolated and characterized.

5.1 Isolation and purification of the LPS

The lipopolysaccharide from *Phaeobacter gallaeciensis* BS107 SA and WT were isolated with hot-phenol-water method (Westphal & Jann, 1965), preceded with wash of the cell pellet with water, ethanol and acetone. The isolated LPS underwent enzymatic digestion with RNase,

DNase and proteinase K, followed by extensive dialysis, proceeded with further purification with a Sephacryl S-200 column chromatography. Finally, the DOC-PAGE analysis unveiled the R-LPS nature of both SA and WT LPS.

5.2 Compositional analysis

The fractions of *Phaeobacter gallaeciensis* BS107 SA and WT underwent monosaccharide and fatty acid analysis with application of acetylated methyl glycoside technique (De Castro, 2010). Both lipopolysaccharides showed the presence of rhamnose (Rha), ribose (Rib), fucose (Fuc), mannose (Man), glucose (Glc), galactose (Gal), heptose (Hep), glucosamine (GlcN) and 3-deoxy-D-manno-oct-2-ulosonic acid (Kdo). Moreover, the quantification of monosaccharides and fatty acids was performed basing on internal standard method and deriving the analytes into acetylated alditols and fatty acid methyl esters respectively. The results are shown in the Table 5.1.

Table 5.1. Composition of the *P. gallaeciensis* BS107 SA. The quantification was performed using the internal standard method with xylose

Neutral sugars	Concentration [nmol/mg]	
Rhamnose (Rha)	40	
Ribose (Rib)	230	
Fucose (Fuc)	62	
Mannose (Man)	36	
Glucose (Glc)	701	
Galactose (Gal)	203	
Heptose (Hep)	64	
3-Deoxy-D-manno-oct-2-ulosonic acid (Kdo)	NQ	
Aminosugars		
Glucosamine (GlcN)	NQ	
Total fatty acids	**Total [nmol/mg]**	**Ester [nmol/mg]**
3OH-10:0	41	23
3OH-12:0	73	0
12:0	Tr	tr
12:1	Tr	Tr
10:0	tr	Tr

NQ - not quantified; tr – trace quantities

The quantitative analysis of the fatty acid methyl esters performed on *Phaeobacter gallaeciensis* BS 107 SA revealed the presence of 10:0, 10:0 (3-OH), 12:0, 12:1, 12:0 (3-OH). The selective hydrolysis of ester linked fatty acids unveiled that all 12:0 (3-OH) were amide linked, whereas 10:0 (3-OH) were partially amide linked. Furthermore, qualitative analysis was made using 17:0 as internal standard (Table 5.1.).

5.3 MALDI-TOF and MS^2 analysis of the lipid A

The complete structure of *P. gallaeciensis* BS107 SA and WT was unveiled basing on MALDI-TOF MS and MS^2 analysis.

The lipid A of *P. gallaeciensis* BS107 SA was obtained applying mild acid hydrolysis in order to cleave the linkage between the non-reducing GlcN of the lipid A and Kdo of the core oligosaccharide. The lipid A was isolated by adding appropriate quantity of methanol and chloroform until a 2:2:1,8 (v/v/v) chloroform/methanol/hydrolysate mixture was obtained (Bligh & Dyer, 1959). Therefore, the moiety was recovered from the organic layer. Subsequently negative ion MALDI-TOF analysis was conducted on the bacterial pellet following the Larrouy-Mamus method (Larrouy-Maumus, 2016).

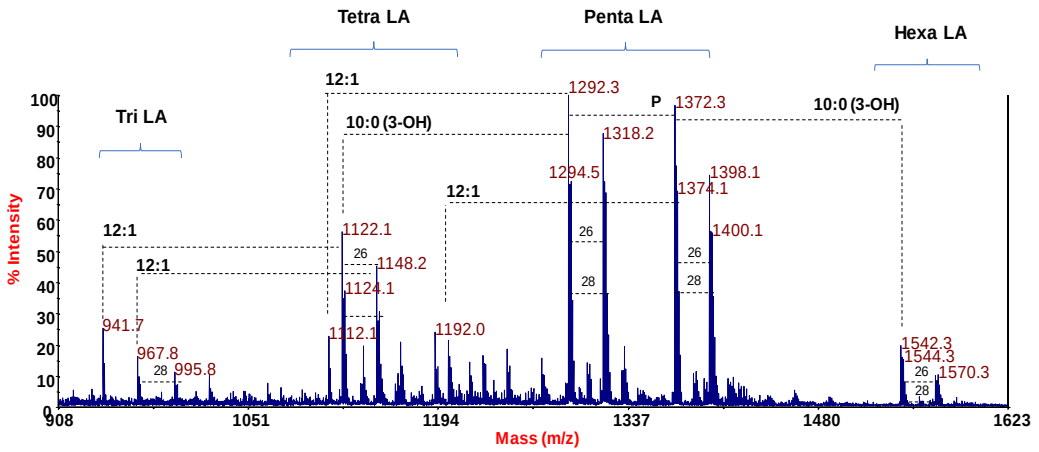

Figure 5.1. Negative ion reflectron MALDI mass spectrum, *Phaeobacter gallaeciensis* BS107 SA lipid A. Tetra-, penta- and hexa-acylated lipid A species are outlined.

The negative ion MALDI mass spectrum of *P. gallaeciensis* BS107 (Figure 5.1.) revealed the presence of peaks in range of *m/z* 941.7-1570.3 relative to deprotonated $[M - H]^-$ lipid A species differing in the nature and number of fatty acid chains and in phosphate content. Four different families of peaks were clearly apparent and matched with tri-, tetra-, penta- and hexa-acylated lipid A species.

On the basis of fatty acid analysis, the highest mass ion at *m/z* 1570.3 was assigned as a *bis*-phosphorylated hexa-acylated lipid A species carrying two 12:0(3-OH), two 10:0(3-OH), one 12:1 and one 10:0. The *bis*-phosphorylated hexa-acylated species around *m/z* = 1544.6, possessing a mass difference Δ*m/z* = 26, carried one 12:1 fatty acid chain instead of a 10:0 residue, and thus possessed two 12:0 (3-OH), two 10:0 (3-OH) and two 10:0. Moreover the clear mass difference of 28 amu (Δ*m/z* = 28) was correlated with substitution of 10:0 into 12:0. Two main peaks were attributed to penta-acylated forms of the lipid A. The first signal at *m/z* 1372.3 was attributed to a *bis*-phosphorylated penta-acylated species carrying two 10:0 (3-OH), one 12:0 (3-OH), 12:1, and 10:0, whereas the signal at *m/z* 1292.3, differing of 80 amu (Δ = *m/z* 80) was assigned as *mono*-phosphorylated form. Also in this case, differences of Δ*m/z* = 26 and Δ*m/z* = 28 were clearly distinguishable. Thereafter main *mono*-phosphorylated tetra-acylated species, related to previously described

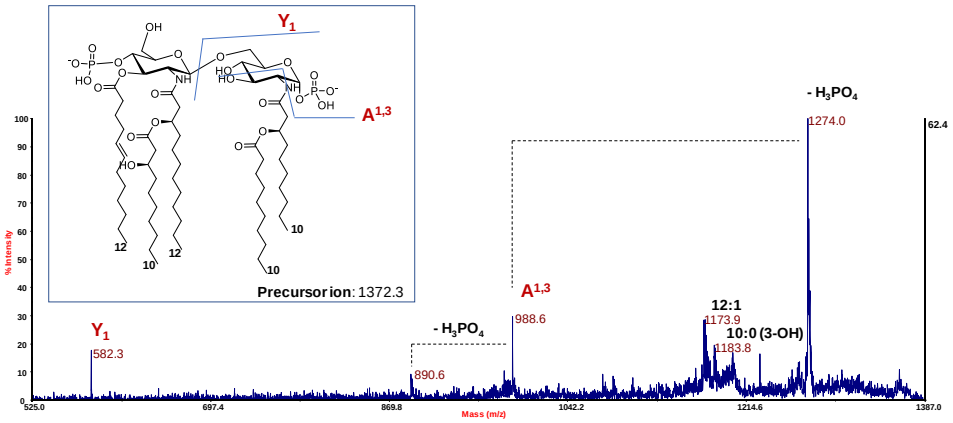

Figure 5.2. Negative-ion MALDI MS^2 spectrum of the penta-acylated lipid A species at *m/z* 1372.3 from *Phaeobacter gallaeciensis* BS107. Fragments assignment is reported in the spectrum. In the inset, the proposed structure for the hexa-acylated lipid A species assignable to the precursor ion at *m/z* 1372.3.

penta-acylated lipid A is found at *m/z* 1122.1. The relative ion with mass difference of 80 amu were connected with presence of bis-phosphorylated species. Finally, the main tri-acylated, mono-phosphorylated species lacking one 12:1 with respect to the ion at *m/z* 1122.1 were assigned to the ion at m/z 941.7.

A negative ion MS^2 analysis was driven in order to locate the acyl moieties and the phosphate groups. The negative ion MS^2 spectrum executed on the precursor ion at *m/z* 1372.3 (Figure 5.2.) corresponding with a *bis*-phosphorylated penta-acylated species revealed presence of the main ion at *m/z* 1274.0 which derived from the loss of one phosphate group. The other fragments at *m/z* 1183.8 and *m/z* 1173.9, matched with the lipid A lacking 10:0 (3-OH) and 12:1 respectively. Key ions were found at *m/z* 988.6 and *m/z* 582.3. The first one was assigned as $^{1,3}A_2$ ion (Domon & Costello, 1988), formed by the cleavage across the glycosidic ring of the reducing GlcN, and was diagnostic for identification of 10:0 and 10:0 (3-OH) as substituents on the distal GlcN. Therefore, the related ion at *m/z* 890.6 was attributed to a further loss of a phosphate group. The ion at *m/z* 582.3 was identified as Y_1 ion formed by the cleavage of the glycosidic bond between two glucosamine residues, suggesting presence of 12:0 (3-OH); 10:0 (3-OH) and 12:1 residues on the non-reducing GlcN. Moreover, the MS^2 spectrum executed on the precursor ion at m/z 1318.6 relative to *mono*-phosphorylated penta-acylated lipid A (data not presented) showed the main product ion at *m/z* 1120.2 attributed to a loss of one 12:1 residue. Thereafter, other product ions associated with sequential loss of a the acyl chains were reported at *m/z* 924.9 and *m/z* 734.7, associated with elimination of two 12:1 residues, and further 10:0 (3-OH) respectively.

In order to unambiguously determine the nature and location of the secondary fatty acids, an aliquot of lipid A was *O*-deacylated through ammonium hydroxide hydrolysis (Silipo, 2002). The MALDI mass spectrum, recorded in negative polarity revealed the presence of two peaks corresponding to di-acylated species at m/z 761.5 and *m/z* 896.0 (Figure 5.3.). The first corresponded to a *mono*-phosphorylated di-acylated lipid A carrying two 10:0 (3-OH) chains, the second at *m/z* 896.0 was associated with a *bis*-phosphorylated di-acylated species carrying two 12:0(3-OH). The ion at *m/z* 1192.5 was identified as a *bis*-phosphorylated

tetra-acylated lipid A species carrying two 10:0 (3-OH), one 12:0 (3-OH) and one 10:0 residue.

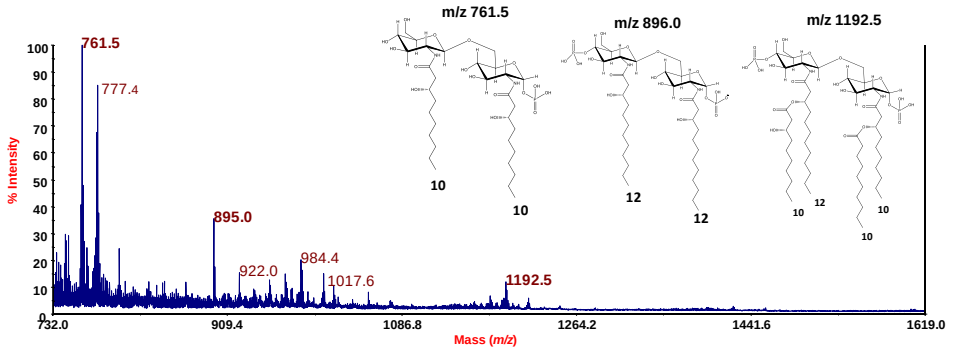

Figure 5.3. Negative ion reflectron MALDI mass spectrum, *Phaeobacter gallaeciensis* BS107 SA lipid A mild ammonium treatment. Proposed structures of products obtained after the treatment.

Finally, the negative mode MALDI-TOF experiments were performed on *Phaeobacter gallaeciensis* BS107 SA (Figure 5.4.a) and WT

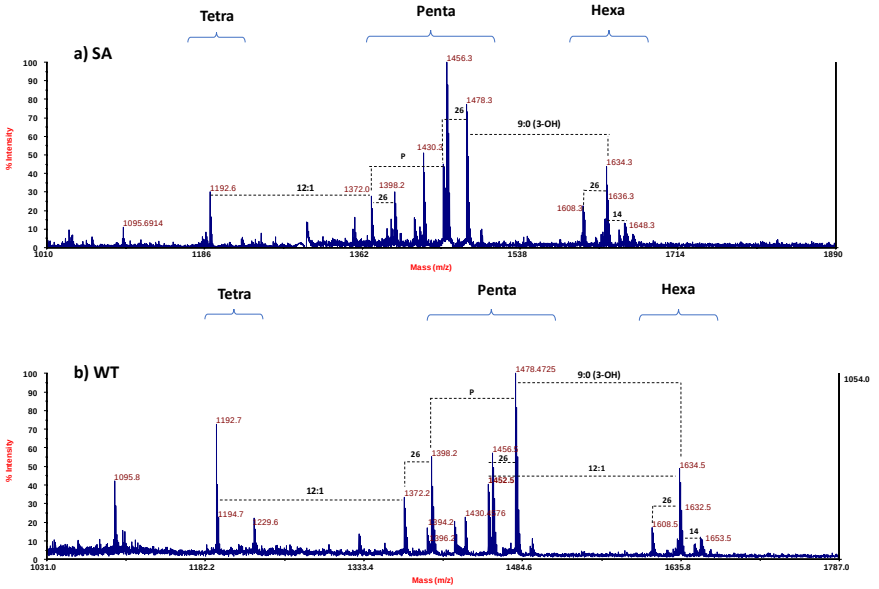

Figure 5.4. Negative ion reflectron MALDI mass spectrum, *Phaeobacter gallaeciensis* BS107 SA (a) and WT (b) lipid A obtained from the native bacterial pellet using Larrouy-Maumus method. Tetra-, penta- and hexa-acylated lipid A species are outlined. The spectrum confirmes structural assignments performed on isolated lipid A.

(Figure 5.4.b) cell pellet, showing a comparable distribution of species although a lower heterogenicity was evident, expecially in the phosphorylation pattern, suggesting removal of some phosphate groups during the acidic treatment. Interestingly, the main ion peaks at *m/z* 1456.3 and 1478.3 corresponding to penta-acylated species carried a pyrophosphate group. The ion at *m/z* 1456.3 was the predominant signal on the spectrum of *Phaeobacter gallaeciensis* BS107 SA, whereas the second, at *m/z* 1478.3 was the highest in the mutualistic WT strain. Moreover, the hexa-acylated forms at *m/z* 1634.3 and 1608.5 were also found to carry three phosphate groups and possess predominantly 9:0 (3-OH) residue instead of 10:0 (3-OH). Finally, a remarkable lower amount of *mono*-phosphorylated species was found. The structure of a hexa-acylated species is showed on Figure 5.5.

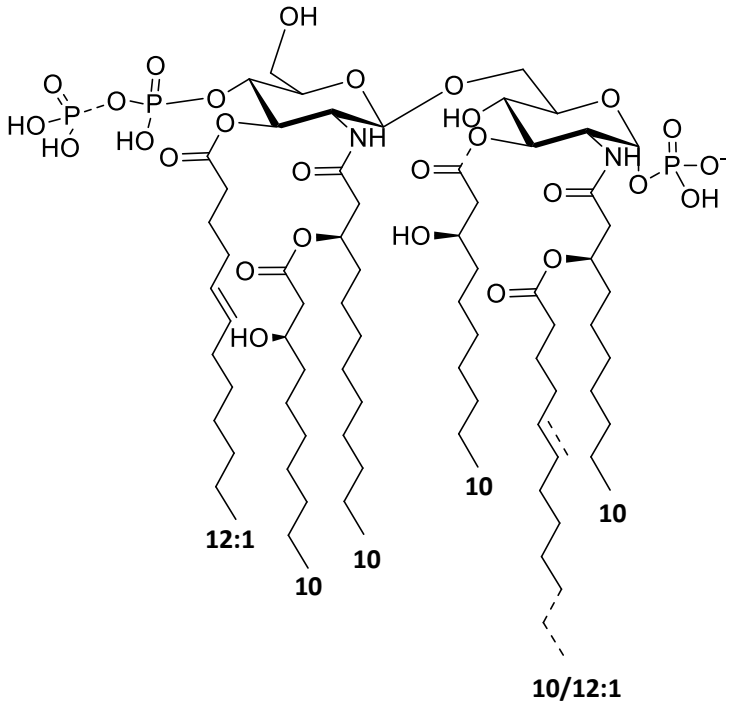

Figure 5.5. Structure of the hexa-acylated *P. gallaeciensis* BS107 lipid A species.

5.4 Immunological studies on *Phaeobacter gallaeciensis* BS107 LPS

The assessment of immunological impact of *Phaeobacter gallaeciensis* BS107 LPS was performed upon exposure of HEK293 cells transfected with human TLR4/CD14/MD-2, and the Monocytes-derived Macrophages (MoMs) to studied LPS in various concentrations (1 ng/mL, 10 ng/mL and 100 ng/mL). Subsequently identical concentrations of agonist *E. coli* O111:B4 LPS and the antagonist, synthetic lipid IV_A were used as controls. Moreover, the untreated cells were considered as the negative control. In detail, the stimulation of hTLR4 HEK293 cells was conducted for 6 h. Thereafter, the activation of NF-κB, so as Chemokine ligand 8 (CXCL-8) release was measured.

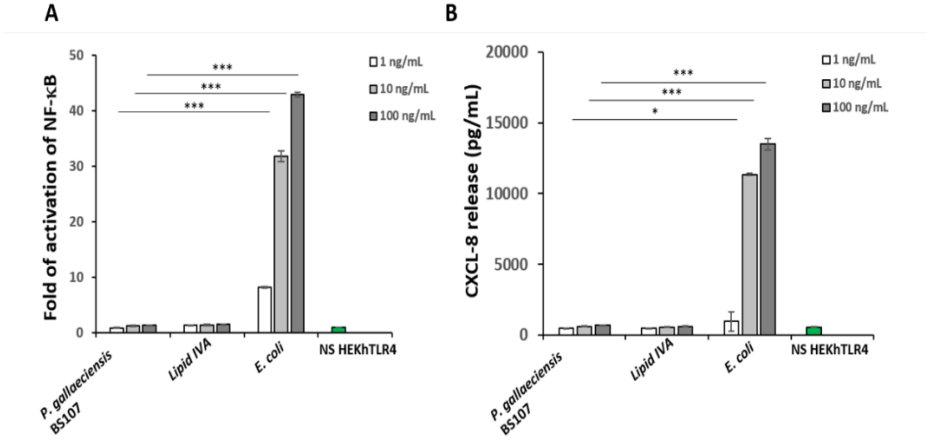

Figure 5.6. Immunopotential analysis of *P. gallaeciensis* BS107 LPS in HEH293 hTLR4/MD-2/CD14. The activation NF-κB (**A**) and release of CXCL-8 (**B**) upon stimulation with 1, 10 and 100 ng/mL of *P. gallaeciensis* LPS for 6 hours. Hexa-acylated *E. coli* LPS and synthetic lipid IV at the same concentrations were used as controls. Data expressed as a mean of three independent repetitions ±SD. * p<0.05; ** p<0.01; *** p<0.001 after t-Students test.

As presented on the Figure 5.6, the LPS derived from *Phaeobacter gallaeciensis* BS107 showed nearly lack of immunostimulant activity. Significantly lower activation of the NF-kB and CXCL-8 release was observed in respect to *E. coli* LPS (*P. gallaeciensis* BS107 LPS vs E. coli LPS p>0,001 for all NF-κB and 10 ng/mL, 100 ng/mL CXCL-8, p>0,001, 1 ng/mL CXCL-8 p>0,05). Interestingly, the results were comparable to the ones obtained on the lipid IV_A.

The immunostimulant properties were further analysed on Monocytes-derived Macrophages (MoMs). The cells expressing TLR4 were exposed for 12 hours to *P. gallaeciensis* BS107 LPS, *E. coli* LPS and lipid IV_A in the concentrations as described above; thereafter release of pro-inflammatory cytokines, including the hTNF-α, IL-10 and IL-6 was measured. Obtained results are presented in Figure 5.7. Also in this case *P. gallaeciensis* LPS showed very poor response in comparison to *E. coli* O111:B4 LPS (*P. gallaeciensis* BS107 LPS vs *E. coli* TNF-α: 1 ng/mL *p< 0,05*; 10 ng/mL, 100 ng/mL *p*< 0,001; IL-10: 1 ng/mL *NS*; 10 ng/mL *p*< 0,001, 100 ng/mL *p*< 0,01; IL-6 1 ng/mL *NS,* 10 ng/mL, 100 ng/mL *p*< 0,001).

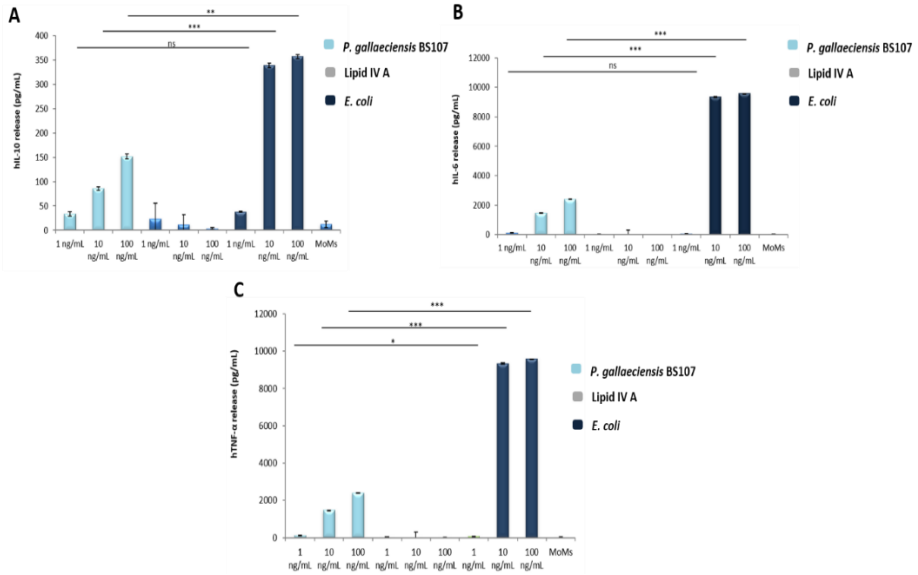

Figure 5.7. Immunopotential analysis of *P. gallaeciensis* BS107 LPS in MoMs. The release of pro-inflammatory cytokines hIL-10 (**A**), hIL-6 (**B**) and hTNF-α (**C**) upon stimulation with 1, 10 and 100 ng/mL of *P. gallaeciensis* LPS for 12 hours. Hexa-acylated *E. coli* LPS and synthetic lipid IV at the same concentrations were used as controls. Data expressed as a mean of three independent repetitions ±SD. * p<0.05; ** p<0.01; *** p<0.001 after t-Students test.

5.5. Discussion

In this study the structural features of *Phaeobacter gallaeciensis* LPS, in particular the lipid A were extensively investigated. The structural assignment of lipid A was conducted basing on a combination of chemical methods and Mass Spectrometry; MALDI-MS and MS^2 experiments were performed on the lipid A isolated by means of mild acidic hydrolysis and

in its native form. The lipid A obtained by acid hydrolysis was composed mostly of *bis*- and *mono*-phosphorylated species, whereas in case of untreated lipid A, species carrying two or three phosphate groups were identified, suggesting the presence of pyrophosphate groups.

The lipid As derived from *P. gallaeciensis* in the symbiotic and pathogenic states (WT and SA respectively) were compared. Both fractions showed the predominant presence of penta-acylated species possessing a disaccharide glucosamine backbone decorated with phosphate and pyrophosphate groups (Figure 5.5.). The main penta-acylated species found in the mutualistic phase carried one 12:0 (3-OH), two 10:0 (3-OH) and two 12:1, whereas in the pathogenic phase a 10:0 on the reducing GlcN substituted the 12:1 ; however, the lipid A in the two mutualistic and parasitic phases did not show significant variations. Presented lipid A was found to possess a 3-hydroxylated fatty acid, namely 10:0 (3-OH), as a secondary residue. This property is rarely observed among lipid As, like *Bdellovibrio bacteriovorus* (Schwudke, 2003), or marine bacteria including *Halobacteroides lacunaris* (Di Lorenzo, 2018) and *Marinomonas vaga* (Krasikova, 2004).

The lipopolysaccharide was further subjected to immunological assays in order to characterize the activation on the TLR4/MD-2 receptorial complex upon exposure to the LPS. Interestingly, the results showed that the molecule was able to activate significantly lower TLR4/MD-2 driven response in comparison to *E. coli*, likely due to the predominant presence of penta-acylated species and the concomitant presence of rather short chain fatty acids, including 10:0 and 10:0 (3-OH) (Rietschel, 1994; Stöver, 2004; Fox, 2010; Molinaro, 2015) (see Chapter 1.8.).

References:

Anwar M.A., Choi S. (2014) Gram-Negative Marine Bacteria: Structural Features of Lipopolysaccharides and Their Relevance for Economically Important Diseases. *Mar. Drugs. 12(5),* 2485-2514.

Bligh E.G., Dyer W.J. (1959) A rapid method of total lipid extraction and purification. *Can. J. Biochem. Phys. 37,* 911-917.

Buchan A., González J.M., Moran M.A. (2005) Overview of the Marine Roseobacter Lineage. *Appl. Environ. Microbiol. 71(10),* 5665-5677.

De Castro C., Parrilli M., Holst O., Molinaro A. (2010) Microbe-associated molecular patterns in innate immunity: extraction and chemical analysis of gram-negative bacterial lipopolysaccharides. *Methods Enzymol. 480,* 89-115.

Di Lorenzo F., Palmigiano A., Paciello I., Pallach M., Garozzo D., Bernardini M.-L., Cono V., Yakimov M.M., Molinaro A., Silipo A. (2017) The Deep-Sea Polyextremophile *Halobacteroides lacunaris* TB21 Rough-Type LPS: Structure and Inhibitory Activity towards Toxic LPS. *Mar. Drugs. 15(7),* e201.

Domon B., Costello C.E.A. (1988) Systematic nomenclature for carbohydrate fragmentations in FAB-MS/MS spectra of glycoconjugates. *Glycoconj. J. 5,* 397-409.

Fox C.B., Friede M., Reed S.G., Ireton G.C. (2010) Synthetic and Natural TLR4 Agonists as Safe and Effective Vaccine Adjuvants. In Sub-cellular biochemistry 53. Endotoxins: Structure, Function and Recognition (Eds. Wang X., Quinn P.J.). Springer, Dordecht, Heidelberg, London, New York, pp 303 – 322.

Genard B., Larouche O., Nicolas J.-L., Miner P., Beaudin M.-L., Tremblay R. (2014) Effect of the probiotic strain *gallaeciensis* after bacterial challenge on the complete larval development of *Pecten maximus. Aquat. Living Resour. 27,* 27-34.

Krasikova I.N., Kapustina N.V., Isakov V.V., Dmitrenok A.S., Dmitrenok P.S., Gorshkova N.M., Solov'eva T.F. (2004) Detailed structure of lipid A isolated from lipopolysaccharide from the marine proteobacterium Marinomonas vaga ATCC 27119. *Eur. J. Biochem. 271,* 2895-2904.

Larrouy-Maumus G., Clements A., Filloux A., McCarthy R.R., Mostowy S. (2016) Direct detection of lipid A on intact Gram-negative bacteria by MALDI-TOF mass spectrometry. *J. Microbiol. Methods. 120,* 68-71.

Maaetoft-Udsen K., Vynne N., Heegaard P.M., Gram L., Frokiaer H. (2013) Pseudoalteromonas strains are potent immunomodulators owing to low-stimulatory LPS. *Innate Immun. 19*, 160-173.

Molinaro A., Holst O., Di Lorenzo F., Callaghan M., Nurisso A., D'Errico G., Zamyatina A., Peri F., Berisio R., Jerala R., Jiménez-Barbero J., Silipo A., Martín-Santamaría S. (2015) Chemistry of lipid A: at the heart of innate immunity. *Chemistry 21(2),* 500-519.

Rietschel E.T., Krikae T., Schade F.U., Mamat U., Schmidt G., Loppnow H., Ulmer A.J., Zahringer U., Seydel U., Di Padova F., Schreier M., Brade H. (1994) Bacterial endotoxin: molecular relationships of structure to activity and function. *FASEB J. 8,* 217-225.

Schwudke D., Linscheid M., Strauch E., Appel B., Zähringer U., Moll H., Müller M., Brecker L., Gronow S., Lindner B. (2003) The obligate predatory *Bdellovibrio bacteriovorus* possesses a neutral lipid A containing α-D-mannoses that replace phosphate residues: similarities and differences between the lipid As and the lipopolysaccharides of the wild type strain *B. bacteriovorus* HD100 and its host-independent derivative HI100. *J. Biol. Chem. 278,* 27502-27512.

Seyedsayamdost M.R., Case R.J., Kolter R., Clardy J. (2011) The Jekyll-and-Hyde chemistry of *Phaeobacter gallaeciensis*. *Nat. Chem. 3(4),* 331-335.

Silipo A., Lanzetta R., Amoresano A., Parrilli M., Molinaro A. (2002) Ammonium hydroxide hydrolysis: a valuable support in the MALDI-TOF mass spectrometry analysis of Lipid A fatty acid distribution. *J. Lipid Res. 43*, 2188-2195.

Slightom R.N., Buchan A. (2009) Surface colonization by marine roseobacters: integrating genotype and phenotype. *Appl. Environ. Microbiol. 75(19),* 6027-6037.

Stöver A. G. , Da Silva Correia J. , Evans J. T. , Cluff C. W. , Elliott M. W., Jeffery E.W. , Johnson D. A. , Lacy M. J. , Baldridge J. R. , Probst P., Ulevitch R. J., Persing D. H., Hershberg R. M. (2004) Structure-activity relationship of synthetic toll-like receptor 4 agonists, J. Biol. Chem., 279, 4440–4449.

Thole S., Kalhoefer D., Voget S., Berger M., Engelhardt T., Liesegang H., Wollherr A., Kjelleberg S., Daniel R., Simon M., Thomas T., Brinkhoff T. (2012) *Phaeobacter gallaeciensis* genomes from globally opposite locations reveal high similarity of adaptation to surface life. *ISME J. 6(12),* 2229-2244.

Vorobeva E.V., Krasikova I.N., Solov'eva T.F. (2006) Influence of lipopolysaccharides and lipids A from some marine bacteria on spontaneous and

Escherichia coli LPS-induced TNF-alpha release from peripheral human blood cells. *Biochem.* 71(7), 759-766.

Wagner-Döbler I., Biebl H. (2006) Environmental biology of the marine *Roseobacter lineage*. *Annu. Rev. Microbiol. 60,* 255-280.

Wang R., Gallant É., Seyedsayamdost M.R. (2016) Investigation of the Genetics and Biochemistry of Roseobacticide Production in the Roseobacter Clade Bacterium *Phaeobacter inhibens*. *MBio. 7(2),* e02118.

Westphal O., Jann K. (1965) Bacterial lipopolysaccharides: extraction with phenol-water and further applications of the procedure. *Methods Carbohydr. Chem. 5,* 83-91.

Chapter VI

Zymomonas mobilis

Premise

Zymomonas mobilis, the etiological agent of beer, wine and cider spoilage, is among the first anaerobic acidophilic bacteria able to synthesize ethanol attracting the interest of researchers (Swings & De Ley, 1977). *Z. mobilis* is notable due to its extraordinarily ability to tolerate ethanolic environment, reaching up to 16% in case of batch culture (Seo, 2005; Yang, 2013). In comparison to most industrially nowadays used ethanologenic organisms as *Saccharomyces cerevisiae*, *Z. mobilis* exhibits a wide range of advantages such as higher ethanol yields, lower biomass production, higher sugar uptake; moreover, it does not require controlled oxygen addition during the fermentation process (Lin & Tanaka, 2006; Panesar, 2006). These peculiarities make it a promising microorganism for a large scale bio-ethanol industrial production (Panesar, 2007).

Bacterial cells use different methods to protect themselves from the external environment; two of the main known microorganism adaptations to highly ethanolic environment are an increased proportion of monounsaturated fatty acids and a high hopanoid content in the bacterial membrane, preventing membrane leakage and decrease of organization (Belin, 2018; Demel & De Kruyff, 1976; Kannenberg, 1980;). Actually *Z. mobilis* is one of the most potent producers of hopanoids (Bringer, 1985; Demel & De Kruyff, 1976; Flesch & Rohmer, 1989) and, furthermore, over 70% of the acyl lipid chains present in the membrane phospholipids were 18:1 (Δ11) (Hermans, 1991; Ingram, 1986). Nevertheless, microorganisms have developed also other strategies letting them survive in harsh conditions, such as the synthesis of polysaccharides and glycoconjugates (Hidalgo-Cantabran, 2014; Nichols, 2005).

Of particular importance are the exopolysaccharides (EPSs), high molecular weight extracellular carbohydrate polymers which exert significant roles in microbial adhesion, protection (Decho, 1990; Nicolaus, 2010), and both symbiotic and pathogenic interactions with the external environment (Flemming & Wingender, 2010; Tytgat & Lebeer, 2014)(see Chapter 1.4). EPSs are indeed often produced by organisms exposed to stressful environmental conditions, providing them a protective barrier against different factors (Kazak, 2010). EPS-secreting microbes produce either homo- or hetero- polysaccharides, nevertheless some bacterial

strains, such as *Serratia marcescens*, *Aeromonas salominicida*, and *Pseudomonas* sp. strain NCIB2021, can also synthesize mixtures of different polysaccharides (Ates, 2015; Kwon, 1994). Some of these EPSs have industrial applications, including xanthan, dextran, gellan and curdlan produced by *Xanthomonas campestris*, lactic acid bacteria, *Pseudomonas elodea* and *Alcaligenes faecalis,* respectively (Mollakhalili, 2015; Nwodo, 2012).

Structure and potential roles of *Z. mobilis* EPS in bacterial survival were here characterised, pursued by the combined use of chemical, spectroscopic and physico-chemical techniques including DOSY NMR and both Static and Dynamic Light Scattering (SLS and DLS). It was showed that *Z. mobilis* produces a mixture of two EPSs, an [→6)-α-D-Man*p*-(1→]$_n$ mannose homopolymer and a galactose containing polysaccharide: [→2)-β-D-Gal*f*-(1→3)-β-D-Gal*p*-(1→]$_n$. Furthermore, it was revealed that the chemical structure of the latter EPS potentially contributes with the *Zymomonas mobilis* high ethanol tolerance.

6.1. Isolation steps of *Zymomnas mobilis* cell wall components

In order to isolate the cell wall components, dried *Zymomonas mobilis* cell pellet underwent a PCP extraction (Galanos, 1969).
The compositional analysis of PCP extract showed predominantly presence of hopanoids, among the main component of the outer membrane, as the abundant Hop-17(21)-ene (Figure 6.1).

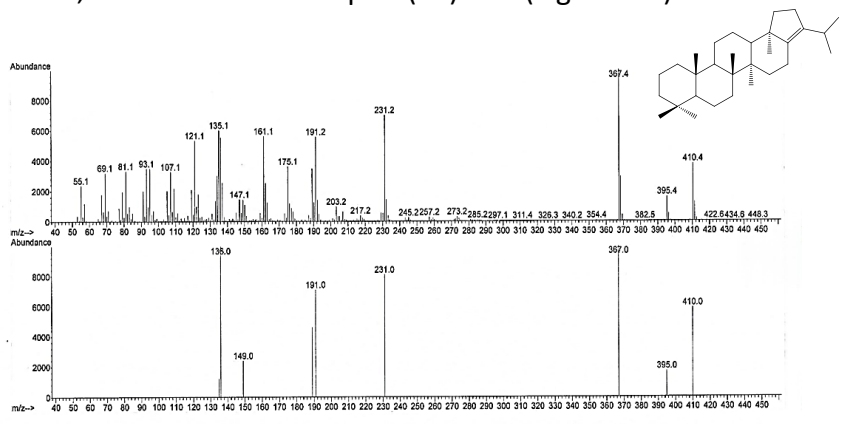

Figure 6.1 EI-MS spectrum and structure of Hop-17(21)-ene, the main hopanoid component of *Z. mobilis* cell membrane. Below the reference spectrum.

Some bacteria, like *Sphingomonas* spp. are devoid of LPS, replaced by another glycolipid, belonging to the Glycosphingolipid (GSL) class (see Chapter 1.5). These compounds are widespread among the α-4 subclass of Proteobacteria, therefore their presence in *Z. mobilis* outer membrane was previously reported in the literature (Kawahara, 1999; Tahara, 1994). The glycosphingolipid of *Zymomonas mobilis* was found to carry 1,3-dihydroxy-2-amino-hexadecane (DS 16:0) substituted with hexadecanoic or tetradecanoic acid ang glucuronic acid (Figure 6.2).

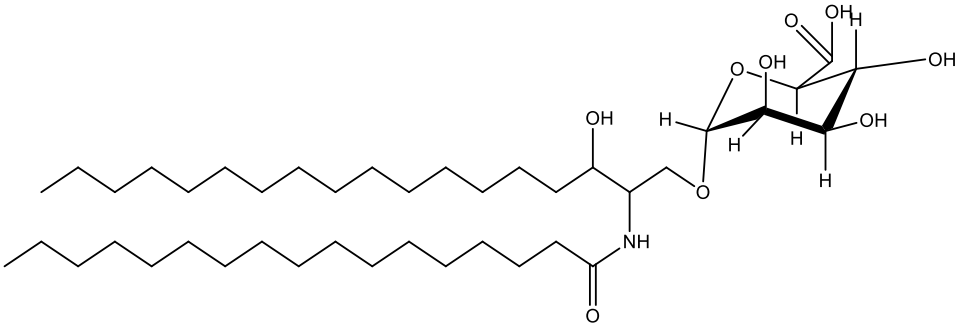

Figure 6.2. Chemical structure of the GSL derived from *Z. mobilis*

6.2 Isolation and compositional analysis of *Zymomonas mobilis* EPS

Two different EPS were isolated and purified from *Z. mobilis* cells by using a hot phenol/water extraction protocol (Westphal & Jann, 1965); the main polysaccharide component, named **PS1**, was found in the water phase (Figure 6.3a, the extraction yield was 15.4%); a fraction containing both **PS1** and a homopolymer, named **PS2**, was indeed isolated from the phenol phase (the extraction yield was 0.8%), with **PS2** being the major component (Figure 6.3b).

Based on the relative abundances of anomeric signals in 1D NMR spectra, **PS1** made up about 86% of extracellular polysaccharide material, whereas **PS2** accounted for about 14%.

Compositional analysis (De Castro, 2010) of both fractions revealed presence of D-galactose (D-Gal) (main sugar residue for **PS1**) and D-mannose. Methylation analysis (Ciucanu & Kerek, 1984) revealed the occurrence of 3-substituted Gal*p*, 2-substituted Gal*f* and 6-substituted Man*p*.

6.3 NMR spectroscopy structural characterization of PS1 and PS2

A combination of NMR experiments was executed to assign the spin systems and to identify the monosaccharide sequence of each polymer (Tables 6.1 and 6.2). The anomeric configuration of monosaccharide units was assigned on the basis of the $^{3}J_{H1,H2}$ coupling constants and the *intra*-residual NOE contacts, whereas the values of the vicinal $^{3}J_{H,H}$ coupling constants allowed the identification of the relative configuration of each residue. Homonuclear and heteronuclear 2D experiments (COSY, TOCSY and HSQC) were used to assign proton and carbon resonances of saccharide spin systems, while the sugar sequence was obtained from the long-range connectivity in the HMBC spectra and supported by the NOE contacts.

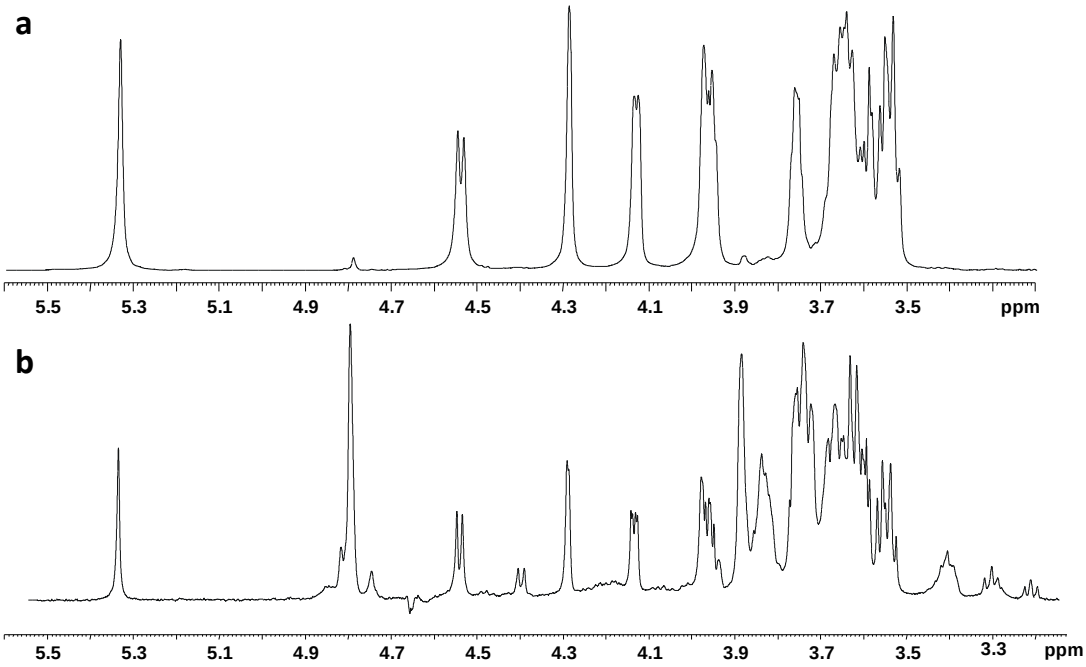

Figure 6.3 ^{1}H NMR spectra of **PS1** and **PS2**; **a)** the water phase mainly contained **PS1**, **b)** the phenol phase contained a mixture of **PS1** and **PS2**.

In the anomeric region of ^{1}H NMR (Figure 6.3a) of **PS1**, two anomeric signals were distinguished (Table 6.1). Spin system **A** (H-1 5.34 ppm, Table 6.1) was identified as a β-galactofuranose residue. The clear downfield shift of all carbon signals within this spin system, the *intra*-residue long range correlation found on the ^{1}H,^{13}C HMBC spectrum between **A**1 and **A**4, were all diagnostic of the presence of a sugar in a furanose ring. Chemical shift of anomeric carbon atom (108.2 ppm) was indicative of a β-configured unit (Molinaro, 2002; Di Lorenzo, 2014). Spin system **B** (H-1 4.54 ppm, $^{1}J_{H1,C1}$ 165 Hz, $^{3}J_{H1,H2}$ 8 Hz) was identified as an β-galactopyranose residue. The β-anomeric configuration was indicated by the *intra*-residue NOE contacts of H-1 with H-3 and H-5 and the downfield chemical shift of C-5, the *galacto* configuration was established by $^{3}J_{H3,H4}$ and $^{3}J_{H4,H5}$.

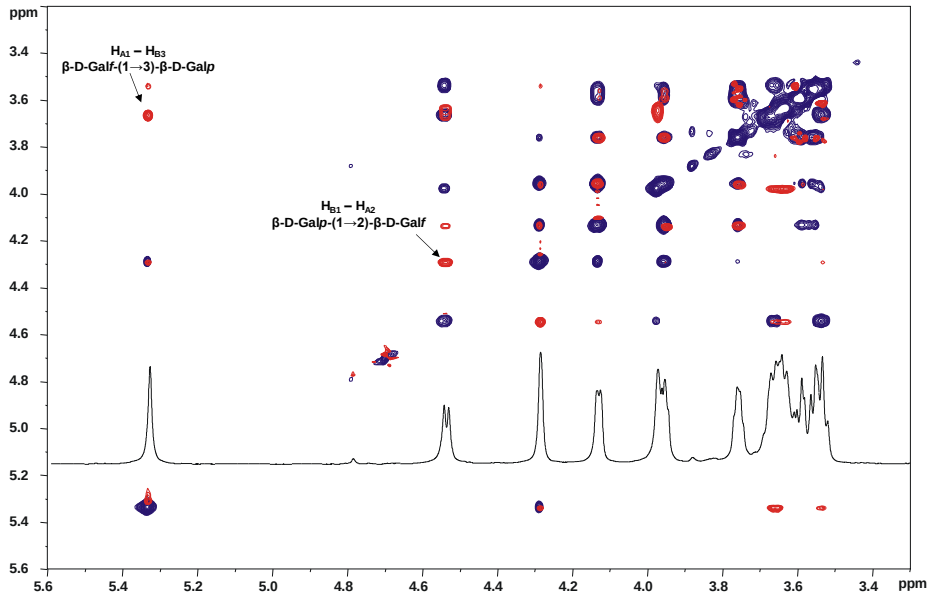

Figure 6.4 Overlapped sections of ROESY and TOCSY spectra of **PS1**. The key inter-residual NOE contacts involving sugar residues of **PS1** are indicated.

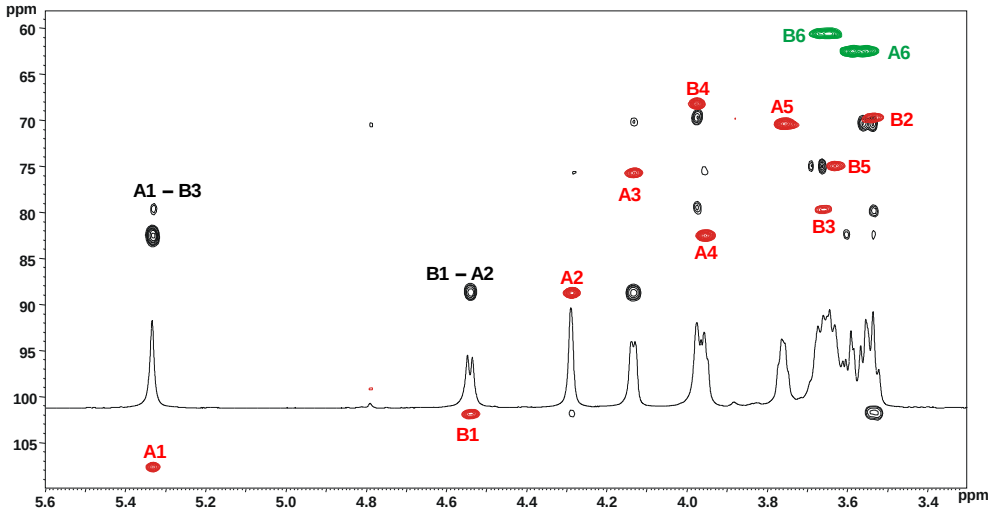

Figure 6.5 Overlapped sections of ^{1}H, $^{1}H^{13}C$ HMBC (black) and $^{1}H^{13}C$ HSQC (red and green) NMR spectra of **PS1**. The key *inter*-residual anomeric long-range correlations are indicated.

Table 6.1 Values of proton (^{1}H) and carbon (^{13}C) NMR shifts of **PS1**.

	Chemical Shift δ (^{1}H/*^{13}C*)					
Unit	**1**	**2**	**3**	**4**	**5**	**6**
A	5.34	4.29	4.14	3.96	3.74	3.55
2-β-D-Gal*f*	*108.2*	*88.9*	*75.9*	*82.6*	*70.5*	*62.5*
B	4.54	3.52	3.66	3.97	3.62	3.64
3-β-D-Gal*p*	*101.9*	*69.6*	*79.8*	*68.4*	*74.9*	*60.5*

The downfield shift of carbon resonances allowed the identification of the glycosylated positions, namely O-2 of **A** and O-3 of **B**. The *inter*-residue NOE contacts between **A**1 and **B**3 and between **B**1 and **A**2 (Figure 6.4) together with the long-range correlations of **A**1 with **B**3 and of **B**1 with **A**2 found in the HMBC (Figure 6.5) spectrum, confirmed the following repeating unit for the polysaccharide **PS1**:

$$[\rightarrow 2)\text{-}\beta\text{-}D\text{-}Gal\mathit{f}\text{-}(1\rightarrow 3)\text{-}\ \beta\text{-}D\text{-}Gal\mathit{p}\text{-}(1\rightarrow]_n\ .$$

The fraction isolated from the phenol phase **PS2** underwent NMR analysis by the same approach as above. Three anomeric protons were identified (Figure 6.3b, Table 6.2), of which two corresponded to the above described **PS1** polysaccharide. Spin system **C** (H-1 4.80 ppm, $^{1}J_{H1,C1}$ 174 Hz) was identified as α-D-Man*p*. The *manno* configuration was established by $^{3}J_{H\text{-}1,H\text{-}2}$ and $^{3}J_{H\text{-}2,H\text{-}3}$ (both below 2 Hz), the anomeric configuration was defined on the basis of the *intra*-residual NOE contacts of H-1 with H-2 (Figure 6.6.). The downfield shift of C-6 signal suggested glycosylation at O-6. Finally, the NOE correlation of H-1 with H-6 and the long-range correlation of C-1 with C-6 (Figure 6.7.) in conjugation with chemical analyses revealed that it was a homopolymer of 6-substituted α-D-Mannopyranose **PS2**:

$$[\rightarrow 6)\text{-}\alpha\text{-}D\text{-}Man\mathit{p}\text{-}(1\rightarrow]_n.$$

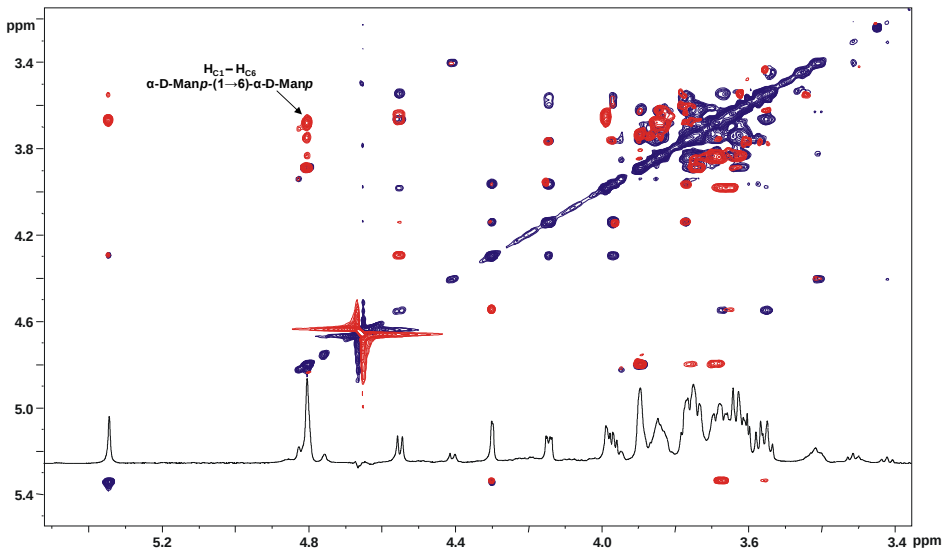

Figure 6.6 Overlapped sections of ROESY and TOCSY spectra of **PS1/PS2**. The key inter-residual NOE contacts involving sugar residues of **PS2** are indicated.

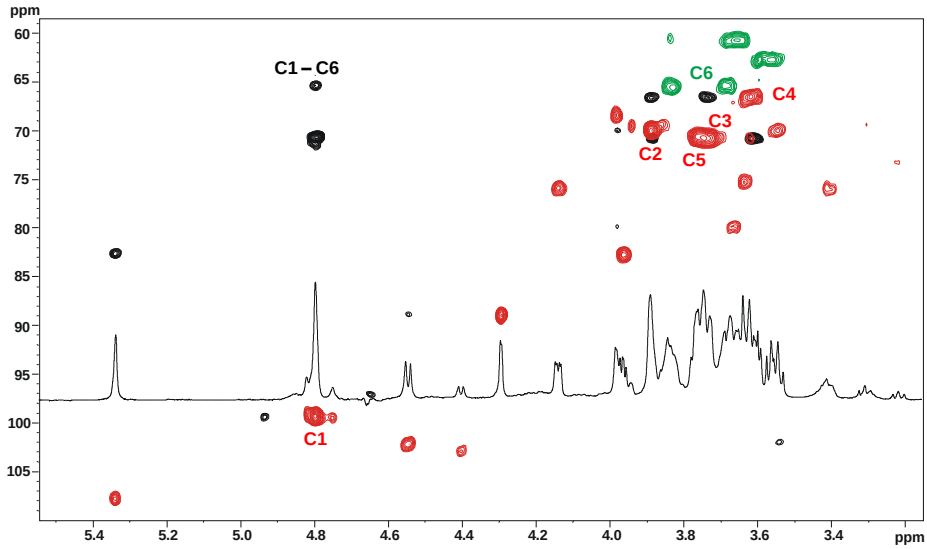

Figure 6.7 Overlapped sections of ^{1}H, ^{1}H-^{13}C HMBC (black) and ^{1}H-^{13}C HSQC (red and green) NMR spectra of **PS1/PS2**. The key *inter*-residual long range correlation of **PS2** is indicated.

Table 6.2 Values of proton (^{1}H) and carbon (^{13}C) NMR shifts of **PS2**.

	Chemical Shift δ (^{1}H/^{13}C)					
Unit	**1**	**2**	**3**	**4**	**5**	**6**
C	4.80	3.89	3.73	3.61	3.74	3.68/3.82
6-α-D-Manp	*99.3*	*69.9*	*70.8*	*66.4*	*70.6*	*65.4*

Therefore, two different exopolysaccharides (Figure 6.8) were identified as *Zymomonas mobilis* EPS components:

[→2)-β-D-Gal*f*-(1→3)- β-D-Gal*p*-(1→]$_n$ **PS1**

[→6)-α-D-Man*p*-(1→]$_n$. **PS2**

Interestingly, the repeating unit of **PS1** was previously reported as component of both capsular polysaccharide and LPS *O*-antigen isolated from an acidophilic bacterium, *Acetobacter methanolicus* strains MB 58/4 and MB70 (Grimmecke, 1991; Grimmecke, 1994).

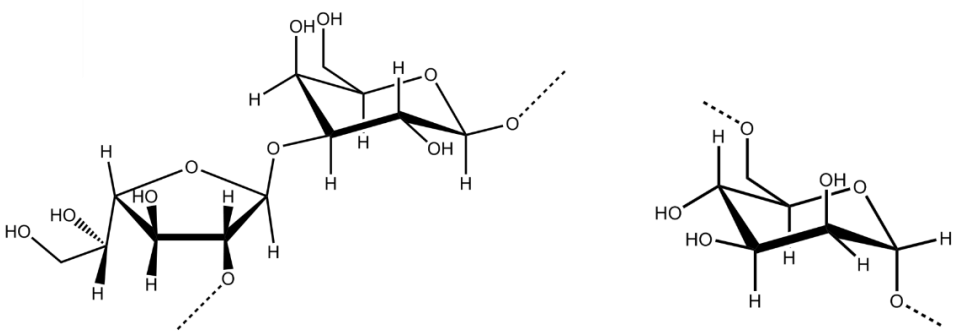

[→2)-β-D-Gal*f*-(1→3)-β-D-Gal*p*-(1→]$_n$

PS1

[→6)-α-D-Man*p*-(1→]$_n$

PS2

Figure 6.8. Structure od the PS1 and PS2

6.4 PFG-NMR and DLS analysis

With the purpose to investigate if and how *Z. mobilis* EPSs were involved in protecting bacteria cells against ethanol-rich environments, a physico-chemical characterization of the behavior of both polysaccharides, **PS1** and **PS2**, in water-ethanol solutions was performed. As a preliminary part of this investigation, the molecular weight of the two EPS was estimated by both PFG-NMR and SLS analysis (see Chapter 6.5). The two independent experimental approaches converge in giving an average molecular weight of about 120 kDa for **PS1** and 4kDa for **PS2**.

The self-diffusion (or, more correctly, intradiffusion) coefficients of both **PS1** and **PS2** in water-ethanol solutions were determined by PFG NMR measurements (Cohen, 2005), following the decay of signal intensity at 5.34 and 4.80 ppm of respectively the anomeric signal of the galactofuranose and the mannopyranose residue (Figure 6.3a and Figure 6.3b). In all cases, the signal decay satisfactorily fits a single exponential curve, indicating low polydispersity of the EPS molecular weight. All the measurements were done at very low **PS1** concentration (~ 0.1 % w/w) so that interactions between different polysaccharide chains could be neglected, as also confirmed by the evidence that the self-diffusion value does not depend on the observation time. This means that the molecules can be assumed to freely diffuse in an isotropic and homogeneous medium. Interestingly, a decrease of **PS1** self-diffusion coefficient, D_{PS1}, was observed (Table 6.3) with increasing ethanol concentration, whereas

the self-diffusion coefficient of **PS2,** D_{PS2}, remained nearly constant. The reduction of the **PS1** mobility can be ascribed either to the increased viscosity or to a change of the chain conformation; to discriminate between these two factors, the polysaccharides hydrodynamic radii at different ethanol concentrations were evaluated. The diffusion of spherical object in a continuous medium is related, indeed, to the object radius, R_h, and to the solvent viscosity, η, by the Stokes-Einstein equation:

$$D_{PS1} = \frac{k_B T}{6\pi\eta R_h}$$

where k_B is Boltzmann constant and T the absolute temperature. The viscosity of the heavy water-ethanol solutions at 25 °C can be calculated from those reported in the literature for the water-ethanol mixtures (González, 2007) using the scaling relationship proposed by Harris (2002), obtaining the values reported in Table 6.3.

Table 6.3. Self-diffusion coefficients, viscosity, hydrodynamic radius and solvation number for the systems water-ethanol-PSx (x = 1,2) at 25 °C. D_{PSx}: self-diffusion coefficient of PSx; D_{et} and $D°_{et}$: self-diffusion coefficient of ethanol in the presence and in the absence of PSx; R_h hydrodynamic radius; η solvent viscosity; $n_{et,PS1u}$: estimated number of ethanol molecules solvating PS1 per repeating unit.

Ethanol wt%	$D_{PSx} \times 10^{11}$ /m^2 s^{-1} [a]	$D_{et} \times 10^{10}$ /m^2 s^{-1} [b]	$D°_{et} \times 10^{10}$ /m^2 s^{-1} [b]	$\eta \times 10^3$ /Pa s	$R_h \times 10^9$ /m [c]	$n_{et,PS1u}$ [d]
			Heavy water-ethanol-PS1			
0	2.64			1.09	7.6	
4	2.19	9.44	9.83	1.25	8.0	10
8	2.03	8.52	8.81	1.40	7.7	13
12	1.72	8.19	8.40	1.53	8.3	17
			Heavy water-ethanol-PS2			
0	14.8			1.09	1.4	
4	14.5	9.72	9.83	1.25	1.2	-
8	15.2	8.85	8.81	1.40	1.0	-
12	15.6	8.51	8.40	1.53	0.9	-

[a] Experimental uncertainty ~ 1%. [c] Uncertainty ~ 2%.

[b] Experimental uncertainty < 0.5%. [d]Uncertainty ~ 30%

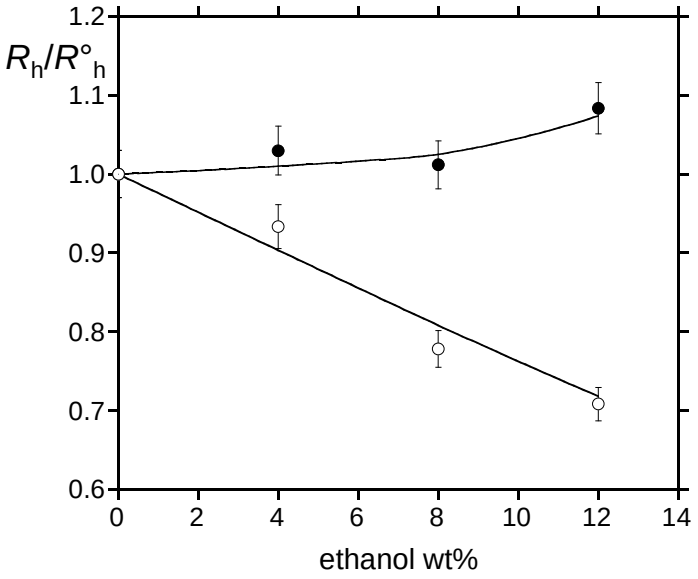

Figure 6.9 Hydrodynamic radius of **PSx (x = 1,2)** in heavy water-ethanol-**PSx** mixtures relative to that observed in the absence of ethanol, $R_h/R°_h$, reported as a function of the ethanol weight percent. Full circles, **PS1**; open circles, **PS2**.

Concerning **PS2**, the constancy of the self-diffusion coefficient with increasing ethanol concentration, corresponded to a significant decrease of the hydrodynamic radius, R_h, of the saccharide chain. In fact, a reduction up to 35 % of R_h was found, that corresponds to a 70% volume reduction. Thus, it appears that the presence of ethanol in the solvent medium causes a dramatic shrinkage of the **PS2** random coil. A similar behavior has been reported in the literature for other polysaccharides (Antoniou & Alexandridis, 2010; Antoniou, 2010). Conversely, presented results (Table 6.3., Figure 6.9.) showed that the R_h values of **PS1** were scarcely sensitive to the presence of ethanol in the system, showing a detectable increase only at the highest considered ethanol concentration.

The reliability of these data was also confirmed by DLS experiments (Figure 6.10), detecting a single population of diffusing objects, identified as the **PS1** coils, at all the considered mixtures. The distribution was centered slightly above 10 nm independently of the

ethanol concentration.

The peculiar behavior of **PS1** in water-ethanol mixtures can be rationalized in terms of the well-established modellization of polymer solvation (Rubenstein & Colby, 2003). In dilute solution, the polymer conformation, and consequently the dimension of the coil it forms, depends on the solvent (or solvent mixture) it is dissolved into. Consequently, for each specific polymer a scale of "solvent quality" can be drawn, which is the result of the combined effects of polymer segment–solvent and segment–segment interactions. A solvent can be "good" (the interactions between the polymer segments and the solvent are favored and the polymer coil expands), "bad" (the polymer coil contracts in order to minimize the disfavored segment–solvent interactions), or "theta" (the coil dimensions remain unperturbed). In mixed solvents a delicate balance between the interactions of the polymer segments and the different solvent molecules present in the mixture is established. It is widely recognized that the solvent quality determines equilibrium properties as well as the dynamics and rheology of polymer solutions. In some cases, the same conceptual framework has been already used to interpret the behavior of polysaccharides in solution (Antoniou, 2010; Antoniou & Alexandridis, 2010; Hilliou, 2009). Basing on obtained results, for **PS2** alike the other polysaccharides reported in the literature, ethanol can be considered as a bad solvent. Interestingly, **PS1** presented a particular behavior; upon addition of ethanol, its coils remained, indeed, nearly unperturbed, indicating that ethanol is a good solvent for this polymer, at least as good as water. Interestingly, ethanol self-diffusion was significantly decreased by the presence of **PS1** (Table 6.3.), differently from what observed for **PS2**. This allows estimating the average number of ethanol molecules diffusing together with each **PS1** saccharide unit (Table 6.3.). The experimental self-diffusion coefficient of ethanol determined in the presence of **PS1**, indeed, is the average of that of ethanol molecules involved in the polysaccharide solvation shell, $D_{\mathrm{et,solv}}$, and that of ethanol molecules freely diffusing in the solution bulk (Costantino, 2000):

$$D_{\mathrm{et}} = \frac{m_{\mathrm{et,solv}}}{m_{\mathrm{et}}} D_{\mathrm{et,solv}} + \frac{m_{\mathrm{et,free}}}{m_{\mathrm{et}}} D_{\mathrm{et,free}}$$

where m_{et} are the ethanol moles in the mixture while $m_{\mathrm{et,solv}}$ and $m_{\mathrm{et,free}}$

are those solvating and not solvating **PS1**, respectively ($m_{et,solv}$ + $m_{et,free}$ = m_{et}). It can be assumed that solvating ethanol molecules diffuse jointly to the solvated macromolecule, i.e., present the same self-diffusion coefficient of PS1 ($D_{et,solv}$ = D_{PS1}).

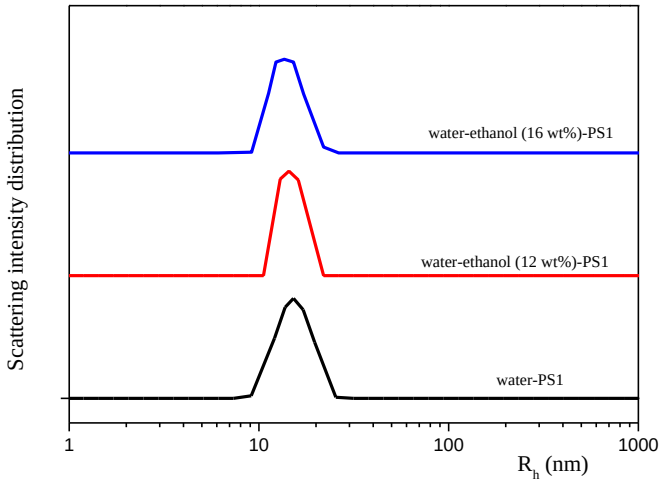

Figure 6.10 Distribution of the **PS1** hydrodynamic radius in water-ethanol-**PS1** mixtures.

On the other hand, considering that the mixtures contain a very low polysaccharide concentration, it can be also assumed that "free" ethanol molecules present the diffusion coefficient determined in **PS1** absence ($D_{et,free}$ = $D°_{et}$), being the obstruction effect exerted by the polymer coils on the ethanol motion negligible. From the knowledge of the **PS1** weight percent and of the saccharide unit molecular weight it is possible to calculate the number of units (expressed as moles) present in the mixture, $m_{PS1,unit}$. Last, the ratio between $m_{et,solv}$ and $m_{PS1,unit}$, represent the number of ethanol molecules involved in the solvation shell of a single saccharide unit, $n_{et,PS1u}$. The $n_{et,PS1u}$ values calculated by this approach are reported in Table 6.3. Since the model neglects the possibility of ethanol molecules physically "entrapped" in a polysaccharide coil but not directly entering the solvation shell of the saccharide units, the $n_{et,PS1u}$ values are roughly upper estimates of the real value.

The results indicated a significant involvement of ethanol in the **PS1** solvation shell, in which more than ten ethanol molecules per repeating unit are present, weakly increasing with the ethanol content in the solvent mixture. It is worth to highlight that this is the first time in which the presence of ethanol in polysaccharide solvation is proven;

indeed, this possibility has been considered negligible so far (Burakowski & Gliński, 2012).

6.5. Calculation of the average molecular mass

6.5.1. Molecular weight estimation by DOSY

The average molecular weight of the two fractions (**PS1** and **PS2**) was estimated by using DOSY (Diffusion-ordered NMR spectroscopy) experiments. As reported in Chapter 6.4., the Stokes – Einstein equation (eq. 1) describes the correlation between the diffusion coefficient of a certain molecule in solution and its molecular size.

$$D = kT/6\pi\eta r_s \, (m^2 \, s^{-1}) \qquad \text{eq. 1}$$

Although the equation 1, from which the analysis of DOSY is derived, holds for spherical molecules, it has been previously reported that diffusion data can be used to provide the molecular weight of uncharged linear and slightly branched, water soluble, oligo- and polysaccharides (Groves, 2004; Iqbal, 2017; Suárez, 2006; Viel, 2003).
Therefore, once measured the diffusion coefficients of the two polysaccharide fractions from 2D DOSY experiments (Figure 6.11), their molecular weight was roughly estimated by using the equation 2

$$D = K \times Mw^{\alpha} \, (m^2 \, s^{-1}) \qquad \text{eq. 2}$$

where K and α are scaling parameters ($K=8.114 \times 10^{-9}$; $\alpha=0.484$) previously determined by Viel et al., (2003).
The interpolation of diffusion data, by using the calibration curve derived by Viel and coworkers from the study of pullulans fractions of known molecular weight, yielded the following molecular masses for each fraction (Figure 6.11):

PS1 ~ 123 kDa

PS2 ~ 3.4 kDa

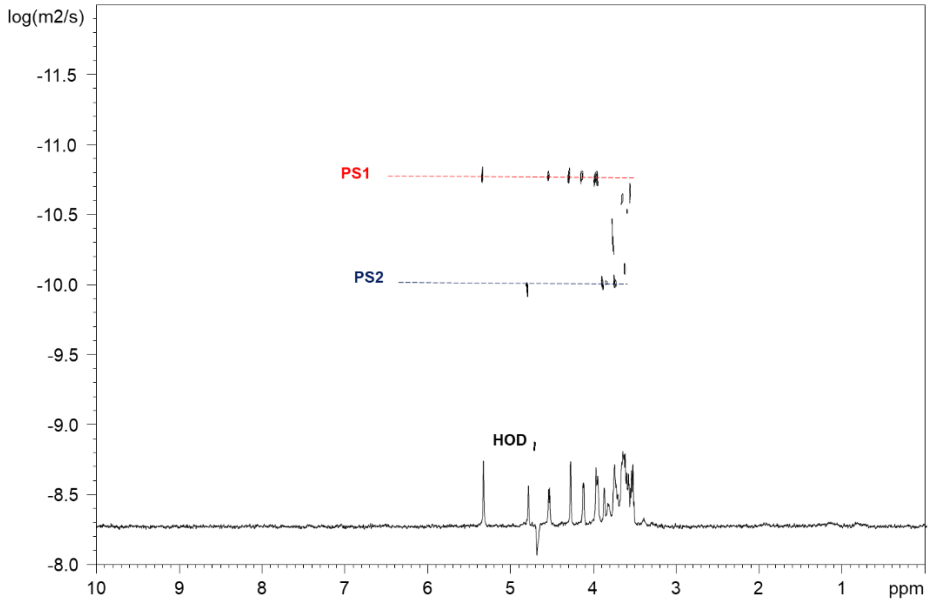

Figure 6.11 Superimposition of ^{1}H NMR and 2D DOSY spectra of the fraction containing both exopolysaccharides, **PS1** and **PS2**.

6.5.2. Molecular Weight estimation by SLS

The mass-average molecular weight of each EPS was determined, in duplicate, by SLS. Samples to be analyzed by SLS were prepared by solubilizing 1 mg of **PS1** or **PS2** in 1 ml of deionized and filtered (0.22 μm) water. Weighed amounts of water were progressively added to the samples to explore lower concentrations. Normally, the mass-average molecular weight, Mw, was obtained from the equation (Schmitz, 1990):

$$\frac{K_{ls}c}{R_\theta} = \left[\frac{1}{Mw} + 2Bc\right]\left[1 + \frac{R_g^2}{3}q^2\right] \qquad \text{eq. 3}$$

where c is the sample mass concentration, B the second virial coefficient, $K_{ls} = 4\pi^2 n_0^2 (dn/dc)^2 / (N_A \lambda^4)$, where $n_0 = 1.33$ is the refractive index of water, $dn/dc = 0.185$ is the refractive index increment (Paduano, 1992), N_A is the Avogadro's number, λ is the laser wavelength in vacuum, R_θ is the excess Rayleigh ratio at 90°. The values of R_θ were obtained from $R_\theta = (I_s - I_{s,0})/I_{s,R} (n_0^2 / n_R^2) R_{\theta,R}$, where I_s is the scattered intensity of the solution, $I_{s,0}$ is the scattered intensity of water, $I_{s,R}$ is the scattering intensity of toluene (the standard), and $n_R = 1.496$ and $R_{\theta,R} = 2.85 \times 10^{-5}$ cm^{-1} are the refractive index and the Rayleigh ratio of toluene, respectively (Kaye & Havlik, 1973), $q = (4\pi n/\lambda) \sin(\theta/2)$ and R_g is the radius of gyration.

As described by Hashim and Ghazy (Hashim, 2014), spherical particles with dimension much smaller than the wavelength of the light beam used for the experiment act as independent scattering centers, generating a symmetrical envelope of scattering light intensity. In this case, it is possible to determine Mw by extrapolation of the data collected at a single angle (Fan, 2014), according to the following equation:

$$\frac{K_{ls}c}{R_\theta} = \left[\frac{1}{Mw} + 2Bc\right] \qquad \text{eq. 4}$$

The mass-average molecular weight of the **PS1** and **PS2** was determined by means of the static light scattering (SLS) through a modified Zimm plot (Figure 6.12) as reported in equation 4, affording the following values:

PS1 ~ (124 ± 2) kDa
PS2 ~ (4.8 ± 0.9) kDa

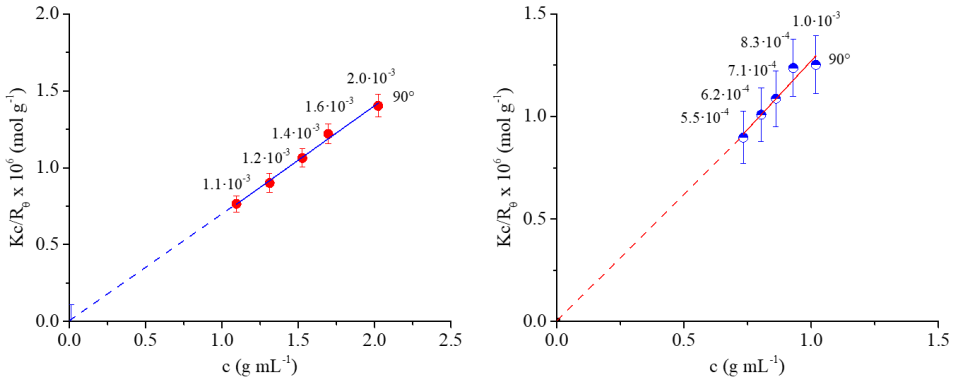

Figure 6.12: Zimm plot for the molecular weight determination of **PS1** and **PS2**.

6.6. Discussion

Z. mobilis is particularly known by its tremendous capability to produce ethanol, and as a result resist to high ethanol concentrations. It is known that the main factors playing a role in this mechanism is related to increased proportion of monounsaturated fatty acids and mean length of the acyl chains in the membrane, nonetheless the pivotal role is played by sterol-like bacterial molecules known as the hopanoids. Indeed, the presence of these cell wall components was reported in the study, with predominant presence of Hop-17(21)-ene which presence was reported in other studies (Hermans, 1991).

Interestingly, *Z. mobilis* represents a narrow group of Gram-negative bacteria which do not synthetize lipopolysaccharide (see Chapter 1.5). Similar to *Sphingomonas* species and other bacteria in the α-group of *Proteobacteria*, close *Zymomonas* produces instead glycosphingolipids (GSL). In case of *Zymomonas mobilis*, the GSL is built of only one monosaccharide unit, namely glucuronic acid, and the ceramide composed of 1,3-dihydroxy-2-amino-hexadecane (DS16:0), and saturated hexadecenoic (16:0) or tetradecanoic (14:0) acid as fatty acid substitution.

Two different EPS components were also isolated and characterizated by means of different spectroscopical and chemical approaches. The properties of both polysaccharides were investigated in relation to the high ethanol tolerance of the bacterium. One of those components, **PS1** was characterized as a galactan built of [→2)-β-D-Gal*f*-(1→3)- β-D-Gal*p*-(1→] repeating unit, and its average molecular size was calculated by means of PFG-NMR and SLS as (124 ± 2) kDa. Interestingly, a similar repeating unit was found as the O-polysaccharide and the core polysaccharide of an acidophilic bacterium, also related to highly ethanolic environment, *Acetobacter methanolicus,* strains MB 58/4 (Grimmecke, 1991) and MB70 (Grimmecke, 1994). The second EPS component, the **PS2** was characterized as a mannose homopolymer with repeating unit as follows: [→6)-α-D-Manp-(1→], and the average molecular mass calculated as (4.8 ± 0.9) kDa.

As widely known, the exopolysaccharides play a role in bacterial adaptation and survival in harsh conditions (see Chapter 1.4). Hence the behaviour of both components was investigated in different ethanol concentration environment using PFG-NMR and DLS. Interestingly, both polysaccharides demonstrated different behaviour upon increase of ethanol concentrations in the environment. The **PS2** possessed similar properties in alcohol to other polysaccharides, namely the polymer coils showed significant tendency to contract observed as significant diminution of the hydrodynamic radius correlated with increased percentage of ethanol. Most interestingly, the **PS1** has shown peculiar features within the increase of alcohol concentration. Unlike other polysaccharides, the galactan coil remained almost unperturbed, as no reduction of hydrodynamic radius was reported, moreover at higher ethanol concentrations a detectable increase of this value was reported. The reliability of the measurements was further confirmed by DLS studies demonstrating that the centred distribution around 10 nm was independent from the ethanol concentration. Moreover, ethanol was shown significantly involve in the solvation shell of the polymer, where more than 10 ethanol molecules were solvating one repeating unit, proportionally to alcohol concentration.

Presented data demonstrate that **PS1,** with its peculiar and interesting behaviour in ethanolic media, likely mediates *Z. mobilis* interaction with the external milieu and finally contributes to its high

ethanol-tolerance mechanisms.

In conclusion, for the first time, an exopolysaccharide whose properties were adapted to resist to such a specific type of environment was described.

References:

Antoniou E., Alexandridis P. (2010) Polymer conformation in mixed aqueous-polar organic solvents. *Eur. Polym. J. 46(2),* 324-335.

Antoniou E., Themistou E., Sarkar B., Tsianou M., Alexandridis P. (2010) Structure and dynamics of dextran in binary mixtures of a good and a bad solvent. *Colloid Polym. Sci. 288(12-13),* 1301-1312.

Ates, O. (2015). Systems biology of microbial exopolysaccharides production. Frontiers in Bioengineering and Biotechnology, 3, 200.

Belin B.J., Busset N., Giraud E., Molinaro A., Silipo A., Newman, D. K. (2018) Hopanoid lipids: From membranes to plant–bacteria interactions. *Nat. Rev. Microbiol*. 16, 304–315.

Bringer S., Härtner T., Poralla K., Sahm H. (1985) Influence of ethanol on the hopanoid content and the fatty acid pattern and continuous cultures of *Zymomonas mobilis*. *Arch. Microbiol. 140(4),* 312-316.

Burakowski A., Gliński J. (2012) Hydration Numbers of Nonelectrolytes from Acoustic Methods. *Chem. Rev. 112(4),* 2059-208.

Ciucanu I., Kerek F. (1984) A simple and rapid method for the permethylation of carbohydrates. *Carbohyd. Res. 131(2),* 209-217.

Cohen Y., Avram L., Frish L. (2005) Diffusion NMR spectroscopy in Supramolecular and Combinatorial Chemistry: An old parameter - New insights. *Angew. Chem. Int. Edit. 44,* 520-554.

Costantino L., D'Errico G., Roscigno P., Vitagliano V. (2000) Effect of urea and alkylureas on micelle formation by a nonionic surfactant with short hydrophobic tail at 25 °C. *J. Phys. Chem. 104(31),* 7326-7333.

De Castro C., Parrilli M., Holst O., Molinaro A. (2010) Microbe-associated molecular patterns in innate immunity: extraction and chemical analysis of gram-negative bacterial lipopolysaccharides. *Methods Enzymol. 480,* 89-115.

Decho A.W. (1990) Microbial exopolymer secretions in ocean environments their roles in food webs and marine processes. *Oceanogr. Mar. Biol. Ann. Rev. 28,* 73-153.

Demel R. A., De Kruyff B. (1976) The function of sterols in membranes. *Biochim. Biophys. Acta, 457,* 109-132.

Di Lorenzo F., Paciello I., Fazio L.L., Albuquerque L., Sturiale L., Da Costa M.S., Lanzetta R., Parrilli M., Garozzo D., Bernardini M.L., Silipo A., Molinaro A. (2014) Thermophiles as potential source of novel endotoxin antagonists: the full structure and bioactivity of the lipo-oligosaccharide from *Thermomonas hydrothermalis. Chembiochem. 15(14),* 2146-2155.

Fan X., Zheng W., Singh D.J. (2014) Light scattering and surface plasmons on small spherical particles. *Light: Sci. Appl. 3,* e179.

Flesch G., Rohmer M. (1989) Prokaryotic triterpenoids. A novel hopanoid from the ethanol-producing bacterium Zymomonas mobilis. *Biochem. J*. 262, 673–675.

Galanos C., Lüderitz O., Westphal O. (1969) New method for the extraction of R lipopolysaccharides. *Eur. J. Biochem*. *9(2),* 245-249.

González K., Calvar N., Gómez E., Domínguez Á. (2007) Density, dynamic viscosity, and derived properties of binary mixtures of methanol or ethanol with water, ethyl acetate, and methyl acetate at T = (293.15, 298.15, and 303.15). *J. Chem. Thermodyn. 39(12),* 1578-1588.

Grimmecke H.D., Knirel Y.A., Shashkov A.S., Kiesel B., Lauk W., Voges M. (1994) Structure of the capsular polysaccharide and the O-side-chain of the lipopolysaccharide from *Acetobacter methanolicus* MB 70, and of oligosaccharides resulting from their degradation by the bacteriophage Acm6. *Carbohyd. Res. 253,* 277-282.

Grimmecke H.D., Mamat U., Lauk W., Shashkov A.S., Knirel Y.A., Vinogradov E.V., Kochetkov N.K. (1991) Structure of the capsular polysaccharide and the O-side-chain of the lipopolysaccharide from *Acetobacter methanolicus* MB 58/4 (IMET 10945), and of oligosaccharides resulting from their degradation by the bacteriophage Acml. *Carbohyd. Res*. 220, 165-172.

Groves P., Rasmussen M.O., Molero M.D., Samain E., Canada F.J., Driguez H., Barbero J.J. (2004) Diffusion ordered spectroscopy as a complement to size exclusion chromatography in oligosaccharide analysis. *Glycobiology 14,* 451-456.

Harris K.R. (2002) Isotope effects and the thermal offset effect for diffusion and viscosity coefficients of liquid water. *Phys. Chem. Chem. Phys. 4,* 5841-5845.

Hermans M.A., Neuss B., Sahm H., (1991) Content and composition of hopanoids in *Zymomonas mobilis* under various growth conditions. *J. Bacteriol.* 173(17), 5592-5595.

Hidalgo-Cantabrana C., Sánchez B., Milani C., Ventura M., Margolles A., Ruas-Madiedoa P. (2014) Genomic overview and biological functions of

exopolysaccharide biosynthesis in Bifidobacterium spp. *Appl. Environ. Microbiol*. 80, 9–18.

Hilliou L., Freitas F., Oliveira R., Reis M.A.M., Lespineux D., Grandfils C., Alves V.D. (2009) Solution properties of an exopolysaccharide from a Pseudomonas strain obtained using glycerol as sole carbon source. *Carbohydr. Polym*. 78, 526–532.

Ingram L. O. (1986) Microbial tolerance to alcohols: role of the cell membrane. *Trends Biotechnol. 4(2),* 40-44.

Iqbal S., Marchetti R., Aman A., Silipo A., Ul Qader S.A.U., Molinaro A. (2017) Enzymatic and acidic degradation of high molecular weight dextran into low molecular weight and its characterizations using novel Diffusion-ordered NMR spectroscopy. *Int. J. Biol. Macromol. 103,* 744-750.

Kannenberg E., Poralla K., Blume A. (1980) A hopanoid from the thermo-acidophilic *Bacillus acidocaldarius* condenses membranes. *Naturwissenschaften. 67,* 458-459.

Kawahara K., Kuraishi H., Zähringer U. (1999) Chemical structure and function of glycosphingolipids of *Sphingomonas* spp. and their distribution among members of the alpha-4 subclass of Proteobacteria. *J. Ind. Microbiol. 23,* 408-413.

Kaye W., Havlik A. (1973) Low angle laser light scattering − absolute calibration. *Appl. Opt. 12,* 541-550.

Kazak H., Öner E.T., Dekker R.F.H. (2010) Extremophiles as sources of exopolysaccharides. In Handbook of carbohydrate polymers (Eds. Ito R., Matsuo Y.). Nova Science Publishers, Inc. New York, pp. 605–619.

Kwon K. J., Park K. J., Kim J. D., Kong J. Y., Kong I. S. (1994) Isolation of two different polysaccharides from halophilic *Zoogloea* sp. *Biotechnol. Lett. 16(8),* 783–788.

Lin Y., Tanaka S. (2006) Ethanol fermentation from biomass resources: current state and prospects. *Appl. Microbiol. Biotechnol. 69,* 627-642.

Molinaro A., Piscopo V., Lanzetta R., Parrilli M. (2002) Structural determination of the complex exopolysaccharide from the virulent strain of *Cryphonectria parasitica*. *Carbohydr. Res. 337(19),* 1707-1713.

Mollakhalili Meybodi N., Mohammadifar M. A. (2015) Microbial exopolysaccharides: A review of their function and application in food sciences. *J. Food Qual. Hazards Control. 2(4),* 112–117.

Nichols C.A., Guezennec J., Bowman J.P. (2005) Bacterial exopolysaccharides from extreme marine environments with special consideration of the southern

ocean, sea ice, and deep-sea hydrothermal vents: A review. *Mar. Biotechnol*. 7, 253–271.

Nicolaus B., Kambourova M., Oner T.O. (2010) Exopolysaccharides from extremophiles: from fundamentals to biotechnology. *Environ. Technol. 31(10),* 1145-1158.

Nwodo U.U., Green E., Okoh A.I. (2012) Bacterial exopolysaccharides: Functionality and prospects. *Int. J. Mol. Sci. 13(11),* 14002-14015.

Paduano L., Sartorio R., Vitagliano V., Albright J.G., Miller D.G. (1992) Measurement of the mutual diffusion coeffi-cients at one composition of the four-component system α-cyclodextrin-L-phenylalanine-monobutylurea-H2O at 25° C. *J. Phys. Chem*. 96, 7478-7483.

Panesar P.S., Marwaha S.S., Kennedy J.F. (2006) *Zymomonas mobilis*: an alternative ethanol producer. *J. Chem. Technol. Biotechnol. 81(4),* 623-635.

Panesar P.S., Marwaha S.S., Kennedy J.F. (2007) Comparison of ethanol and temperature tolerance of *Zymomonas mobilis* strain in glucose and molasses medium. *Indian J. Biotechnol. 6,* 74-77.

Rubinstein M., Colby R. (2003). Polymer solution. Polymer physics. Oxford University Press, New York, pp. 171–196.

Schmitz K. S. (1990) An Introduction to Dynamic Light Scattering. Academic Press Inc., San Diego, pp 11-30.

Seo J.-S., Chong H., Park H.S., Yoon K.-O., Jung C., Kim J.J., Hong J.H., Kim H., Kim J.-H., Kil J.-I., Park C.J., Oh H.-M., Lee J.S., Jin S.-J., Um H.-W., Lee H.-J., Oh S.-J., Kim J.Y., Kang H.L., Lee S.Y., Lee K.J., Kang H.S. (2005) The genome sequence of the ethanologenic bacterium *Zymomonas mobilis* ZM4. *Nature Biotechnol*. 23, 63-68.

Suárez E.R., Syvitski R., Kralovec J.A., Noseda M.D., Barrow J.C., Ewart H.S., Lumsden D.M., Grindley T.B. (2006) Immunostimulatory polysaccharides from *Chlorella pyrenoidosa*. A new galactofuranan. Measurement of molecular weight and molecular weight dispersion by DOSY NMR. *Biomacromolecules. 7(8),* 2368-2376.

Swings J., De Ley J. (1977) The biology of *Zymomonas mobilis*. *Bacteriol. Rev. 41,* 1-46.

Tahara Y., Kawazu M. (1994) Isolation of glucuronic acid-containing glycosphingolipid from *Zymomonas mobilis*. *Biosci. Biotechnol. Biochem. 58,* 586-587.

Tytgat H.L., Lebeer S. (2014) The Sweet Tooth of Bacteria: Common Themes in Bacterial Glycoconjugates. *Microbiol. Mol. Biol. Rev. 78(3),* 372–417.

Viel S., Capitani D., Mannina L., Segre A. (2003) Diffusion ordered NMR spectroscopy: A versatile tool for the molecular weight determination of uncharged polysaccharides. *Biomacromolecules. 4(6),* 1843-1847.

Westphal O., Jann K. (1965) Bacterial Lipopolysaccharides Extraction with Phenol-Water and Further Applications of the Procedure. *Methods Carbohydr. Chem. 5,* 83-91.

Yang S., Pan C., Tschaplinski T.J., Hurst G.B., Engle N.L., Zhou W., Dam P.A., Xu Y., Rodriguez Jr M., Dice L., Johnson C.M., Davison B.H., Brown S.D. (2013) Systems Biology Analysis of *Zymomonas mobilis* ZM4 Ethanol Stress Responses. *PLOS ONE.* 7, 1-14.

SECTION III

Experimental section

Chapter VII

Materials and methods

7.1. *Acetobacter pasteurianus* CIP103108

Extraction and purification of A. pasteurianus CIP103108 LPS

The dried *A. pasteurianus* CIP103108 cells underwent washing with ethanol, water and acetone. Afterwards hot phenol-water procedure was performed in order to isolate the cell walls components (Westphal & Jann, 1965). Thereafter, obtained waster phase (WP) and (PP) was extensively dialyzed (cut off 12-14 kDa) against distilled water and followed by enzymatic digestion with DNase, RNAse (37°C, 5 h) and proteinase K (56°C, 16 h) and again extensively dialyzed (cut off 12-14 kDa) against distilled water. WP and PP were subjected to 14% sodium deoxycholatepolyacrylamide gel electrophoresis (DOC-PAGE) followed by silver nitrate gel staining (Kittelberger, 1993). Moreover, an ultracentrifugation step (100,000 *g*, 4°C, 16 h) was performed to further purify the WP. The LPS material from the WP was further purified applying size exclusion chromatography with Sephacryl-S200 column in denaturing conditions (0.25% DOC at pH 8). Obtained fractions were freeze-dried and DOC was removed by ethanol washing followed by extensive dialysis against distilled water. Finally, the fractions were analysed by sodium dodecyl sulfate-polyacrylamide gel electrophoresis (SDS-PAGE) followed by silver nitrate gel staining.

Monosaccharide compositional analysis of A. pasteurianus

The composition of neutral sugars was established with acetylated alditols method (De Castro, 2010). Weighted aliquot of LPS was hydrolysed with 2 M TFA solution at 120°C for 120 minutes. Thereafter liberated monosaccharides were reduced with $NaBH_4$ to alditols and acetylated twice with equal amounts of pyridine and acetic anhydride at 85°C for 10 minutes. Acetylated alditols were further analysed using gas-liquid chromatography/mass spectrometry (GC-MS). Thereafter 3 µg of internal standard xylose was added to the sample. Aminosugars were liberated applying 16 h hydrolysis in 4 M HCl at 100°C proceeded by reduction and acetylation as described above. Uronic acids were quantified as described for neutral sugars, applying an additional step of carboxyl group reduction with $NaBD_4$. The identification of ulosonic acids was carried out with acetylated methyl glycosides method (De Castro, 2010). An aliquot of sample underwent 16 h methanolysis with 1.25 M HCl/MeOH at 85°C and was further acetylated as described above. The absolute configuration of monosaccharides was unveiled by deriving the

saccharide residues to acetylated *O*-oct-2-yl glycosides (Leontein, 1978). Shortly, the derivates were obtained by reaction with 2-(-)-octanol and acetyl chloride at 85°C for 16 h and acetylation with Ac_2O and Pyr as described above. The products were analysed by GC-MS. The linkage analysis was performed applying Ciucanu-Kerek's method (Ciucanu & Kerek, 1984). The methylation was performed by iodomethane in presence of NaOH in DMSO. Furthermore, the product was hydrolysed with 2 M TFA for 120 minutes at 120°C, liberated partially methylated monosaccharides reduced with $NaBD_4$ and peracetylated twice with Ac_2O and Pyr twice at 85°C for 10 minutes. Obtained products were analysed with GC-MS as described: GLC [HP 6890 N gas chromatograph with FID and a column (Agilent Technologies, 30 m × 0.25 mm, film thickness 0.25 µm) of PhenylMethylSiloxane HP-5MS] with temperature programmes follows: 120°C for 3min, then 5°C min^{-1} to 320°C.

Fatty acid analysis of A. pasteurianus

The fatty acids were characterized and quantified applying the fatty acid methyl esters (FAME) method (De Castro, 2010). Weighted aliquot of LPS underwent 4 h hydrolysis in 4 M HCl at 100°C. Thereafter the sample was neutralised adding 5 M NaOH and heating for 30 min at 100°C. The pH was further brought to 3 and liberated fatty acids extracted vigorously shaking with chloroform. Organic phase was dried and methylated diazomethane at room temperature. The FAME were injected to the GLC and characterized basing on retention time comparison with the standards. The quantification was made adding 17:0 as an internal standard. The position of hydroxyl groups was elucidated basing on 2 h derivatization with *N,O-bis*-(trimethylsilyl)trifluoroacetamide (BSTFA) at 65°C and GC-MS analysis of obtained products. The ester linked fatty acids were characterized by an hour hydrolysis with 0.5 M NaOH in water: methanol solution (1:1) followed by an extraction and methylation of fatty acids as described above. The FAME were characterized basing on a GLC analysis. GLC [HP 6890 N gas chromatograph with FID and a column (Agilent Technologies, 30 m × 0.25 mm, film thickness 0.25 µm) of PhenylMethylSiloxane HP-5MS]with temperature programmes follows: 120°C for 3 min, then 5°C min^{-1} to 320°C.

Isolation of O-polysaccharide and lipid A domains from A. pasteurianus

An aliquot (16 mg) of pure, *Acetobacter pasteurianus* CIP103108 S-LPS containing fraction underwent mild acid hydrolysis using acetate

buffer at pH 4.4 for 5h at 100°C. Thereafter the hydrophilic carbohydrate fraction and glycolipid fraction were separated applying Bligh-Dyer's method (Bligh & Dyer, 1959). A mixture of chloroform and methanol was added to the hydrolysate until a chloroform/methanol/hydrolysate 2:2:1.8 (v/v/v) ratio was obtained. The mixture was vortexed and centrifugated, thereafter the organic and water phases were separated and freeze dried. The hydrophobic glycolipid fraction was analysed by MALDI-MS, whereas the hydrophilic part underwent size exclusion chromatography step on a GE Healthcare Life Sciences Superdex 75 column eluted with 50 mM ammonium bicarbonate. Obtained fractions were monitored with ^{1}H NMR.

MALDI-TOF and MS²

The reflectron MALDI-TOF MS and MS^2 analysis were conducted on an ABSCIEX TOF/TOF™ 5800 Applied Biosystems mass spectrometer equipped with an Nd:YLF laser with a λ of 345 nm, a b500-ps pulse length and a repetition rate of up to 1000 Hz. *Acetobacter pasteurianus* CIP 103108 lipid A fraction was solved in in $CHCl_3$/MeOH (1:1, v/v) as described (Silipo, 2004; Di Lorenzo, 2017a). As the matrix hydroxyacetophenone (THAP) dissolved in CH_3OH/0.1% TFA/CH_3CN (7:2:1, v/v/v) at a concentration of 75 mg ml^{-1} was used (Molinaro, 2002). 0.5 µl, of matrix solution and lipid A solution was deposited on the MALDI plate and dried at room temperature. The MALDI spectra were accumulation of 1500 shots, whereas MS^2 experiments were 6000–7000 shots.

NMR A. pasteurianus CIP103108

The structural assignments of isolated polysaccharides and glycoconjugates were performed basing on ^{1}H NMR and 2D NMR spectra, recorded in D_2O at pD 7 at 278K with a cryoprobe-equipped Bruker 600 DRX spectrometer. The total correlation spectroscopy (TOCSY) experiments were performed with spinlock times of 100 ms using data sets (t1 × t2) of 4096 × 512 points. Double-quantum-filtered phase-sensitive correlation spectroscopy (DQF-COSY) experiments were registered using data sets of 4096 × 912 points. nuclear Overhauser enhancement spectroscopy (NOESY) and Rotating-frame Overhauser enhancement spectroscopy (ROESY) experiments were performed using data sets (t1 × t2) of 4096 × 512 points and with mixing times between 100 and 400 ms. All homonuclear experiments data matrix was zero-filled

in both dimensions to give a matrix of 4 K × 2 K points and was resolution-enhanced in both dimensions using a cosinebell function before Fourier transformation. Finally, coupling constants were determined by 2D phase-sensitive DQF-COSY measurements. $^{1}H^{13}C$ Heteronuclear single-quantum coherence (HSQC) and $^{1}H^{13}C$ heteronuclear multiple-bond correlation (HMBC) experiments were carried out in the ^{1}H-detection mode by single-quantum coherence with proton decoupling in the ^{13}C domain using data sets of 2048 × 400 points. The $^{1}H^{13}C$ HSQC experiments were carried out with sensitivity improvement and in the phase-sensitivemode applying echo/antiecho gradient selection, with multiplicity editing during the selection step (States, 1982). Furthermore, $^{1}H^{13}C$ HMBC was optimized on long-range coupling constants, along with a low-pass J filter in order to suppress one-bond correlations, with use of gradient pulses for selection. Thereafter, a 60 ms delay had been used for the evolution of long-range correlations. Moreover, $^{1}H^{13}C$ HMBC spectra were optimized for 6 – 15 Hz coupling constants. The data matrix was extended to 2048 × 1024 points by using a forward linear prediction extrapolation in all the heteronuclear experiments (Stern, 2002).

Finally, the ^{31}P and $^{1}H^{31}P$ HSQC were performed on a Bruker DRX-400 spectrometer. Aqueous 85% phosphoric acid was used as external reference (SIG = 0.00 ppm). $^{1}H^{31}P$ HSQC experiments were optimized for an 8 Hz coupling constant. The data matrix was extended to 2048 × 1024 points by applying a forward linear prediction extrapolation.

TLR4/MD-2 activation assay with HEK-Blue hTLR4 cells

The culture of HEK-Blue hTLR4 cells was done in DMEM high glucose medium supplemented with 10% fetal bovine serum (FBS), 2 mM glutamine, antibiotics and 1× HEK-BlueTM Selection (Invivogen). Thereafter the cells were detached from the Petri dish, quantified and finally seeded in a 96-well plate at a density of 4×10^{4} cells per well and incubated overnight (37 °C, 5% CO_2, 95% humidity). Thereafter the supernatant was removed and replaced with only DMEM w/o Phenol Red. The activation assay was performed upon 16 hour cell stimulation with different concentrations (0.1, 1, 10, 100 ng/mL) of *Acetobacter pasteurianus* CIP103108 LPS or *E. coli* O55:B5 LPS (Sigma-Aldrich) as positive control. To competition assay was conducted pre-incubating HEK-Blue hTLR4 cells with *Aacetobacter pasteurianus* CIP103108 LPS (0.1, 1, 10, 100 ng/mL) for 30 minutes followed by addition of 1 ng/mL of *E. coli* O55:B5 LPS and further incubation for 16 h. Thereafter the supernatants

containing SEAP were collected and incubated with paranitrophenylphosphate (pNPP) for 2 − 4 hours blocking the access of light at room temperature. The optical density of all wells was measured with a microplate reader set to λ = 405 nm. Obtained results were normalized to untreated cells (activation assay) or *E. coli* O55:B5 LPS stimulated cells (competition assay), expressed as the mean of percentage ± SEM of at least three independent experiments.

7.2 *Endozoicomonas* sp. HEX 311

Isolation and purification

The LPS from *Endozoicomonas* sp. HEX 311 was isolated from dried cell-pellet applying the hot phenol-water extraction (Westphal & Jahn, 1965) followed by dialysis against Milli-Q water (cut-off 12 – 14 kDa). Obtained product was further digested with DNase and RNase (37°C, 5 h) and proteinase K (56°C, 16 h) and one more dialysed against Milli-Q water (cut-off 12 – 14 kDa). Thereafter the dialysate was subjected to an ultracentrifugation step at 4°C, 100.000 x g for 48 h. The nature of obtained product was further analysed by DOC-PAGE followed by silver staining (Kittelberger, 1993). Finally, the LPS was purified by a Sephacryl S-400 column (GE Healthcare Lifesciences) and eluted with 50 mM ammonium bicarbonate.

Compositional analysis

The monosaccharide content was determined applying the acetylated *O*-methylglycosides technique (De Castro, 2010). An aliquot (500 µg) of material was methanolysed in 1.25 M HCl/MeOH solution and further acetylated with equal amounts of Ac_2O and Pyr for 30 minutes at 85°C. Absolute configuration of sugar residues was designed basing on the acetylated *O*-octyl glycosides method as described (De Castro, 2010). Thereafter 1 mg of sample underwent linkage analysis with Ciucanu-Kerek's method (Ciucanu & Kerek, 1984). Briefly, the sample suspended in DMSO was methylated with iodomethane in presence of sodium hydroxide, hydrolysed with 2 M THA in 120°C for 120 minutes, the carbonyl groups reduced with $NaBD_4$ and finally acetylated as described above. The total fatty acid content was characterized upon 4 h hydrolysis in 4 M aqueous HCl solution at 100°C, followed by treatment with 5 M NaOH for 30 minutes in 100°C. The fatty acids were isolated with chloroform after acidifying the solution (pH = 3). The products were

further methylated twice with diazomethane at room temperature and obtained fatty acid methyl esters analysed by GC-MS. The FAME were also obtained upon methanolysis of the LPS with 1 M HCl/MeOH solution at 80°C 16 h followed by extraction with hexane. The organic phase was further investigated with GC-MS. Finally, the absolute configuration was characterized as described previously (Rietschel, 1976). All GC-MS analysis were conducted on Agilent Technologies gas chromatograph 6850A equipped with a mass selective detector 5973N. Separations were performed on a Zebron ZB-5 capillary column (Phenomenex, 30 m x 0.25 mm internal diameter, flow rate 1 mL min^{-1}, He as carrier gas). The program as follows: 120°C for 3 min, then 5°C min^{-1} to 320°C.

Isolation of the lipid A

An aliquot of lipid A was dissolved in acetate buffer at pH 4.4 and heated at 100°C for 2 h in order to cleave the lipid A from saccharide domain. The hydrolysate was further mixed with chloroform and methanol in order to reach chloroform/methanol/hydrolysate ratio 2:2:1.8, vortexed and centrifugated. The organic phase was recovered and washed with the water phase of freshly prepared Bligh-Dyer (Bligh &Dyer, 1959) mixture and pooled phases dried. Obtained product underwent further MALDI-TOF analysis.

Ammonium hydroxide treatment

An aliquot of isolated, pure lipid A was suspended in 10% ammonium hydroxide and heated at 37°C for 16 h (Silipo, 2002). The product was dried and analysed by MALDI-MS.

MALDI MS and MS^2

All MALDI-TOF and MS^2 experiments were performed on an ABSCIEX TOF/TOFTM 5800 Applied Biosystems mass spectrometer, equipped with an Nd:YLF laser with a λ of 345 nm, a <500 ps pulse length, and a repetition rate of up to 1000 Hz. The lipid A fractions were dissolved chloroform/methanol 1:1 (v/v) solution ad described (Silipo, 2004; Di Lorenzo, 2017a). As a matrix 75 mg mL^{-1} trihydroxyacetophenone (THAP) dissolved in methanol/0.1 % trifluoracetic acid/acetonitrile (7:2:1,v/v/v) was used. Thereafter the ammonium treatment product was dissolved in chloroform-trifluoroethanol (4:1, v/v) solution and DHB in acetonitrile 0.2 % trifluoroacetic acid (7:3, v/v) was used as a matrix (Molinaro, 2002). 0.5 µL of the lipid A preparation and 0.5 µL of the matrix were deposited on a MALDI plate and dried at room temperature. The bacterial cell pellet

was prepared following Larrouy-Mammus approach (Larrouy-Maumus, 2016). The matrix solution was 10 mg mL^{-1} 2,5-dihydroxybenzoic acid (DHB) in chloroform/methanol (9:1, v/v). The cell pellet preparation of 0.5 µL and 0.5 µL of the matrix were deposited on a stainless MALDI plate and dried at room temperature. All spectra were performed in negative polarity accumulating 1500 laser shots, whereas MS^2 experiments were a sum of whereas 6000–7000 shots.

7.3 *Phaeobacter gallaeciensis* BS107 SA and WT

Isolation and purification of the LPS

Dried and pre-washed with ethanol, water and acetone *Phaeobacter gallaeciensis* BS107 SA and WT cells underwent hot phenol/water extraction (Westphal & Jann, 1965) preceded by the PCP extraction (light petroleum/chloroform/phenol, 7:5:3 v/v/v) (Galanos, 1969). After extensive dialysis against Milli-Q water the phases were destined to enzymatic digestion with DNAse, RNAse (37°C, 5 h) and proteinase K (56°C, 16 h) followed by another step of dialysis against Milli-Q water. Thereafter the fractions underwent 14% DOC-PAGE analysis followed by silver nitrate staining (Kittelberger, 1993). The material obtained from *Phaeobacter gallaeciensis* BS107 WT was subjected to another purification step with Sephacryl S-300 column (GE Healthcare Lifesciences) eluted with 50 mM ammonium bicarbonate.

Compositional and methylation analysis

The neutral sugar composition of *Phaeobacter gallaeciensis* BS107 SA was analysed using acetylated alditols method (De Castro, 2010). An aliquot of sample underwent 2 h hydrolysis at 120°C in 2 M TFA, 16 h reduction with $NaBD_4$ and acetylation with use of equal amounts of pyridine and acetic anhydride for 10 minutes in 85°C. The products were analysed by GC-MS. The quantification was made by internal standard method with 3 µg of allose as reference. In parallel determination of lipopolysaccharide composition of *Phaeobacter gallaeciensis* BS107 SA and WT and SA strains was performed by metanalysis in 1.25 M HCl/MeOH at 85°C, 16 h, flowed by acetylation (85°C, 30 min). Obtained products were analysed with GC-MS.

Amino sugar constitution was established by 16 h hydrolysis of LPS in 100°C with 4 M HCl. Obtained products were reduced and acetylated as above.

Total fatty acids were analysed as fatty acid methyl esters (FAME) (De Castro, 2010). An aliquot of *Phaeobacter gallaeciensis* BS107 SA LPS was hydrolysed for 4 h at 100°C with 4 M HCl, thereafter the sample was brought to basic pH with 5 M NaOH solution. The hydrolysis was continued for 30 min at 100°C. In order to quantify the ester linked fatty acids a hydrolysis with 0,5 M NaOH in H_2O/MeOH 1:1 (v/v) at 85°C for 2 h was performed. Fatty acids were extracted with chloroform from acidic (pH = 3) solution and were methylated twice using diazomethane at room temperature for 5 minutes. The products were analysed by GC-MS, the quantification was performed with use of GC and 17:0 as the internal standard. The hydroxy-fatty acids composition was confirmed using the BSTFA derivatives. Moreover, *Phaeobacter gallaeciensis* BS107 SA and WT LPS fatty acid content was also characterized basing on methanolysis performed with 1.25 M HCl/MeOH at 85°C for 16 h followed by isolation with hexane and analysis with GC-MS.

Isolation of LPS constituents

The *Phaeobacter gallaeciensis* BS107 SA LPS underwent mild acid hydrolysis. The sample was dissolved in 1% acidic acid solution and heated for 150 min at 100°C. Water soluble and insoluble constituents were separated by Blight-Dyers extraction (Bligh & Dyer, 1959). A mixture of methanol and chloroform was added until the ratio of chloroform/methanol/hydrolysate 2:2:1,8 (v/v/v). The mixture was shaken vigorously, and phases separated with centrifugation.

MALDI-TOF MS and MS^2

Reflectron MALDI-TOF MS and MS^2 analysis were performed using ABSCIEX TOF/TOF™ 5800 Applied Biosystems mass spectrometer. The intact bacterial cell pellet was treated as described in the literature (Larrouy-Maumus, 2016). 2,5-dihydroxybenzoic acid (DHB) was dissolved in $CHCl_3$/MeOH solution 9:1, v/v) at the final concentration 10 mg ml^{-1} and was used as the matrix solution. 0,5 µl of matrix solution and 0,5 µl of bacterial cells preparation were deposited on plate and left drying at room temperature.

The lipid A was dissolved in $CHCl_3$/MeOH (1:1, v/v) until the concentration 25 pmol μl^{-1}. Trihydroxyacetophenone (THAP) was dissolved in MeOH/0,1% TFA/CH_3CN (7:2:1, v/v/v) at concentration of 75 mg ml^{-1} was used as matrix. Like in the previous case, 0,5 µL of the matrix solution and 0,5 µL of lipid A solution was placed on a MALDI plate and left drying at room temperature. Spectra were recorded accumulating 1500 laser shots in case of MS, MS^2 were a sum of 6000-7000 shots (Sturiale, 2011).

Immunological assays

HEK293 cell line transfected with hTLR4/MD-2-CD14 (InvivoGen) were seeded on a 96-well plate at concentrations 1 x 10^5 cells/mL. After 48 h HEK cells were transfected by PolyFect Transfection Reagent (Qiagen) with a reaction mix containing 15 ng of *Renilla* luciferase reporter plasmid and 150 ng of Firefly luciferase reporter con-structs, pGL3.ELAM.tk (which harbours nuclear factor kappa B (NF-κB) promoter sequences). The following day cells were incubated with different concentrations (1, 10, and 100 ng/mL) of *P. gallaeciensis* BS107 LPS, E. coli O111:B4 LPS (LPS-EB ultrapure; InvivoGen) or synthetic lipid IV a for 6h. The NF-κB activation (Dual Luciferase Reporter Assay System, Promega) and release of CXCL-8 release (DuoSet R&D System) was measured.

Human CD 14+ monocytes were isolated from human peripheral blood monocytes (PBMCs) of healthy adult blood donors and differentiated in macrophages (MoMs). Ethical approval for blood sampling from consenting healthy volunteers was granted by the Ethics Review Board of Sapienza University. The human CH14+ monocytses were isolated as described (Di Lorenzo, 2017b). The macrophages were seeded in a 24-well plates (2.5 x 10^5 cells/well) and stimulated with 1, 10 and 100 ng/mL of *P. gallaeciensis* BS107 LPS and subsequently with the same concentrations of *E. coli* O111:B4 LPS (LPS-EB ultrapure; InvivoGen) or synthetic lipid IV a for 12 h. Thereafter the cells were recovered and cytokine release characterized by ELISA (R&D System).

7.4 *Zymomonas mobilis*

Zymomonas mobilis bacterial growth

Zymomonas mobilis cells were grown in a cell medium consisting of Bactopeptone (10 g L^{-1}), glucose (20 g L^{-1}) and yeast extract (10 g L^{-1}) shaken at 150 rpm for 72 or 96 h, at 30 °C. The medium was removed after

centrifugation at 4000 rpm for 30 min. Finally, the cell pellet was freeze-dried.

Isolation of exopolysaccharides PS1 and PS2

Primarly Z. mobilis cell pellet underwent the PCP extraction as described (Galanos, 1969). Both exopolysaccharide fractions (**PS1** and **PS2**) were isolated from dried *Zymomonas mobilis* cell pellet applying hot phenol/water method (1:1 v/v) (Westphal & Jann, 1965), thereafter the water phase (WP), so as the phenol phase (PP) underwent extensive step of dialysis against deionized water. The water phase containing predominantly **PS1** was subjected to enzymatic digestion with DNase and RNase (38°C, 5 h) and proteinase K (56°C, 16 h) followed by another dialysis step against deionised water. Thereafter, the WP were subjected to gel filtration chromatography a Sephacryl S-300 column, eluted with 50 mM ammonium bicarbonate. Obtained fractions were monitored with ^{1}H NMR. The PP containing **PS2** underwent ultracentrifugation at 4°C, 147.000 x g for 48 h. The supernatant was further subjected to a Sephacryl S-500 column, eluted with 50 mM ammonium bicarbonate, obtained fractions freeze fried and monitored with ^{1}H NMR. Moreover, both fractions were found to remain at the start of silver stained (Kittelberger, 1993) SDS-PAGE lane.

Compositional methylation

The sugar compositional analysis was performed deriving the monosaccharides into *O*-methyl glycosides (De Castro, 2010). Purified EPS underwent methanolysis in 1.25 M HCl/MeOH solution at 85°C for 16 h, thereafter the products were acetylated with equal quantities of acetic anhydride and pyridine for 30 minutes in 85°C. Obtained acetylated *O*-methyl glycosides were subjected to GC-MS analysis. Absolute configuration was examined by deriving each monosaccharide to *O*-oct-2-yl glycosides by reaction with 2-(-)-octanol and acetyl chloride at 85°C for 16 hours proceeded with acetylation as described above and analysis with GC-MS (Leontein, 1978). The linkage analysis was carried out by Ciucanu-Kerek's method (Ciucanu & Kerek, 1984). An aliquot of sample was suspended in DMSO, thereafter methylation with methyl iodide in presence of sodium hydroxide was performed at room temperature for 4 h. The methylated polysaccharide underwent hydrolysis with 2 M TFA at 120°C for 2 h followed by reduction with $NaBD_4$. Finally, the partially methylated alditols were acetylated as above and analysed with GC-MS.

All GC-MS analyses were carried out using Agilent Technologies 6850 A gas chromatograph equipped with a mass selective detector 5973 N and a Zebron ZB-5 capillary column (Phenomenex, 30 m × 0.25 mm i.d., flow rate 1 mL/min, He as carrier gas). The temperature program used as follows: gradient of 150°C (3 min) to 280°C at 3°C min^{-1}.

PFG-NMR

The Pulsed-Field Gradient (PFG)-NMR experiments were performed at 298,15K. Fractions containing separately **PS1** and **PS2** (0.8 mg) were dissolved in 600 µL pre-formed D_2O/ethanol mixtures with increasing concentration of ethanol (0%, 4%, 8%, and 12% by volume). HDO signal was used as the internal standard. Furthermore, a stimulated echo sequence with bipolar gradient pulses and one spoil gradient (stebpgp1s1d from Bruker library) with a longitudinal eddy current delay was applied. The experiments were optimized as follows: echo delay was Δ = 250 ms for the determination of **PS1** and **PS2** self-diffusion coefficients and Δ = 150 ms for the determination of ethanol self-diffusion coefficient and the gradient duration δ = 6 ms for **PS1** and **PS2**, and δ = 2.5 ms for ethanol. Thereafter the sequence was run as a 2D NMR experiment with a linear gradient G incremented, in 16 steps, from 2% to 95% of the maximum gradient amplitude (5.35 G cm^{-1}). Afterward Fourier transformation and baseline correction of ^1H spectra (F2 dimension), the diffusion dimension (F1) of the 2D DOSY spectra were processed with TopSpin software (version 3.1). The self-diffusion coefficients of both EPSs, namely **PS1** and **PS2** so as the ethanol present in the mixtures were calculated basing on proton signal intensity decay. Thus, for both exopolysaccharides, the decay of anomeric signals at 5.34 ppm and 4.80 ppm, for **PS1** and **PS2** respectively was observed, whereas the signals at 3.52 ppm and 1.05 ppm were considered for ethanol. Normalized integral intensities of every proton were further fitted to an exponential decay, according to equation below:

$$I = I_0 \exp(-Dk)$$

where: I is the integral intensity, normalized to the integral obtained at the lowest gradient amplitude; I_0 is the signal intensity in the absence of any applied magnetic field gradient; γ is the magnetogyric ratio of the proton D is the intradiffusion coefficient and with $k = (G \gamma \delta)^2 (\Delta - \delta/3 - \tau/2)$ where G is the strength of the magnetic field gradient pulses; γ is the magnetogyric ratio of the proton; δ is their duration; Δ is the distance

between the leading edges of the gradient pulses and corresponds to the experimental diffusion time and finally τ is the gradient recovery time. There was no Δ effect observed on the signal decay, single exponential equation satisfactorily interpolating the data in all cases which finally lead to the same self-diffusion coefficient for a given component in each sample.

Dynamic and static light scattering

The light scattering experiments, namely Static light scattering (SLS) and Dynamic light scattering (DLS) were conducted with a setup composed by a Photocor compact goniometer, a SMD 6000 Laser Quantum 50mW light source operating at 5325 Å, a photomultiplier (PMT-120-OP/B) and a correlator (Flex02-01D) obtained from Correlator.com. The measurements were conducted at 298,15 K with temperature controlled by a thermostat bath. The scattering angle of all experiments was 90° (θ). Furthermore, the scattering vecor value $q=4\pi n / \lambda \sin(\theta/2)$ was calculated by assuming the refractive index of solution as n = 1.33. Samples for SLS analysis were prepared by dissolving 1 mg of both **PS1** and **PS2** in 1 mL of deionized filtered (0.22 µm pore size) water. Thereafter weighed amounts of samples were progressively added to the samples in order to explore lower exopolysaccharide concentrations. The average-masses were determined in duplicate. The regularization algorithm was used to analyse the scattered intensity correlation function (Lomakin, 2005). In order to prepare samples for DLS 1 mg of **PS1** was dissolved in 1 mL of water and pre-formed water-ethanol mixtures (12 and 16% ethanol by volume). for each analysed sample at least three independent diffusion coefficient measurements were performed.

7.5. LPS/MD-2 interaction studies

LPS isolation

The dried cell pellet from *Bradyrhizobium* BTAi-1 Δshc, previously washed with ethanol, water, acetone and light petroleum was subjected to hot phenol water extraction (Westphal & Jahn, 1965) followed by extensive dialysis against Milli-Q water (cut-off 12 - 14 kDa). Thereafter the product was digested with DNase, RNase (37°C, 5h) and proteinase K (56°C, 16 h) and dialysed against Milli-Q water (cut-off 12 - 14 kDa). Finally, the dialysate was subjected to an ultracentrifugation step at 4 °C,

147.000 x g for 48 h. The pellet was recovered and freeze-dried. Nature and purity were examined with DOC-PAGE electrophoresis and compared to the literature data. The isolation of *Acetobacter pasteurianus* LPS was described in Chapter 3.1 and 9.1.

Expression and Purification of hMD-2

The purification of His-tagged hMD-2 was performed by means of immobilized metal affinity chromatography (IMAC) using high density nickel resin as reported (Facchini, 2018). 0.5 M Tris/HCl pH 7.5 and 1.5 M NaCl was added to *Pichia* medium until the concentration 50 mM Tris/HCl 150 mM NaCl. Thereafter the medium was passes through a high-density nickel column, pre-washed with 50 mM Tris/HCl pH 7.5 and 150 mM NaCl. The hMD-2 was eluted with gradient of imidazole 0 – 1 M.

The use of standard Nickel-column approach was not successful due to presence of contaminants in the hMD-2 fraction, moreover, the column did not show significant affinity as the recombinant protein was present on the dead volume fraction.

Further approach was performed using a cobalt-based TALON® column. The resin was added to *Pichia pastoris* medium and inubated 16 h in the *Pichia pastoris* medium with agitation at 4°C. Thereafter, the protein was eluted with 1 M imidazole; 1.5 mL of eluate was recovered for every fraction. The purification was monitored using SDS-PAGE electrophoresis, visualized with Coomassie Blue staining

Cobalt-based resin has shown high affinity to the column. Fractions were recovered and concentrated using 3 kDa filters.

NMR experiments

The ^{1}H NMR and DOSY experiments recorded on a Bruker Avance III 800 MHz spectrometer equipped with a TCI cryoprobe.

The ^{1}H NMR experiments were recorded with a concentration of the compounds was set to 0.9 mg/mL (LPS from *Acetobacter pasteurianus*) and 1 mg/mL (LPS from *Bradyrhizobium BTAi-1 Δshc*) in perdeuterated PBS 50 mM in D2O, uncorrected pH meter reading 7.5, with 64 scans.

All DOSY spectra were recorded at 298 K with the ledbpgppr2s pulse sequence by acquisition of 64 scans, with a diffusion time of Δ = 500 ms (for LPS from *Acetobacter pasteurianus)* or Δ = 300 ms (for LPS from *Acetobacter pasteurianus)*, a gradient length of δ = 4 ms (in both cases),

and a gradient ramp from 5% to 95% in 32 linear steps. Was used the same conditions for acquisition of the sample in presence of hMD-2.

Transmission Electron Microscopy

Samples analysed using Cryo-TEM were dissolved in PB (50 mM) pH 7.5 and vitrified on Quantifoil 2/2 grids, using vitrobot (FEI) and analyzed at nitrogen liquid temperature with a TEM operated at 200 kV in low-dose conditions. Micrographs were taken at low radiation dose on a JEM-2200FS/CR transmission electron microscope JEOL, Japan) operated at 200 kV and equipped with an UltraScan4000 SP (4008x4008 pixels) cooled slow-scan CCD camera (GATAN, UK).

References:

Bligh E.G., Dyer W.J. (1959) A rapid method for total lipid extraction and purification. *Can. J. Biochem. Physiol. 37,* 911-917.

Ciucanu, I., Kerek, F. (1984) A simple and rapid method for the permethylation of carbohydrates. *Carbohydr. Res. 131,* 209–217.

De Castro C., Parrilli M., Holst O., Molinaro A. (2010) Microbe-associated molecular patterns in innate immunity: extraction and chemical analysis of gram-negative bacterial lipopolysaccharides. *Methods Enzymol. 480,* 89-115.

Di Lorenzo F. (2017a) The lipopolysaccharide lipid A structure from the marine sponge-associated bacterium *Pseudoalteromonas* sp. 2A. *Antonie Leeuwenhoek. 110,* 1401-1412.

Di Lorenzo F., Palmigiano A., Al Bitar-Nehme S., Sturiale L., Duda K.A., Gully D., Lanzetta R., Giraud E., Garozzo D., Bernardini M.L., Molinaro A., Silipo A. (2017b) The Lipid A from *Rhodopseudomonas palustris* Strain BisA53 LPS Possesses a Unique Structure and Low Immunostimulant Properties. *Chem. Eur. J. 23,* 3637-3647.

Domon B., Costello C.E. (1988) Structure elucidation of glycosphingolipids and gangliosides using high-performance tandem mass spectrometry. *Biochemistry. 27(5),* 1534-1543.

Facchini F.A., Zaffaroni L., Minotti A., Rapisarda S., Calabrese V., Forcella M., Fusi P., Airoldi C., Ciaramelli C., Billod J.M., Schromm A.B., Braun H., Palmer C., Beyaert R., Lapenta F., Jerala R., Pirianov G., Martin-Santamaria S., Peri F. (2018) Structure-Activity Relationship in Monosaccharide-Based Toll-Like Receptor 4 (TLR4) Antagonists. *J. Med. Chem. 61(7),* 2895-2909.

Galanos C., Luderitz O., Westphal O. (1969) A new method for the extraction of R lipopolysaccharides. *Eur. J. Biochem*. *9*, 245-249.

Kittelberger R., Hilbink F. (1993) Sensitive silver-staining detection of bacterial lipopolysaccharides in polyacrylamide gels. *J. Biochem. Biophys. Methods*. *26(1),* 81-86.

Larrouy-Maumus G., Clements A., Filloux A., McCarthy R.R., Mostowy S. (2016) Direct detection of lipid A on intact Gram-negative bacteria by MALDI-TOF mass spectrometry. *J. Microbiol. Methods. 120,* 68-71.

Leontein K., Lönngren J. (1978) Determination of the absolute configuration of sugars by Gas-Liquid Chromatography of their acetylated 2-octyl glycosides. *Methods Carbohydr. Chem. 62,* 359-362.

Lomakin A., Teplow D.B., Benedek G.B. (2005) Quasielastic light scattering for protein assembly studies. In Amyloid Proteins: Methods and Protocols Vol. 299 (Eds. Sigurdsson E.M.). Human Press, Totowa pp. 153-174.

Molinaro A., Piscopo V., Lanzetta R., Parrilli M. (2002) Structural determination of the complex exopolysaccharide from the virulent strain of *Cryphonectria parasitica*. *Carbohydr. Res. 337(19),* 1707-1713.

Rietschel, E.T. (1976) Absolute configuration of 3-Hydroxy fatty acid present in lipopolysaccharides from various bacterial groups. *Eur. J. Biochem. 64*, 423-428.

Silipo A., Lanzetta R., Amoresano A., Parrilli M., Molinaro A. (2002) Ammonium hydroxide hydrolysis: a valuable support in the MALDI-TOF mass spectrometry analysis of Lipid A fatty acid distribution*. J. Lipid Res. 43,* 2188-2195.

Silipo A., Sturiale L., Garozzo D., De Castro C., Lanzetta R., Parrilli M., Grant W.D., Molinaro A. (2004) Structure elucidation of the highly heterogeneous lipid a from the lipopolysaccharide of the gram-negative extremophile bacterium *Halomonas magadiensis* Strain 21 M1. *Eur. J. Org. Chem. 10,* 2263-2271

States D.J., Haberkorn R.A., Ruben D.J. (1982) A two-dimensional nuclear Overhauser experiment with pure absorption phase in four quadrants. *J. Magn. Reson. 48,* 286-292.

Stern A.S., Li K.B., Hoch J.C. (2002) Modern spectrum analysis in multidimensional NMR spectroscopy: comparison of linear-prediction extrapolation and maximum-entropy reconstruction. *J. Am. Chem. Soc. 124,* 1982-1993.

Sturiale L., Palmigiano A., Silipo A., Knirel Y.A., Anisimov A.P., Lanzetta R., Parrilli M., Molinaro A. (2011) Reflectron MALDI TOF and MALDI TOF/TOF mass spectrometry reveal novel structural details of native lipooligosaccharides. *J. Mass. Spectrom. 46,* 1135-1142.

Westphal O., Jann K. (1965) Bacterial lipopolysaccharides: extraction with phenol-water and further applications of the procedure. *Methods Carbohydr. Chem*. *5*, 83-91.

Conclusion

The lipopolysaccharides are among the most important PAMPs in Gram-negative bacteria infection. Although the recognition of those molecules by the innate immune system upon binding to the TLR4/MD-2 is beneficial for the host, excessive levels of LPS can lead to an uncontrolled release of pro-inflammatory cytokines and finally to life threatening septic shock. Furthermore, the activation of innate immune response is strictly connected to the lipid A structure, and structural modifications of this region influence significantly the immunostimulant properties of the whole molecule, diminishing or even deactivating the lipid A immunological potential. The study of lipid A molecules from non-human pathogenic bacteria can have several therapeutic implications to identify lipid A molecules that, in human cells, display inhibitory activity and may inhibit the activation of the immune system caused by agonistic lipid A/LPS.

Acetobacter pasteurianus CIP103108 is an acetic acid bacterium, used in production process of traditional Japanese black rice vinegar, *kurozu* whose consumption is believed to carry significant health benefits. The lipopolysaccharide structure possessed many particular features. Firstly, the microbe was found to carry two distinct and novel O-polysaccharides, structurally reassembling ones found in other *Acetobacter* strains. Thereafter the core region was shown to possess a very rare Ko unit directly linked to the lipid A, likely crucial for the microbe to survive in such acidic conditions, as the linkage does not show significant acid lability, contrarily to "classical" ketosidic bond formed with Kdo. Furthermore, the core region was variously phosphorylated on the Kdo residue. The immunological assays on HEK298 cells showed very weak immunostimulant activity and interestingly, minor capability to inhibit the response caused by agonistic *E. coli* LPS.

Recently reported, striking similarities of the sponge and mammalian immune system drove interest to the lipid A of a sponge symbiont, *Endozoicomonas* sp. HEX 311. The lipid A was predominantly composed of a mixture of hexa- to tri-acylated species, the main *hypo*-acylated. The sugar skeleton was substituted by "short" chain fatty acids, many odd-numbered, as *iso*-9:0 and *iso*-11:0. Finally the hexa-acylated

species was shown possessed a 3+3 symmetry. All those features suggest a low immunopotential of the lipid A, worth elucidating in the future.

Another LPS was isolated from *Phaeobacter gallaeciensis* BS107, a bacterium living in a particular symbiont-pathogen system with a microalgae *Emiliana huxleyi*. The lipid A was predominantly made up of penta- and tetra- acylated species and carried a pyrophosphate group. Moreover, the lipid A isolated from *Phaeobacter gallaeciensis* in symbiotic and pathogenic phases showed almost the same structural features. Finally, the immunological assays performed with HEK298 cells and Monocytes-derived Macrophages shown very weak capability of the molecule to induce TLR4/MD-2 driven immune response.

Zymomonas mobilis is a bacterium showing promising potential in bio-ethanol production, is able to extraordinarily tolerate high ethanol concentrations. Interestingly, this Gram negative bacterium does not synthetize the lipopolysaccharide, substituting it with other glycolipid, the glycosphingolipid. Significant amount of exopolysaccharides was isolated and characterized. Two distinct EPS were identified, and studies were conducted to correlate their presene to the high ethanol tolerance. Indeed, as shown by DOSY-NMR and DLS, the galactose containing exopolisaccharide exhibited interesting stability upon increasing ethanol concentration, thus contributing to the protection of the bacterial cell.

Finally, interactions were studied between a key protein involved in the LPS signalling pathway, the MD-2 with *A. pasteurainus* and *Bradyrhizobium* sp. *Δshc* LPS. As an amphiphilic molecule, the lipopolysaccharides form aggregated in the aqueous medium. Therefore, the behaviour of the micelles upon addition of MD-2 was studied by NMR and Cryo-EM. Interestingly both LPSs shown opposite behaviours in presence of protein.

Summary

Articles directly related to the thesis :

- **Pallach M.**, Di Lorenzo F., Facchini F.A., Gully D., Giraud E., Peri F., Duda K.A., Molinaro A., Silipo A. Structure and inflammatory activity of the LPS isolated from *Acetobacter pasteurianus* CIP103108. Int. J. Biol. Macromol. 119 (2018) 1027–1035. doi: 10.1016/j.ijbiomac.2018.08.035

- **Pallach M.**, Marchetti R., Di Lorenzo F., Fabozzi A., Giraud E., Gully D., Paduano L., Molinaro A., D'Errico G., Silipo A. *Zymomonas mobilis* exopolysaccharide structure and role in high ethanol tolerance, Carbohyd. Polym. 201 (2018) 293-299. doi:10.1016/j.carbpol.2018.08.072

- **Pallach M.**, Di Lorenzo F., Duda K.A., Le Pennec G., Molinaro A., Silipo A., The Lipid A structure from the marine sponge symbiont *Endozoicomonas* sp. HEX 311. Chembiochem. (2018) (Accepted). doi:10.1002/cbic.201800441

Articles not related to the thesis:

- Lembo-Fazio L,. Billod J.-M., Di Lorenzo F., Paciello I., **Pallach M.**, Vaz-Francisco S., Holgado A., Beyaert R., Fresno M., Shimoyama A., Lanzetta R., Fukase K., Gully D., Giraud E., Martín-Santamaría S., Bernardini M.-L., Silipo A. *Bradyrhizobium* Lipid A: Immunological Properties and Molecular Basis of its Binding to the Myeloid Differentiation Protein-2/Toll-Like Receptor 4 Complex. Front. Immunol. 9 (2018) e1888. doi: 10.3389/fimmu.2018.01888

- Di Lorenzo F., Palmigiano A., Albitar-Nehme S., **Pallach M.**, KokoulinM., Komandrova N.,Romanenko L., Bernardini M.-L., Garozzo D., Molinaro A., Silipo A. Lipid A Structure and Immunoinhibitory Effect of the Marine Bacterium *Cobetia pacifica* KMM 3879^{T}. Eur. J. Org. Chem. (2018) 2707–2716. doi:10.1002/ejoc.20180027

- Di Lorenzo F., Palmigiano A., Paciello I,. **Pallach M.**, Garozzo D,. Bernardini M.-L., Cono V., Yakimov M.M., Molinaro A., Silipo A. The Deep-Sea Polyextremophile *Halobacteroides lacunaris* TB21 Rough-Type LPS: Structure and Inhibitory Activity towards Toxic LPS. Mar Drugs. 15 (2017) pii: E201. doi: 10.3390/md15070201

- Di Lorenzo F., Palmigiano A., Duda K.A., **Pallach M.**, Busset N., Sturiale L., Giraud E., Garozzo D., Molinaro A., Silipo A. Structure of the Lipopolysaccharide from the *Bradyrhizobium* sp. ORS285 rfaL Mutant Strain. ChemistryOpen. 6 (2017) 541-553. doi: 10.1002/open.201700074

Papers related to the thesis in preparation:

- **Pallach M.**, Di Lorenzo F., Gully D., Giraud E., Duda K.A., Molinaro A., Silipo A. Structure of *Acetobacter pasteurianus* CIP103108 lipooligosaccharide (Manuscript in submission).

- **Pallach M.**, Di Lorenzo F., Lembo-Fazio L, Bernardini M.-L., Duda K.A., Molinaro A., Silipo A Structure and low inflammatory activity of *Phaeobacter gallaeciensis* BS107 lipid A (Manuscript in submission).

- **Pallach M.**, Coelho H., Zaffaroni L., Di Lorenzo F., Delgado S., Peri F., Jiménez-Barbero J., Molinaro A., Silipo A. Interactions of MD-2 with lipopolysaccharides (Manuscript in preparation).

Courses attended at University of Naples Federico II

Date	Speaker	Title
5-12 July 2016	Prof. Michelangelo Parrilli, Dr. Emiliano Bedini	Glycoscience
12-15 July 2016,	Prof. Pietro Pucci	Advanced Mass spectrometry
12-19 June 2017	Prof. Antonio Evidente	Spettroscopia Intrepretativa NMR Organica

11-14 July 2017	Prof. Delia Picone	NMR of Biomolecules
7,9,14,16 May 2018	Prof. Giovanni Pagano	Ecotoxicology: principles and main applications
2 – 4 July 2018	Prof. Alfonso Iadonisi	Organic reactions in biological systems

Seminaries attended at University of Naples Federico II

Date	Speaker	Title
20 November 2015	Dr. Francesco Berti	Innovative approaches for polysaccharide-based vaccines
22-24 February 2016	Dr. Guido Pintacuda	Solid State NMR
16 March 2016	Dr. Giulia Bianchetti	Basics of detergents formulations and challenges
17 March 2016	Dr. Vicenzo Benessere	Progettazione risk assessment e controllo qualità del packaging alimentare: il ruolo intteso del consulente chimico
12 October 2016	Prof. Angela Lombardi	Metalloproteins, mimics by design
26 October 2016	Dr. Francesca Viganò	Biomolecule analytics using microscale thermophoresis
19 December 2016	Prof. Herman Overkleeft	Chemical Biology and medicinal chemistry of glycoscphingolipid metabolism
8 June 2017	Dr. Paul Sotta	Non-entropic contribution to reinforcement in filled elastomers
8 June 2017	Prof. Neri Niccolai	Structural Bioinformatics: a window to observe new asects of protein behavious
23 July 2018	Prof. Jun-Ichi Tamura	Chemical synthesis and characterization of chondroitin sulfate

24 September 2018	Prof. Sabine Flitch	The golden age of glycoscience – new tools in synthesis and analysis
24 September 2018	Prof. Carmen Galan	Novel synthetic glycol-tools for biology research

Attendance on training events outside University of Naples Federico II

- 24 – 27 May 2016; TOLLerant 2nd, Madrid, Spain
- 28 June - 1 July 2016; Structural Glycoscience, Grenoble, France
- 14 – 16 December 2016; TOLLerant 3rdMeeting, Ljubljana, Slovenia
- 5 - 7 June 2017, TOLLerant 4th Meeting**,** Napoli, Italy
- 12 - 15 December 2017, TOLLerant 5th Meeting, Ghent, Belgium

Visiting periods in other laboratories:

Date	Host institution	Topic
6 Fubuary - 31 March 2017	Research Center Borstel - Leibniz Lung Center, Borstel, Germany	Advanced derivatization techniques in glycolipid and carbohydrate analysis
6 November – 8 December 2017	Lofarma S.P.A, Milan, Italy	Industrial secondment in pharmaceutical company
12 March – 27 April 2018	CIC bioGUNE, Derio, Bilbao, Spain	Carbohydrate-protein interaction studies

Attendance on conferences:

- 19 - 22 June 2016; XV Convegno-Scuola sulla Chimica dei Carboidrati (XV Convent-School on Carbohydrate Chemistry), Certosa di Pontignano – Siena, Italy
- 25-29 September 2016; 7th Baltic Meeting on Microbial Carbohydrates, Güstrow–Rostock, Germany
- 2 – 6 July 2017; 19th European Carbohydrate Symposium, Barcelona, Spain
- 10 July 2017; 1st NapOsaka Meeting, Naples, Italy
- 12 – 13 September 2017; Bioactive Polysaccharides, Cambridge, UK

- 17-20 June 2018; XVI Convegno-Scuola sulla Chimica dei Carboidrati (XVI Convent-School on Carbohydrate Chemistry); Certosa di Pontignano – Siena, Italy
- 25 June 2018; 2nd NapOsaka Meeting, Naples, Italy
- 11 - 13 July 2018; Immunoshape International Symposium on Glycoimmunology, San Sebstian, Spain
- 15 – 19 July 2018; 29th International Carbohydrate Symposium, Lisbon, Portugal
- 09 – 12 September 2018; 8th Baltic Meeting on Microbial Carbohydrates, Dublin, Ireland

Conference presentations

Oral communications:

- **Pallach M.**, Di Lorenzo F., Facchini F.A., Peri F.,Duda K.A., Molinaro A., Silipo A. Structural and immunostimulant studies on *Acetobacter pasteurianus* and *Phaeobacter gallaeciensis* lipopolysaccharide, 8th Baltic Meeting on Microbial Carbohydrates, Dublin, 09 – 12 September 2016
- **Pallach M.**, Di Lorenzo F., Facchini F.A., Peri F.,Duda K.A., Molinaro A., Silipo A. Structural and immunological features of *Acetobacter pasteurianus* CIP103108 lipopolysaccharide, 29th International Carbohydrate Symposium, Lisbon, 15 – 19 July 2018 (Flash presentation)
- **Pallach M.**, Di Lorenzo F., Facchini F.A., Peri F., Duda K.A., Molinaro A., Silipo A. Lipipolysaccharides and the Innate Immunity: Structural and Immunostimulant Studies on *Acetobacter pasteurianus* CIP103108 and *Phaeobacter gallaeciensis* BS107 Lipopolysaccharide, XVI Convegno-Scuola sulla Chimica dei Carboidrati (XVI Convent-School on Carbohydrate Chemistry), Certosa di Pontignano – Siena, 17-20 June 2018
- **Pallach M.** Structure of potential LPS TLR4/MD-2 agonists and antagonists from different bacterial sources, 2nd NapOsaka Meeting, Naples, Italy, 25 June 2018
- **Pallach M.**, Di Lorenzo F., Facchini F.A., Peri F., Duda K.A., Molinaro A., Silipo A.; Structural and immunostimulant studies on *Acetobacter pasteurianus* CIP103108 and *Phaeobacter*

gallaeciensis BS107 lipopolysaccharide, Immunoshape International Symposium on Glycoimmunology, San Sebstian, 11 - 13. July 2018

- **Pallach M.** Structure of potential LPS TLR4/MD-2 agonists and antagonists from different bacterial sources, 1st NapOsaka Meeting, Naples, Italy, 10 July 2017
- **Pallach M.** Structure of potential LPS TLR4/MD-2 agonists and antagonists from different bacterial sources, Bioactive Polysaccharides, 12 – 13 September 2017 (Flash presentation)
- **Pallach M.**, Di Lorenzo F., Molinaro A., Silipo A. Lipopolysaccharides and Innate Immune System, 7th Baltic Meeting on Microbial Carbohydrates, Güstrow–Rostock, 25-29 September 2016

Posters:

- **Pallach M**., Di Lorenzo F., Facchini F.A. ,Peri F.,Duda K.A., Molinaro A., Silipo A., ICS Structural and immunological features of *Acetobacter pasteurianus* CIP103108 lipopolysaccharide, 29th International Carbohydrate Symposium, Lisbon, 15 – 19 July 2018 ***(ChemBioChem Poster Prize)***

- **Pallach M**., Di Lorenzo F., Molinaro A., Silipo A. Structural Studies on *Endozoicomonas* sp. HEX 311 and *Zymomonas mobilis* Cell Wall Components, 19th European Carbohydrate Symposium, Barcelona 2 – 6 July 2017
- **Pallach M.**, Di Lorenzo F., Molinaro A., Silipo A. Structural studies on marine bacterium *Endozoicomonas* sp. O-polysaccharide; XV Convegno-Scuola sulla Chimica dei Carboidrati (XV Convent-School on Carbohydrate Chemistry), Certosa di Pontignano – Siena, 19 - 22 June 2016